Chapter 10
Messengers from the High-Energy Universe

By combining observations of a single phenomenon using different related particles, it is possible to achieve a more complete understanding of the properties of the sources; this approach is known as multi-messenger astrophysics. Multi-messenger astrophysics has developed in the beginning of the century using mostly information coming from charged particles and from photons at different wavelengths. In the very recent years simultaneous measurements involving also the detection of neutrinos and gravitational waves have been performed, expanding the horizon of astronomy.

Cosmic rays[1] were discovered at the beginning of the twentieth century (see Chap. 3). Since then an enormous number of experiments were performed on the Earth's surface, underground/underwater, on balloons, or on airplanes, or even on satellites. We know today that particles of different nature, spanning many decades in energy, are of cosmic origin, travel through the interstellar space and come to us. Their origin and composition is a challenging question. The combined study of charged and neutral cosmic rays of different nature and energies, called multi-messenger astrophysics, can solve fundamental problems, in particular related to physics in extreme environments, and unveil the presence of new particles produced in high-energy phenomena and/or in earlier stages of the Universe.

As we have seen in Chap. 1, we believe that the ultimate engine of the acceleration of cosmic rays is gravity. In gigantic gravitational collapses, such as those occurred in supernovae (energetic explosions following the collapse of stars) and in the accretion of supermassive black holes in the center of galaxies at the expense of the surrounding matter, part of the potential gravitational energy is transformed into kinetic energy

[1] In this textbook we define as *cosmic rays* all particles of extraterrestrial origin. It should be noted that other textbooks instead define as cosmic rays only nuclei, or only protons and ions – i.e., they separate gamma rays and neutrinos from cosmic rays.

A. De Angelis and M. Pimenta, *Introduction to Particle and Astroparticle Physics*, Undergraduate Lecture Notes in Physics,
https://doi.org/10.1007/978-3-319-78181-5_10

of particles. The mechanism is not fully understood, although we can model part of it; we shall give more details in this chapter. The essential characteristics of regions near collapsed matter are for sure the presence of protons, electrons, hydrogen and helium atoms (and possibly heavier atoms and ions), photons, and variable magnetic fields. A high density kernel is likely to be the center of "shock waves", expanding boundaries between regions of different density.

As usual in physics, experimental data are the key to understand how these ingredients lead to the production of high-energy particles: we need to know as accurately as possible the origin, composition, and energy spectrum of cosmic rays. Different kinds of cosmic particles act as complementary messengers: the production and propagation mechanisms can be, in particular, different. This is the basis of multimessenger astrophysics, the "New Astronomy" for the XXI century.

Multimessenger astrophysics is based on the combined information from:

- Charged cosmic rays. We shall see that this study is extremely difficult, since they can "point" to their sources only when their energy exceeds tens of EeV.
- Gamma rays. We shall see that the Universe is essentially transparent to gamma rays in a region up to some 100 GeV; beyond this energy the interaction with background photons in the Universe entails an absorption effect through the interaction $\gamma\gamma \to e^+e^-$.
- Neutrinos. Because of their small interaction cross section they travel almost undisturbed through cosmic distances, but they are very difficult to detect,
- Gravitational waves. Astronomy with gravitational waves has just started.

Cosmic rays are mainly protons ($\sim$90 %) and heavier nuclei, with a small fraction of electrons, a few per mil of the total flux. Antiprotons fluxes are even smaller (about four orders of magnitude) and so far compatible with secondary production by hadronic interactions of primary cosmic rays with the interstellar medium. Up to now there is no evidence for the existence of heavier anti-nuclei in cosmic rays. Photons and neutrinos are also a small fraction of the cosmic rays.

The energy spectrum of the charged cosmic rays reaching the atmosphere spans over many decades in flux and energy (Fig. 10.1). Above a few GeV the intensity of the cosmic ray flux follows basically a power law $E^{-\gamma}$, the differential spectral index γ being typically between 2.7 and 3.3, with two clear changes in the slope: the "knee" around $E \simeq 5 \times 10^{15}$ eV, and the "ankle" around $E \simeq 5 \times 10^{18}$ eV. A strong suppression of the flux at the highest energies, $E \gtrsim 5 \times 10^{19}$ eV, is nowadays clearly established; it may result from the destructive interaction of highly energetic particles with the Cosmic Microwave Background (CMB), or from a limit to the maximum energies of the cosmic accelerators (see Sects. 10.3.3.3 and 10.4.1.6).

Charged cosmic rays arrive close to the solar system after being deflected from the galactic magnetic fields (about 1 μG in intensity) and possibly by extragalactic magnetic fields (between 1 nG and 1 fG), if they are of extragalactic origin; when getting close to the Earth they start interacting with stronger magnetic fields—up to $\mathcal{O}$(1G) at the Earth's surface, although for shorter distances. The radius of curvature in the galaxy

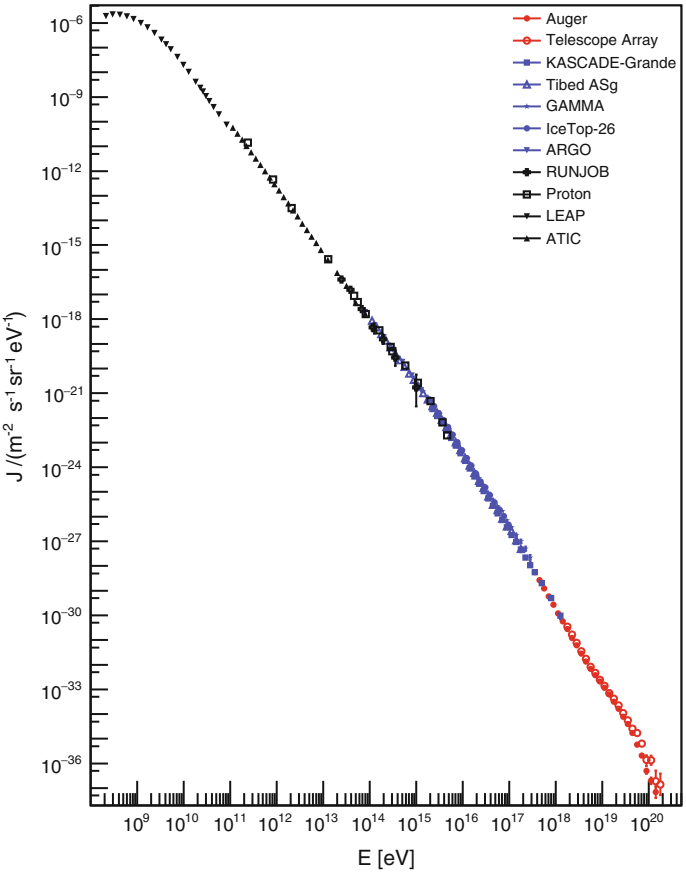

Fig. 10.1 Energy flux of charged cosmic rays. Courtesy of dr. Ioana Maris, Univ. Libre Bruxelles

$$\frac{R_L}{1\text{kpc}} \simeq \frac{E/1\text{EeV}}{B/1\text{mG}}, \tag{10.1}$$

is shorter than the distance to the galactic center (GC) for energies smaller than $\sim 10^{19}$ eV – much above the knee – and thus astronomy with charged cosmic rays is extremely difficult. To do astronomy with cosmic rays one must use photons. High-energy astrophysical processes generate photon radiation over a large range of wavelengths. Such photon radiation can be associated to the emitters, which is an advantage with respect to charged cosmic rays. In addition, photon radiation, besides being interesting in itself, can give insights on the acceleration of charged particles, being photons the secondary products of accelerated charged particles. In addition, photons are likely to be present in the decay chain of unstable massive particles, or in the annihilation of pairs of particles like dark matter particles.

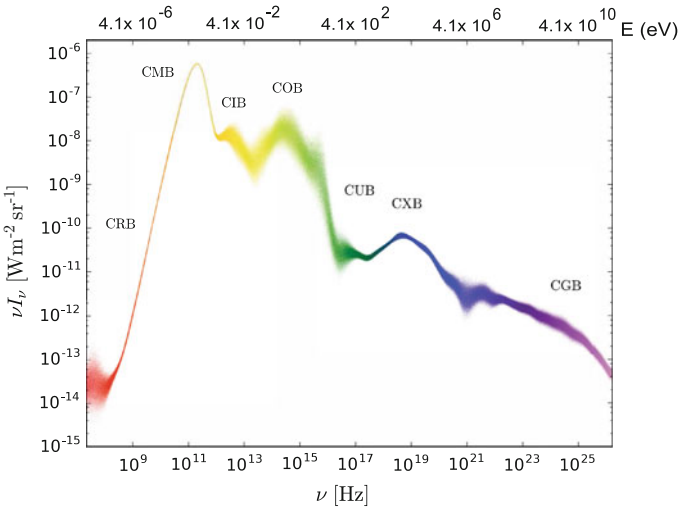

Fig. 10.2 Spectral energy distribution of the diffuse extragalactic background radiation. Adapted from R. Hill, K.W. Masui, D. Scott, https://arxiv.org/abs/1802.03694v1

Experimental data on cosmic photon radiation span some 30 energy decades (Fig. 10.2). The general behavior of the yield at high energies can be approximated by an energy dependence as a power law $E^{-2.4}$. There is little doubt on the existence of photons in the PeV–EeV range, but so far cosmic gamma rays have been unambiguously detected only in the low (MeV), high (GeV) and very (TeV) high-energy domains: upper limits are plotted above the TeV in the Figure.

A look at the sources of cosmic gamma rays in the HE region shows a diffuse background, plus a set of localized emitters. Some 5500 emitters above 100 MeV have been identified up to now, mostly thanks to the 4th catalog issued by the *Fermi*-LAT after 8 years of operation, and some 200 of them are VHE emitters as well (Fig. 10.3). About half of the gamma ray emitters are objects in our galaxy; at VHE most of them can be associated to supernova remnants (SNRs), while at MeV to GeV energies they are mostly pulsars. The remaining half are extragalactic, and the space resolution of present detectors (slightly better than 0.1°) is not good enough to associate them with particular points in the host galaxies; we believe, however, that they are produced by accretion of supermassive (up to billion solar masses) black holes in the centers of the galaxies. These are the so-called Active Galactic Nuclei (AGN).

Among cosmic messengers, gamma rays are important because they point to the sources. Present gamma-ray detectors have imaged may sources of high-energy gamma rays, which might likely be also sources of charged cosmic rays, neutrinos and other radiation. Abrupt increases of luminosity ("flares") are sometimes detected, in particular in galactic emitters and in active galactic nuclei (AGN); the most spectacular phenomenon is the explosion being of gamma ray bursts.

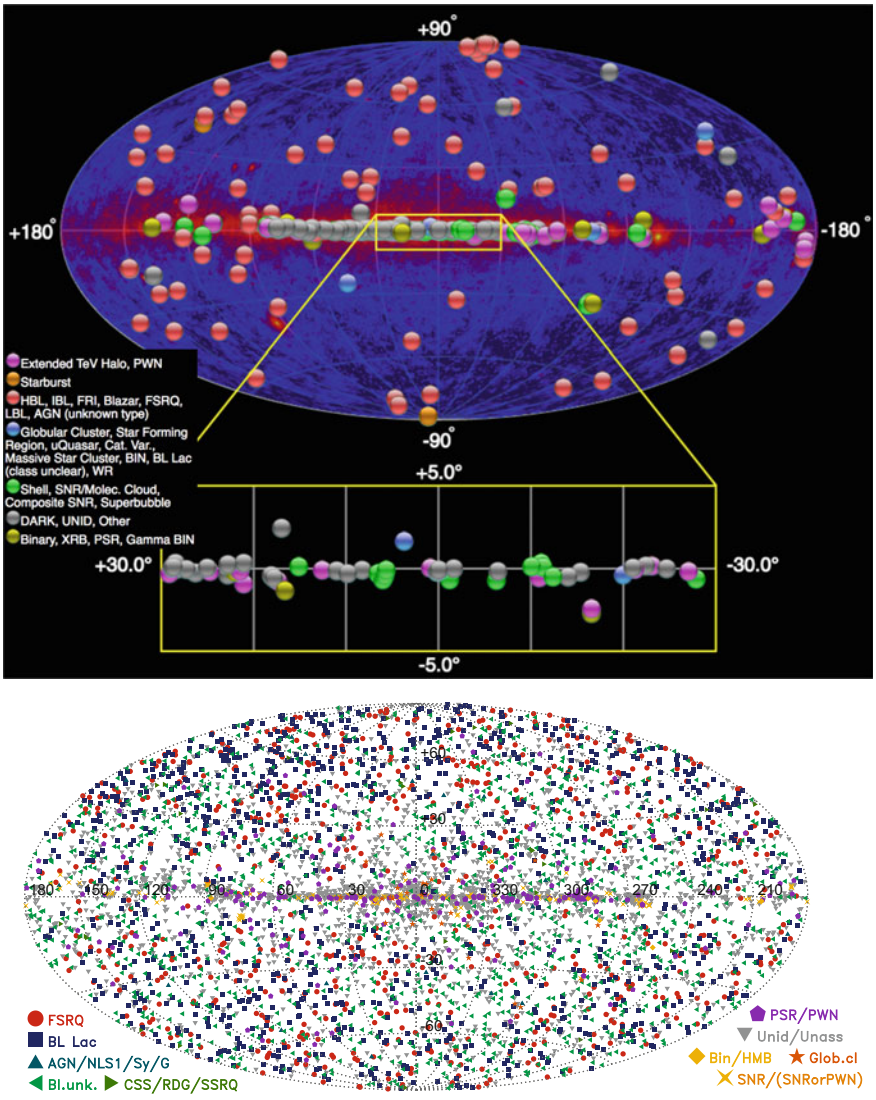

Fig. 10.3 On the top, sources of gamma-ray emission above 100 GeV plotted in galactic coordinates. The background represents the high-energy gamma ray sources detected by *Fermi*-LAT. The region near the galactic center is enlarged. From the TeVCat catalog, http://tevcat.uchicago.edu/, February 2018. The sources detected by the *Fermi* LAT above 100 MeV after 8 years of data taking are shown in detail on the bottom

Gamma Ray Bursts (GRBs), recorded almost daily, are extremely intense shots of gamma radiation of extragalactic origin. They last from fractions of a second (the so-called "short" GRBs, recently associated to neutron star-neutron star mergers), to a few seconds and more ("long" GRBs), associated to the collapse of a very large mass star (hundreds of solar masses), and a very energetic supernova (a "hypernova"). They are often followed by "afterglows" after minutes, hours, or days.

In the past few years the first observation of very-high-energy-neutrinos of astrophysical origin and the first direct detections of gravitation waves were announced. New channels to observe and understand the Universe and its evolution are now available. It has been possible to locate some sources of astrophysical neutrinos (Sect. 10.4.3.3) and of gravitational waves (Sect. 10.4.4).

10.1 How Are High-Energy Cosmic Rays Produced?

We shall discuss two basic scenarios for the production of cosmic rays: a top-down and a bottom-up scenario.

In top-down scenarios, cosmic rays come from the decays of heavier, exotic particles with masses ranging from the typical 100 GeV – 1 TeV scale of supersymmetry to the 10^{11} GeV scale of superheavy particles up to the GUT scale, $M_{GUT} \sim 10^{24}$ eV and beyond – in this last case the GZK cutoff can be avoided, since protons can be produced in the Earth's vicinity. We shall write more on this in Sect. 10.1.3.

The production of protons in particle acceleration processes in sources is instead referred to as the bottom-up scenario. At a scientific conference in 1933, Zwicky and Baade advanced a revolutionary conjecture: massive stars end their lives in explosions which blow them apart; such explosions produce cosmic rays, and leave behind a collapsed star made of densely packed neutrons. Many of the high-energy gamma-ray emitters correspond positionally to SNRs, thus indirectly confirming this conjecture– indeed we are convinced nowadays that most of the accelerators of cosmic rays in our Galaxy are SNRs. But how can a supernova remnant (or whatever remnant of a gravitational collapse) accelerate particles? By which mechanisms cosmic rays are "reprocessed" interacting with molecular clouds in the universe? It took 16 years after the conjecture by Zwicky and Baade before Enrico Fermi could devise a model in which this conjecture could be explained.

10.1.1 Acceleration of Charged Cosmic Rays: The Fermi Mechanism

Charged cosmic rays produced by particle ejection in several possible astrophysical sources may be accelerated in regions of space with strong turbulent magnetic fields. Permanent magnetic fields are not a good candidate since they cannot accelerate particles; static electric fields would be quickly neutralized; variable magnetic fields

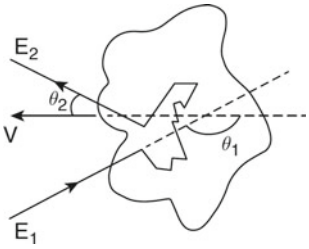

Fig. 10.4 Scattering of a cosmic ray by a moving gas cloud. From T. Gaisser, "Cosmic Rays and Particle Physics," Cambridge University Press 1990

may instead induce variable electric fields and thus accelerate, provided the particles are subject to many acceleration cycles.

In 1949 Fermi proposed a mechanism in which particles can be accelerated in stochastic collisions; this mechanism could model acceleration in shock waves which can be associated to the remnant of a gravitational collapse–for example, a stellar collapse, but also, as we know today, the surrounding of a black hole accreted in the center of a galaxy.

Let us suppose (see Fig. 10.4) that a charged particle with energy E_1 (velocity v) in the "laboratory" frame is scattering against a moving boundary between regions of different density (a partially ionized gas cloud). Due to the chaotic magnetic fields generated by its charged particles, the cloud will act as a massive scatterer. Let the cloud have a velocity $\beta = V/c$, and let θ_1 and θ_2 be the angles between, respectively, the initial and final particle momentum and the cloud velocity. Let us define $\gamma = 1/\sqrt{1-\beta^2}$.

The energy of the particle E_1^* (supposed relativistic) in the cloud reference frame is given by (neglecting the particle mass with respect to its kinetic energy):

$$E_1^* \simeq \gamma E_1 (1 - \beta \cos\theta_1) \,.$$

The cloud has an effective mass much larger than the particle's mass, and thus it acts as a "magnetic mirror" in the collision. In the cloud reference frame $E_2^* = E_1^*$ (collision onto a wall), and in the laboratory frame the energy of the particle after the collision is:

$$E_2 \simeq \gamma E_2^* (1 + \beta \cos\theta_2^*) = \gamma^2 E_1 (1 - \beta \cos\theta_1)\,(1 + \beta \cos\theta_2^*).$$

Thus the relative energy change is given by:

$$\frac{\Delta E}{E} = \frac{1 - \beta\cos\theta_1 + \beta\cos\theta_2^* - \beta^2 \cos\theta_1 \cos\theta_2^*}{1-\beta^2} - 1 \,. \tag{10.2}$$

The collision is the result of a large number of individual scatterings suffered by the particle inside the cloud, so the output angle in the c.m. is basically random. Then

$$\left\langle \cos\theta_2^* \right\rangle = 0 \,.$$

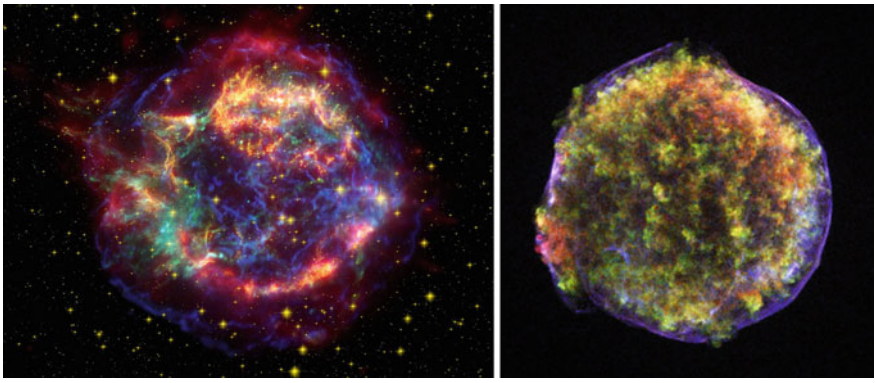

Fig. 10.5 Left: The Cassiopeia A supernova remnant is a bright remnant of a supernova occurred approximately 300 years ago (this is what we call a young SNR), 11 000 light-years away within the Milky Way. The expanding cloud of material left over from the supernova now appears approximately 10 light-years across; it is very likely a site of hadron acceleration. The image is a collage in false colors of data from the Spitzer Space Telescope (infrared, depicted in red), from the Hubble Space Telescope (visible, depicted in orange), and from the Chandra X-ray Observatory (blue and green). By Oliver Krause et al., Public Domain, https://commons.wikimedia.org/w/index.php?curid=4341500. Right: A Chandra image of another young SNR: Tycho, exploded in 1572 and studied by Tycho Brahe, at a distance of about 8000 ly and large ∼20 ly across. Shock heated gas (filamentary blue) expands with a 3000 km/s blast wave. By NASA/CXC/Chinese Academy of Sciences/F. Lu et al

The probability P to have a collision between a cosmic ray and the cloud is not constant as a function of the relative angle θ_1; it is rather proportional to their relative velocity (it is more probable that a particle hits a cloud that is coming against it, than a cloud that it is running away from it):

$$P \propto (v - V\cos\theta_1) \lessapprox (1 - \beta\cos\theta_1)$$

and thus

$$\langle\cos\theta_1\rangle \simeq \frac{\int_{-1}^{1}\cos\theta_1(1-\beta\cos\theta_1)d\cos\theta_1}{\int_{-1}^{1}(1-\beta\cos\theta_1)d\cos\theta_1} = -\frac{\beta}{3}\,. \tag{10.3}$$

The energy after the collision increases then on average by a factor

$$\left\langle\frac{\Delta E}{E}\right\rangle \simeq \frac{1-\beta\langle\cos\theta_1\rangle}{1-\beta^2} - 1 \simeq \frac{1+\beta^2/3}{1-\beta^2} - 1 \simeq \frac{4}{3}\beta^2\,. \tag{10.4}$$

This mechanism is known as the second-order Fermi acceleration mechanism. It is not very effective, since the energy gain per collision is quadratic in the cloud velocity, and the random velocities of interstellar clouds in the galaxy are very small, $\beta \sim 10^{-4}$; also the diffusion velocities directly measured, for example, in the observations of supernova remnants (see Fig. 10.5), are small ($\beta \sim 10^{-3} - 10^{-2}$).

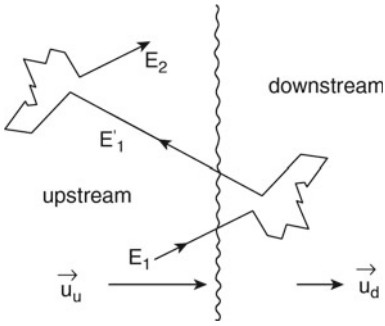

Fig. 10.6 Cosmic ray acceleration for a diffusing shock wave, in the reference frame of the shock. Adapted from T. Gaisser, "Cosmic Rays and Particle Physics," Cambridge University Press 1990

An energy gain linear in β (1st order Fermi acceleration) is needed instead to explain the cosmic ray spectrum, and we are going now to see that this happens in the Diffusive Shock Acceleration (DSA). What changes in this case is that the directions of the clouds, instead of being randomly distributed, are strongly correlated: they are approximately fronts of a plane wave. This is what occurs, for example, when a supernova ejects a sphere of hot gas into the interstellar medium, and rapidly moving gas, faster than the local speed of sound, i.e., of the speed of pressure waves, is ejected into a stationary gas, this last behaving as an obstacle for the expansion.

A shock wave creates a high-density region propagating with a locally plane wave front, acting like a piston. A shocked gas region runs ahead of the advancing piston into the interstellar medium. We assume that there is an abrupt discontinuity between two regions of fluid flow, and in the undisturbed region ahead of the shock wave, the gas is at rest. In the reference frame of the shock front, the medium ahead (upstream) runs into the shock itself with a velocity $\mathbf{u_u}$, while the shocked gas (downstream) moves away with a velocity $\mathbf{u_d}$ (Fig. 10.6); according to the kinetic theory of gases, in a supersonic shock propagating through a monoatomic gas $|u_u| \sim 4|u_d|$. In the laboratory system, a particle coming from upstream to downstream meets in a head-on collision a high-density magnetized gas. The particle inverts the direction of the component of its initial velocity parallel to the shock front direction, crosses the shock front itself, and scatters with the gas upstream; it can bounce again and again within such a pair of parallel magnetic mirrors. Note that, although the system is equivalent from the point of view of the dynamics of the bouncing particle to a pair of mirrors approaching with a net relative velocity $V = |\mathbf{u_u} - \mathbf{u_d}|$, the two mirrors do not actually approach, since the molecules acting as mirrors belong for different rebounds to different regions of the gas, and the distance is approximately constant if the diffusion velocity does not vary.

If we put ourselves in the frame of reference of one of the clouds (upstream or downstream), each bound-rebound cycle is equivalent from the point of view of the energy gain to a collision in the laboratory with a head-on component into a cloud moving with speed V (see Fig. 10.4). Being the target gas coherently moving, the component of the velocity of the particle perpendicular to the direction of propagation of the shock wave will have a negligible change, while the component parallel to the

direction itself will be inverted. If we call θ the angle between the (fixed) direction of the expansion and the direction of the incident particle, with the same convention as in Fig. 10.4, Eq. 10.2 becomes

$$\frac{\Delta E}{E} \simeq -2\beta \cos\theta\,, \tag{10.5}$$

the angle θ between the particle initial velocity and the magnetic mirror being now constrained to the specific geometry: $-1 \leq \cos\theta \leq 0$. The probability of crossing the wave front is proportional to $-\cos\theta$, and Eq. 10.3 becomes:

$$\langle \cos\theta \rangle \simeq \frac{\int_{-1}^{0} -\cos^2\theta \, d\cos\theta}{\int_{-1}^{0} -\cos\theta \, d\cos\theta} = -\frac{2}{3}. \tag{10.6}$$

The average energy gain for each bound-rebound cycle is:

$$\left\langle \frac{\Delta E}{E} \right\rangle \simeq -2\beta \langle \cos\theta \rangle \simeq \frac{4}{3}\beta \equiv \epsilon\,. \tag{10.7}$$

After n cycles the energy of the particle is:

$$E_n = E_0(1+\epsilon)^n \tag{10.8}$$

i.e., the number of cycles needed to a particle to attain a given energy E is:

$$n = \ln\left(\frac{E}{E_0}\right) / \ln(1+\epsilon)\,. \tag{10.9}$$

On the other hand, at each cycle a particle may escape from the shock region with some probability P_e, which can be considered to be proportional to the velocity V, and then the probability P_{E_n} that a particle escapes from the shock region with an energy greater or equal to E_n is:

$$P_{E_n} = P_e \sum_{j=n}^{\infty} (1-P_e)^j = (1-P_e)^n\,. \tag{10.10}$$

Replacing n by the formula Eq. 10.9 one has:

$$P_{E_n} = (1-P_e)^{\ln\left(\frac{E}{E_0}\right)/\ln(1+\epsilon)}$$

$$\ln P_{E_n} = \frac{\ln\left(\frac{E}{E_0}\right)}{\ln(1+\epsilon)} \ln(1-P_e) = \frac{\ln(1-P_e)}{\ln(1+\epsilon)} \ln\left(\frac{E}{E_0}\right)\,.$$

Then

$$\frac{N}{N_0} = P_{E_n} = \left(\frac{E}{E_0}\right)^{-\alpha} \Longrightarrow \frac{dN}{dE} \propto \left(\frac{E}{E_0}\right)^{-\Gamma} \tag{10.11}$$

with

$$\alpha = -\frac{\ln(1-P_e)}{\ln(1+\epsilon)} \cong \frac{P_e}{\epsilon} \;\; ; \;\; \Gamma = \alpha + 1\,. \tag{10.12}$$

The 1st order Fermi mechanism predicts then that the energy spectrum is a power law with an almost constant index (both ϵ and P_e are proportional to $\langle\beta\rangle$).

In the case of the supersonic shock of a monoatomic gas α is predicted by the kinetic theory of gases (see for example the volume on Fluid Mechanics by Landau and Lifshitz) to be around 1 ($\Gamma \sim 2$). The detected spectrum at Earth is steeper. In its long journey from the galactic sources to the Earth the probability that the particle escapes from the galaxy is proportional to its energy (see Sect. 10.3.3):

$$\left|\frac{dN}{dE}\right|_{\text{Earth}} \propto \left(\frac{dN}{dE}\right)_{\text{sources}} \times E^{-\delta} \propto \left(\frac{E}{E_0}\right)^{-\Gamma-\delta}\,. \tag{10.13}$$

Using the measured ratios of secondary to primary cosmic rays (e.g., B/C), δ can be estimated to be between 0.3 and 0.6 (see later). The 1st order Fermi model provides thus a remarkable agreement with the observed cosmic ray spectrum; however, V has been assumed to be nonrelativistic, and a numerical treatment is needed to account for relativistic speeds.

Note that one can approximate

$$P_e \simeq \frac{T_{cycle}}{T_e}\,, \tag{10.14}$$

where T_e is the characteristic time for escape from the acceleration region, and T_{cycle} is the characteristic time for an acceleration cycle. Thus, if E_0 is the typical energy of injection into the accelerator,

$$E < E_0(1-\epsilon)^{\tau/T_{cycle}} \;: \tag{10.15}$$

the maximum energy reachable by an accelerator is constrained by the lifetime τ of the accelerator (typically ~ 1000 years for the active phase of a SNR).

SNRs through Fermi first-order acceleration mechanisms are commonly recognized nowadays as responsible for most of the high-energy cosmic rays in the galaxy. However, the proof that this mechanism can accelerate cosmic rays all the way up to the knee region is still missing.

To summarize, the main ingredients of acceleration are magnetic fields and shock waves. These can be present in several types of remnants of gravitational collapses, in particular SNRs, AGN, GRBs. In these objects, clouds of molecular species, dust,

photon gas from bremsstrahlung and synchrotron radiation are likely to be present, and accelerated charged particles can interact with them.

10.1.2 Production of High-Energy Gamma Rays and Neutrinos

The study of sources of gamma rays and neutrinos is crucial for high-energy astrophysics: photons and neutrinos point back to their source allowing the identification of high-energy accelerators. Usually the spectrum of photons and neutrinos is measured as the energy flux in erg (or in eV or multiples) per unit area per unit time per unit frequency ν (in Hz), and fitted, where possible, to a power law; the spectral index characterizes the source. Another important quantity is the energy flux νF_ν, usually expressed in erg cm^{-2} s^{-1}, called the spectral energy distribution (SED). Equivalent formulations use the spectral photon (neutrino) flux dN/dE, and the relation holds:

$$\nu F_\nu = E^2 \frac{dN}{dE} \,. \tag{10.16}$$

High-energy photons can be produced by radiative and collisional processes, in particular those involving the interaction of high-energy charged particles (for example, electrons, protons, ions accelerated by the shock waves of remnants of gravitational collapses) with nuclear targets such as molecular clouds or radiation fields (magnetic fields, photon fields). We distinguish between purely leptonic mechanisms of production and models in which photons are secondary products of hadronic interactions; the latter provide a direct link between high-energy photon production and the acceleration of charged cosmic rays (Sect. 10.2.5), and produce, in general, also neutrinos. Since neutrinos cannot be practically absorbed nor radiated, and in bottom-up processes they come only through hadronic cascades, the neutrino is a unique tracer of hadronic acceleration.

Positron annihilation and nuclear processes associated with neutron capture and de-excitation of nuclei dominate the gamma-ray production at MeV energies.

An alternative mechanism (top-down scenario) could be the production via the decay of heavy particles; this mechanism works also for neutrinos.

10.1.2.1 Leptonic Gamma Ray Production Models

Photons cannot be directly accelerated; however, mechanisms exist such that photons of rather large energies are radiated. We examine in this subsection radiation processes just involving leptons (they are called "leptonic" photoproduction mechanisms). In particular, we shall sketch the simplest self-sustaining acceleration mechanism, the synchrotron self-Compton restricted to a single acceleration region.

Synchrotron Radiation. High-energy photon emission in a magnetic field is in the beginning generally due to synchrotron radiation. The dynamics of charged particles is strongly influenced through the Lorentz force by the magnetic fields present in astrophysical environments. Accelerated relativistic particles radiate synchrotron photons; the power loss for a charged particle of mass M and charge Ze can be expressed as

$$-\frac{dE}{dt} \simeq 2.6 \frac{\text{keV}}{\text{s}} \left(\frac{Zm_e}{M}\right)^4 \left(\frac{E}{1\,\text{keV}}\right)^2 \left(\frac{B}{1\,\text{G}}\right)^2 . \tag{10.17}$$

It is immediately evident from Eq. 10.17 that synchrotron energy loss is by far more important for electrons than for protons.

Compton scattering and "inverse Compton" process. The Compton scattering of a photon by an electron is a relativistic effect, by which the frequency of a photon changes due to a scattering. In the scattering of a photon by an electron at rest, the wavelength shift of the photon can be expressed as

$$\frac{\lambda' - \lambda}{\lambda} = \frac{\hbar\omega}{m_e c^2}(1 - \cos\alpha) ,$$

where α is the angle of the photon after the collision with respect to its line of flight. As evident from the equation and from the physics of the problem, the energy of the scattered photon cannot be larger than the energy of the incident photon. However, when low-energy photons collide with high-energy electrons instead than with electrons at rest, their energy can increase: such process is called inverse Compton (IC) scattering. This mechanism is very effective for boosting (for this reason it is called "inverse") the photon energy, and is important in regions of high soft-photon energy density and energetic electron density.

Synchrotron Self-Compton. The simplest purely leptonic mechanism we can draw for photon "acceleration"—a mechanism we have seen at work in astrophysical objects—is the so-called self-synchrotron Compton (SSC) mechanism. In the SSC, ultrarelativistic electrons accelerated in a magnetic field—such as the field present in the accretion region of AGN, or in the surrounding of SNR—generate synchrotron photons. The typical values of the fields involved are such that the synchrotron photons have an energy spectrum peaked in the infrared/X-ray range. Such photons in turn interact via Compton scattering with their own parent electron population (Fig. 10.7); since electrons are ultrarelativistic (with a Lorentz factor $\gamma_e \sim 10^{4-5}$), the energy of the rescattered photon can be boosted by a large factor.

For a power law population of relativistic electrons with a differential spectral index q and a blackbody population of soft photons at a temperature T, mean photon energies and energy distributions can be calculated for electron energies in the Thomson regime and in the relativistic Klein–Nishina regime:

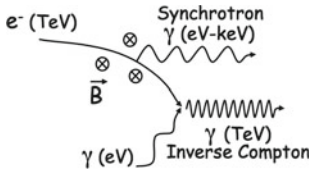

Fig. 10.7 Scheme of the SSC mechanism

$$\langle E_\gamma \rangle \simeq \tfrac{4}{3}\gamma_e^2 \langle \eta \rangle \quad \text{for } \gamma_e \eta \ll m_e c^2 \text{ (Thomson limit)} \tag{10.18}$$

$$\simeq \tfrac{1}{2}\langle E_e \rangle \quad \text{for } \gamma_e \eta \gg m_e c^2 \text{ (Klein–Nishina limit)} \tag{10.19}$$

$$\frac{dN_\gamma}{dE_\gamma} \propto E_\gamma^{-\frac{q+1}{2}} \quad \text{for } \gamma_e \eta \ll m_e c^2 \text{ (Thomson limit)} \tag{10.20}$$

$$\propto E_\gamma^{-(q+1)} \ln(E_\gamma) \quad \text{for } \gamma_e \eta \gg m_e c^2 \text{ (Klein–Nishina limit)} \tag{10.21}$$

where E_γ denotes the scattered photon's energy, E_e denotes the energy of the parent electron, and η denotes the energy of the seed photon. Note that an observer sees a power-law synchrotron spectrum only if no absorption of photons happens. Sources in which all produced photons are not absorbed are called optically thin. In an optically thick source, significant self-absorption can happen, modifying the shape of the synchrotron spectrum and typically sharpening the cutoff.

A useful approximate relation linking the electron's energy and the Comptonized photon's energy is given by:

$$E_\gamma \simeq 6.5 \left(\frac{E_e}{\text{TeV}}\right)^2 \left(\frac{\eta}{\text{meV}}\right) \text{GeV}\,.$$

The Compton component can peak at GeV–TeV energies; the two characteristic synchrotron and Compton peaks are clearly visible on top of a general E_γ^{-2} dependence. Figure 10.8 shows the resulting energy spectrum. This behavior has been verified with high accuracy on the Crab Nebula and on several other emitters, for example on active galactic nuclei. If in a given region the photons from synchrotron radiation can be described by a power law with spectral index p, in the first approximation the tails at the highest energies from both the synchrotron and the Compton mechanisms will have a spectral index p. Note, however, that since he Klein–Nishina cross section is smaller than the Thomson cross section, the Compton scattering becomes less efficient for producing gamma rays at energies larger than ∼50 TeV.

A key characteristics of the SSC model is a definite correlation between the yields from synchrotron radiation and from IC during a flare (it would be difficult to accommodate in the theory an "orphan flare," i.e., a flare in the IC region not accompanied by a flare in the synchrotron region). Although most of the flaring activities occur almost simultaneously with TeV gamma ray and X-ray fluxes, observations of 1ES 1959+650 and other AGN have exhibited VHE gamma ray flares without their coun-

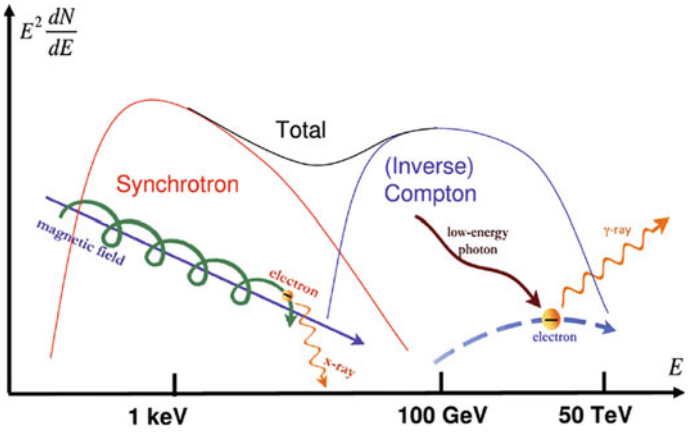

Fig. 10.8 Differential energy spectrum of photons in the SSC model

terparts in X-rays. The SSC model has been very successful in explaining the SED of AGN, but flares observed in VHE gamma rays with absence of high activity in X-rays are difficult to reconcile with the standard SSC.

10.1.2.2 Hadronic Models and the Production of Gamma Rays and Neutrinos

Alternative and complementary models of VHE emission involve cascades initiated by primary protons/nuclei that had been accelerated in the system. The beam of accelerated hadrons collides with a target of nucleons (for example, a molecular cloud) or with a sea of photons, coming from the synchrotron radiation or the bremsstrahlung of electrons accelerated or starlight (hadronic photoproduction).

In either case, the energy of the primary protons is expected by the physics of hadronic cascades to be one-two orders of magnitude larger than the energy of gamma rays, since the dominant mechanism for photon production is the decay of the secondary π^0 mesons into $\gamma\gamma$ pairs at the end of the hadronic cascade. The study of γ rays can thus provide insights on the acceleration of charged cosmic rays. Photons coming from π^0 decay have in general energies larger than photons from synchrotron radiation.

A characteristics of hadroproduction of gamma rays is a peak at $\simeq m_\pi c^2/2 \simeq 67.5$ MeV in the spectral energy distribution, which can be related to a component from π^0 decay; this feature, which is almost independent of the energy distribution of π^0 mesons and consequently of the parent protons, is called the "pion bump", and can be explained as follows. In the rest frame of the neutral pion, both photons have energy $E_\gamma = m_\pi c^2/2 \simeq 67.5$ MeV and momentum opposite to each other. Once boosted for the energy E of the emitting π^0, the probability to emit a photon of energy E_γ is constant over the range of kinematically allowed energies (the interval between

$E(1 - v/c)/2$ and $E(1 + v/c)/2$, see Exercise 2). The spectrum of gamma rays for an arbitrary distribution of neutral pions is thus a superposition of rectangles for which only one point at $m_\pi c^2/2$ is always present. This should result in a spectral maximum independent of the energy distribution of parent pions.

The existence of a hadronic component has been demonstrated from the experimental data on galactic SNRs and from the region of the GC (see later), and could explain the production of cosmic ray hadrons at energies up to almost the knee. The detection of orphan AGN flares and, more recently, of a simultaneous gamma ray-neutrino flare from an AGN, indicated evidence for hadronic production of gamma rays in such sources powered by supermassive black holes.

Let us shortly examine the relation between the high-energy part of the spectra of secondary photons and the spectra of primary cosmic rays (we shall assume protons) generating them. We shall in parallel examine the case of the spectra of secondary neutrinos, which are copiously produced in the decays of $\pi^\pm$, also present in the final states, and whose rate is closely related to the π^0 rate– neutrinos could become, if large enough detectors are built, another powerful tool for the experimental investigation. We shall follow here an analytical approach; it should be noted however that Monte Carlo approaches in specialized software programs called SIBYLL, QGSJet, EPOS and DPMJet provide much more precise results, and are normally used in scientific publications.

Proton-nucleon collisions. In beam dump processes of protons against molecular clouds, at c.m. energies much larger than the pion mass, the cross section is about 30–40 mb. The final state is dominated by particles emitted with small transverse momentum (soft or low-p_T processes). Almost the same number of π^0, π^- and π^+ are produced, due to isospin symmetry. The π^0s decay immediately into two gamma rays; the charged pions decay into $\mu\,\nu_\mu$, with the μ decaying into $e\nu_e\nu_\mu$ (charge conjugates are implicitly included). Thus, there are three neutrinos for each charged pion and three neutrinos for every gamma ray; each neutrino has approximately 1/4 of the $\pi^\pm$ energy in the laboratory, while each photon has on average half the energy of the π^0.

We assume the cross section for proton-proton interactions to be constant, $\sigma_{pp} \simeq 3 \times 10^{-26}$ cm^2. If generic hadrons of mass number A constitute the beam instead of protons, one can approximate $\sigma_{Ap} \sim A^{2/3}\sigma_{pp}$. The average pion multiplicity (shared democratically among each pion species π^0, π^- and π^+) is approximately proportional to the square root of the c.m. energy as modeled by Fermi and Landau (Chap. 6); we can approximate, for incident protons,

$$N_\pi \sim 3\left(\frac{E_p - E_{th}}{\text{GeV}}\right)^{1/4} \sim 3\left(\frac{E_p}{\text{GeV}}\right)^{1/4}, \tag{10.22}$$

where E_{th} is the threshold energy for pion production, less than 1 GeV - we can neglect it at large proton energies. Consequently, the average pion energy at the source is related to the proton energy, in the direction of flight of the proton, by

$$\langle E_\pi \rangle \sim \frac{1}{3}\left(\frac{E_p}{\mathrm{GeV}}\right)^{3/4},$$

where γ_p is the Lorentz boost of the proton.

The generic pion distribution from the hadronic collision, assuming equipartition of energy among pions, can be written as

$$q_\pi \simeq n_H l \sigma_{pp} \int_{E_{th}}^{\infty} dE_p\, j_p \left(\frac{E_p}{\mathrm{GeV}}\right)^{3/4} \delta(E_\pi - \langle E_\pi \rangle), \tag{10.23}$$

where n_H is the density of hadrons in the target, l is the depth ($N_H = n_H l$ is the column density), j_p is the proton rate. If the differential proton distribution per energy and time interval at the source is

$$j_p(E_p) = A_p E_p^{-p}, \tag{10.24}$$

making in the integral (10.23) the substitution $E_p \to E_\pi^{4/3}$ the pion spectrum at the source is

$$q_\pi(E_\pi) \propto E_p^{-\frac{4}{3}p+\frac{1}{3}}. \tag{10.25}$$

The photon spectrum is finally

$$q_\gamma(E_\gamma) = A_\gamma E_\gamma^{-\frac{4}{3}p+\frac{1}{3}}, \text{ with } A_\gamma \simeq 800 N_H A_p \sigma_{pp}. \tag{10.26}$$

This simple analytic result comes from an approximation of the interaction, but the result is not far from that of a complete calculation. Equation (10.26) provides us with an estimate of the total photon flux at the source. The spectral behavior of the protons can be estimated from diffusive shock acceleration and a spectral index -2 can be assumed.

The treatment of the neutrino case proceeds along the same line; one has

$$q_\nu(E_\nu) \simeq A_\nu (24 E_\nu/\mathrm{GeV})^{-\frac{4}{3}p+\frac{1}{3}}\ ;\ A_\nu \simeq 300 N_H A_p \sigma_{pp}. \tag{10.27}$$

Photoproduction interactions have a cross section of a fraction of mb, smaller than the proton-proton interaction by two orders of magnitude. They are thus important in environments where the target photon density is much higher than the matter density – this is the case of many astrophysical systems, like the neighborhood of SMBHs in AGN.

One can imagine that photoproduction of neutrinos and photons happens mainly via the Δ^+ resonance: $p\gamma \to N\pi$. The cross sections for the processes $p\gamma \to p\pi^0$ and $p\gamma \to n\pi^+$ at the Δ resonance are in the approximate ratio of 2:1, due to isospin balance (Chap. 5). The process happens beyond the threshold energy for producing a Δ^+:

$$4 E_p \epsilon \gtrsim m_\Delta^2, \tag{10.28}$$

where ϵ is the energy of the target photon. The cross section for this reaction peaks at photon energies of about 0.35 $m_p c^2$ in the proton rest frame. In the observer's frame the energy ϵ of the target photon is such that $\epsilon E_p \sim 0.35$, with E_p in EeV and ϵ in eV. For UV photons, with a mean energy of 40 eV, this translates into a characteristic proton energy of some 10 PeV.

The photon and neutrino energies are lower than the proton energy by two factors which take into account (i) the average momentum fraction carried by the secondary pions relative to the parent proton[2] ($\langle x_F \rangle \simeq 0.2$) and (ii) the average fraction of the pion energy carried by the photon in the decay chain $\pi^0 \to \gamma\gamma$ (1/2) and by the neutrinos in the decay chain $\pi^+ \to \nu_\mu \mu^+ \to e^+ \nu_e \bar{\nu}_\mu$ (roughly 3/4 of the pion energy because equal amounts of energy are carried by each lepton). Thus:

$$E_\gamma \sim \frac{E_p}{10} \; ; \; E_\nu \sim \frac{E_p}{20} \, . \tag{10.29}$$

The photon and neutrino spectra are related. All the energy of the π^0 ends up in photons and 3/4 of the π^+ energy goes to neutrinos, which corresponds to a ratio of neutrino to gamma luminosities (L_ν / L_γ)

$$\frac{L_\nu}{L_\gamma} \simeq \frac{3}{8} \, . \tag{10.30}$$

This ratio is somewhat reduced taking into account that some of the energy of the accelerated protons is lost to direct pair production ($p + \gamma \to e^+ e^- p$).

If a source is occulted by the presence of thick clouds or material along the line of sight to the Earth, however, gamma rays are absorbed while neutrinos survive.

An approximate expression for the relation between the neutrino and the gamma-ray fluxes produced from hadronic cascades holds if the proton energy spectrum can be described by a power law, or by an exponential:

$$E_\nu^2 \frac{dN_\nu}{dE_\nu}(E_\nu) \sim \frac{3}{4} K E_\gamma^2 \frac{dN_\gamma}{dE_\gamma}(E_\gamma) \; ; \; K = 1/2 \; (2) \; \text{for} \; \gamma p \; (pp) \, . \tag{10.31}$$

The production rate of gamma rays is not necessarily the emission rate observed: photons can be absorbed, and the photon field reduces the pionic gamma rays via pair production.

10.1.2.3 Nuclear Processes and Gamma Rays in the MeV Range

Protons at energies below the pion production threshold (about 300 MeV) can be at the origin of gamma rays through nuclear excitation of the ambient medium.

[2] The variable x_F (Feynman x), defined as the ratio between the longitudinal momentum of a particle and the maximum allowed value, is used in the discussion of hadronic interactions at large energies. It displays approximate scaling with energy.

De-excitation of the target nuclei leads to gamma ray lines in the energy region between several hundred keV to several MeV. The most distinct features in the overall nuclear gamma-ray spectrum appear around 4.4 MeV (from ^{12}C), 6.1 MeV (from ^{16}O), 0.85 MeV (from ^{56}Fe), etc.

Gamma ray line emission is expected also from radioactive isotopes synthesised in stellar interiors or during supernova explosions. Since nucleosynthesis can be effective only in very dense environments, to survive and be observed gamma-ray lines should be produced by abundant isotopes with long lifetimes. The best candidates are lines from ^{26}Al and ^{60}Fe for the production of diffuse galactic emission, and from ^{7}Be, ^{44}Ti and ^{56}Ni produced during transient phenomena.

10.1.3 Top-Down Mechanisms; Possible Origin from Dark Matter Particles

Finally, top-down mechanisms might be at the origin of high energy particles (hadrons, gamma rays, neutrinos, ...).

In the GeV-TeV region, photons and neutrinos might come from the decay of heavier particles (dark matter particles for example), or from blobs of energy coming from the annihilation of pairs of such particles. Experimental data collected up to now do not support the existence of such mechanisms—which are anyway searched for actively, especially for photons which are easier to detect, since they might shed light on new physics.

The top-down mechanism implies also an excess of antimatter: differently from the bottom-up mechanism, which privileges matter with respect to antimatter due to the abundance of the former in the Universe, decays of heavy particles should have approximately the same matter and antimatter content. An excess of antimatter at high energy with respect to what expected by standard production (mostly photon conversions and final states from collisions of CRs with the ISM) is also searched for as a "golden signature" for dark matter. Some even believe that at the highest energy cosmic rays are the decay products of remnant particles or topological structures created in the early universe. A topological defect from a phase transition in grand unified theories with typical energy scale of 10^{24} eV could suffer a chain decay into GUT mediators X and Y (see Chap. 7) that subsequently decay to known particles; in the long term the number of neutral pions (decaying into photons) is two orders of magnitude larger than the number of protons. Therefore, if the decay of topological defects is the source of the highest energy cosmic rays, the final state particles must be photons and neutrinos, which are difficult to detect.

Features in the spectra of known particles, in the GeV–TeV range, could show up if these particles originate in decays of exotic particles of very large mass possibly produced in the early Universe. Such long-lived heavy particles are predicted in many models, and the energy distribution of particles coming from their decay should be radically different from what predicted by the standard emission models from astrophysical sources.

Special care is dedicated to the products of the decays of particles in the 100-GeV mass range, since this is the order of magnitude of the mass we expect (Sect. 8.4.1) for candidate dark matter particles.

10.1.3.1 Origin from WIMPs

Dark matter candidates (WIMPs in particular, as discussed in Chap. 8) are possible sources of, e.g., photons, electrons and positrons, and neutrinos via a top-down mechanism.

As discussed in Chap. 8, the normalized relic density of dark matter (DM) particles χ can be expressed as

$$\frac{\Omega_\chi}{0.2} \simeq \frac{3 \times 10^{-26} \mathrm{cm}^3 \mathrm{s}^{-1}}{\langle \sigma_{\mathrm{ann}} v \rangle} .$$

The value for the interaction rate $\langle \sigma_{\mathrm{ann}} v \rangle$ corresponds to a cross section of the order of 10 pb, typical for weak interactions at a scale $\sim$100 GeV. This is the so-called "WIMP miracle": a weakly interacting massive particle would be a good DM candidate. WIMP masses can be expected in the range between 10 GeV and a few TeV.

Given the expected amount of WIMP dark matter in the current Universe and the annihilation cross section, it is likely that DM is subject to self-annihilations. To be able to self-annihilate, the DM particle must either coincide with its antiparticle, or be present in both the particle and antiparticle states. In the annihilation (or decay) of the dark matter particles all allowed standard model particles and antiparticles could be produced, and gamma rays and/or charged particles are present in the final states (in the last case, with no preference between matter and antimatter, contrary to the standard sources of cosmic rays).

Where dark matter densities ρ are large, the probability that WIMPs encounter each other and annihilate is enhanced, being proportional to ρ^2. The problem is that we know the dark matter density in the halos of galaxies, while the extrapolation to big density cores (like, for example, galactic centers are expected to be) relies on models – this fact holds also for the Milky Way. If one can trust the extrapolations of DM density, one can predict the expected annihilation signal when assuming a certain interaction rate $\langle \sigma v \rangle$ or put limits on this quantity in the absence of a signal (see Sect. 10.4.2.4).

10.2 Possible Acceleration Sites and Sources

In Sect. 10.1.1 we explained how a particle can be accelerated. In which astrophysical objects such acceleration process can take place?

In order to effectively accelerate a particle, the source must have at least a size R of the order of the particle *Larmor radius* r_L:

$$r_L = \frac{pc}{ZeBc} \tag{10.32}$$

where Z is the atomic number of the nucleus.

Note that the charged particle acceleration in a given magnetic field depends thus on the ratio of its linear momentum and of its electric charge, parameter defined usually as the *rigidity*:

$$\mathcal{R} = r_L Bc = \frac{pc}{Ze}. \tag{10.33}$$

The rigidity is measured in volt V and its multiples (GV, TV).

In convenient units, the energy of the accelerated particles, the magnetic field and the source size are related as:

$$\frac{E}{1\,\mathrm{PeV}} \simeq Z \frac{B}{1\,\mu\mathrm{G}} \times \frac{R}{1\,\mathrm{pc}} \simeq 0.2Z \frac{B}{1\,\mathrm{G}} \times \frac{R}{1\,\mathrm{AU}}\,. \tag{10.34}$$

This entails the so-called Hillas relation, which is illustrated in Table 10.1 and Fig. 10.9. We remind that the energies in the Hillas plot are maximum attainable energies: besides the containment, one must have an effective acceleration mechanism.

In the following, known possible acceleration sites are described.

10.2.1 Stellar Endproducts as Acceleration Sites

We have seen that most VHE gamma-ray emissions in the galaxy can be associated to supernova remnants. More than 90 % of the TeV galactic sources discovered up to now are, indeed, SNRs at large (we include here in the set of "SNR" also pulsar wind nebulae, see later).

The term "supernova" indicates a very energetic "stella nova", a term invented by Galileo Galilei to indicate objects that appeared to be new stars, that had not been observed before in the sky. The name is a bit ironic, since Galilei's diagnosis was wrong: supernovae are actually stars at the end of their life cycle with an explosion. Five supernovae have been recorded during the last millennium by eye (in the year

Table 10.1 Typical values of radii and magnetic fields in acceleration sites, and the maximum attainable energy

Source	Magnetic field	Radius	Maximum energy (eV)
SNR	30 μG	1 pc	3×10^{16}
AGN	300 μG	10^4 pc	$>10^{21}$
GRB	10^9 G	10^{-3} AU	0.2×10^{21}

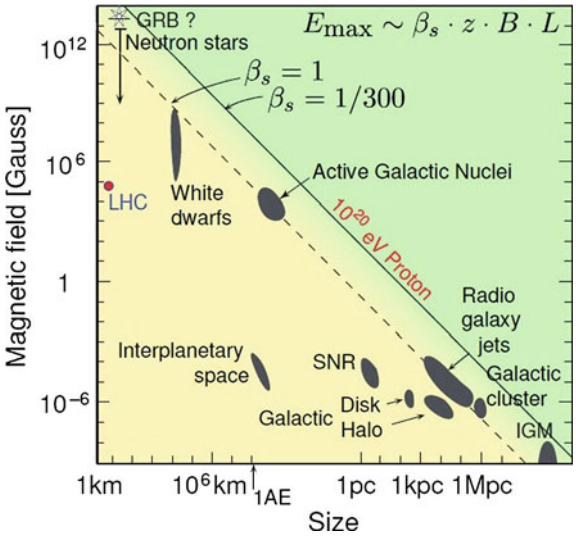

Fig. 10.9 The "Hillas plot" represents astrophysical objects which are potential cosmic ray accelerators on a two-dimensional diagram where on the horizontal axis the size R of the accelerator, and on the vertical axis the magnetic field strength B, are plotted. The maximal acceleration energy E is proportional to $ZRB\beta_s$, where β_s expresses the efficiency of the accelerator and depends on the shock velocity and on the geometry, and Z is the absolute value of the particle charge in units of the electron charge. Particular values for the maximal energy correspond to diagonal lines in this diagram and can be realized either in a large, low field acceleration region or in a compact accelerator with high magnetic fields. Typical β_s values go from $\sim$1 in extreme environments down to $\sim 1/300$. From http://astro.uni-wuppertal.de/kampert

1006; in the year 1054–this one was the progenitor of the Crab Nebula; in the year 1181; in 1572, by Tycho Brahe; and by Kepler in 1604); more than 5000 have been detected by standard observatories–nowadays, a few hundreds supernovae are discovered every year by professional and amateur astronomers. Only one core collapse supernova has been detected so far in neutrinos: SN1987a in the Large Magellanic Cloud at a distance of about 50 kpc. In modern times each supernova is named by the prefix SN followed by the year of discovery and a by a one- or two-letter designation (from A to Z, then aa, ab, and so on).

Supernovae are classified taxonomically into two "types". If a supernova's spectrum contains lines of hydrogen it is classified Type II; otherwise it is classified as Type I. In each of these two types there are subdivisions according to the presence of lines from other elements or the shape of the light curve (a graph of the supernova's apparent magnitude as a function of time). It is simpler, however, to classify them by the dynamic of the explosion:

1. **Core-collapse supernovae (type II, Ib, Ic)**. In the beginning, a massive star burns the hydrogen in its core. When the hydrogen is exhausted, the core contracts until the density and temperature conditions are reached such that the fusion $3\alpha \rightarrow {}^{12}\mathrm{C}$ can take place, which continues until helium is exhausted. This pattern (fuel exhaustion, contraction, heating, and ignition of the ashes of the previous cycle) might repeat several times depending on the mass, leading finally to an explosive burning. Almost the entire gravitational energy of about 10^{53} erg is released in MeV neutrinos of all flavors in a burst lasting seconds. A 25-solar mass star can go through a set of burning cycles ending up in the burning of Si to Fe in a total amount of time of about 7 My (as discussed in Chap. 1, Fe is stable with respect to fusion), with the final stage taking a few days.
2. **Type Ia supernovae**, already discussed in Chap. 8 as "standard candles", occur whenever, in a binary system formed by a small white dwarf and another star (for instance a red giant), the white dwarf accretes matter from its companion reaching a total critical mass of about 1.4 solar masses. Beyond this mass, it re-ignites and can trigger a supernova explosion.

A supernova remnant (SNR) is the structure left over after a supernova explosion: a high-density neutron star (or a black hole) lies at the center of the exploded star, whereas the ejecta appear as an expanding bubble of hot gas that shocks and sweeps up the interstellar medium. A star with mass larger than 1.4 times the mass of the Sun cannot die into a white dwarf and will collapse; it will become a neutron star or possibly, if its mass is larger than 3–5 times the mass of the Sun, a black hole. The most frequent elements heavier than helium created by the fusion processes are carbon, nitrogen, oxygen (this set is just called "CNO"), and iron.

10.2.1.1 Neutron Stars; Pulsars

When a star collapses into a neutron star, its size shrinks to some 10–20 km, with a density of about 5×10^{17} kg/m^3. Since angular momentum is conserved, the rotation can become very fast, with periods of the order of a few ms up to 1 s. Neutron stars in young SNRs are typically pulsars (short for pulsating stars), i.e., they emit a pulsed beam of electromagnetic radiation. Since the magnetic axis is in general not aligned to the rotation axis, two peaks corresponding to each of the magnetic poles can be seen for each period (Fig. 10.10).

The rotating period for young pulsars can be estimated using basic physics arguments. A star like our Sun has a radius $R \sim 7 \times 10^5$ km and a rotation period of $T \simeq 30$ days, so that the angular velocity is $\omega \sim 2.5 \times \mu$rad/s. After the collapse, the neutron star has a radius $R_{NS} \sim 10$ km. From angular momentum conservation, one can write:

$$R^2\omega \sim R_{NS}^2\omega_{NS} \Longrightarrow \omega_{NS} = \omega\frac{R^2}{R_{NS}^2} \Longrightarrow T_{NS} \simeq 0.5\,\mathrm{ms}\,.$$

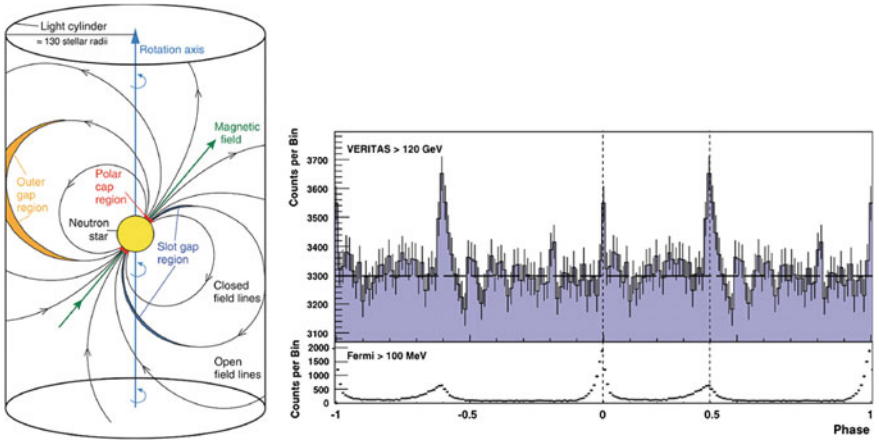

Fig. 10.10 Left: Schematic of the Crab Pulsar. Electrons are trapped and accelerated along the magnetic field lines of the pulsar and can emit electromagnetic synchrotron radiation. Vacuum gaps or vacuum regions occur at the "polar cap" close to the neutron star surface and in the outer region; in these regions density varies and thus one can have acceleration. From MAGIC Collaboration, Science 322 (2008) 1221. Right: Time-resolved emission from the Crab Pulsar at HE and VHE; the period is about 33 ms. From VERITAS Collaboration, Science 334 (2011) 69

The gravitational collapse amplifies the stellar magnetic field. As a result, the magnetic field B_{NS} near the NS surface is extremely high. To obtain an estimate of its magnitude, let us use the conservation of the magnetic flux during the contraction. Assuming the magnetic field to be approximately constant over the surface,

$$B_{\text{star}} R^2 = B_{NS} R_{NS}^2 \Longrightarrow B_{NS} = B_{\text{star}} \frac{R^2}{R_{NS}^2} .$$

For a typical value of $B_{\text{star}} = 1$ kG, the magnetic fields on the surface of the neutron star is about 10^{12} G. This estimate has been experimentally confirmed by measuring energy levels of free electrons in the pulsar strong magnetic fields. In a class of neutron stars called *magnetars* the field can reach 10^{15} G.

Typical pulsars emitting high-energy radiation have cutoffs of the order of a few GeV. More than hundred HE pulsars emitting at energies above 100 MeV have been discovered by the *Fermi*-LAT until 2013. They are very close to the solar system (Fig. 10.11, left), most of the ones for which the distance has been measured being less that a few kpc away. A typical spectral energy distribution is shown in Fig. 10.11, right. The pulsar in Crab Nebula is not typical, being one of the two (together with the Vela pulsar) firmly detected up to now in VHE (Fig. 10.12)—Crab and Vela were also the first HE pulsars discovered in the late 1970s.

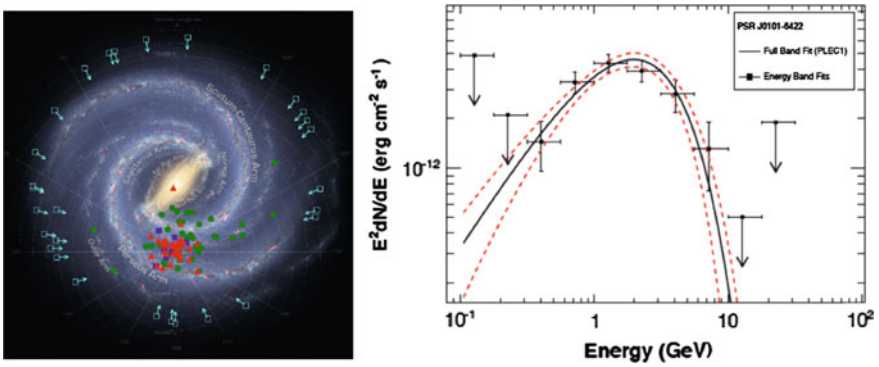

Fig. 10.11 Left: Map of the pulsars detected by the *Fermi*-LAT (the Sun is roughly in the center of the distribution). The open squares with arrows indicate the lines of sight toward pulsars for which no distance estimates exist. Credit: NASA. Right: Spectral energy distribution from a typical high-energy pulsar. Credit: NASA

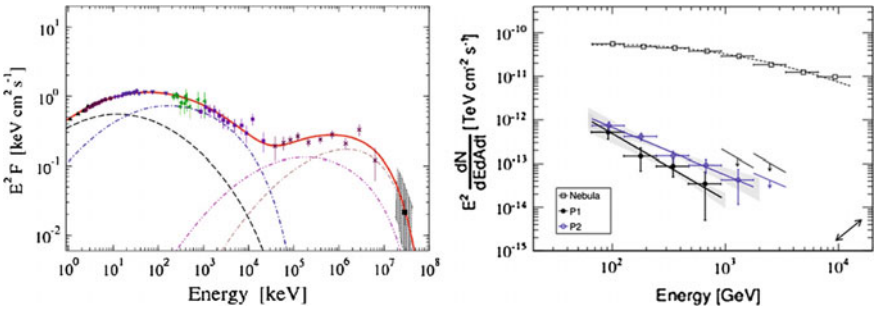

Fig. 10.12 Left: Spectral energy distribution of the Crab Pulsar. Right: The VHE energy emission, compared with the emission from the pulsar wind nebula powered by the pulsar itself. The two periodical peaks are separated. Credit: MAGIC Collaboration

10.2.1.2 Binary Systems

Neutron stars and BHs and other compact objects are frequently observed orbiting around a companion compact object or a non-degenerate star (like in the binary LS I+61 303). In binary systems mass can be transferred to the (more) compact object, accreting it. Shocks between the wind of the massive companion and the compact object can contribute to the production of non-thermal emission in X-rays or even in gamma rays. Due to the motion of ionized matter, very strong electromagnetic fields are produced in the vicinity of the compact object, and charged particles can be accelerated to high energies, generating radiation.

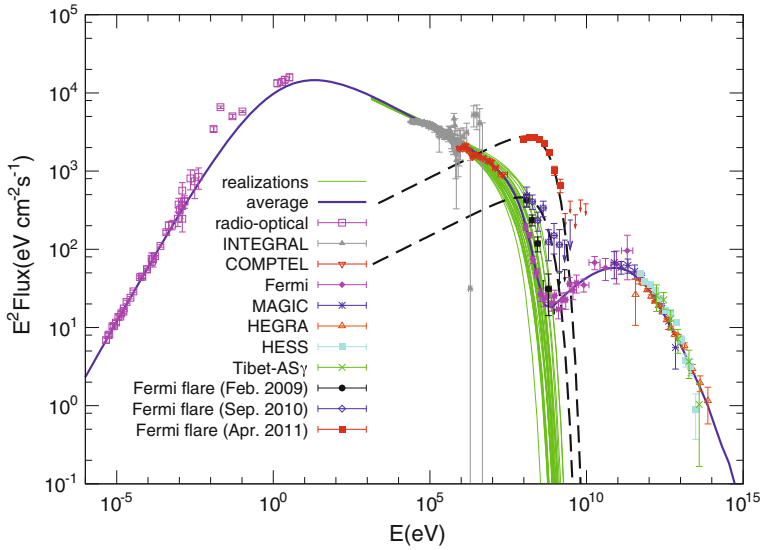

Fig. 10.13 Spectral energy distribution of the Crab Nebula (data from radio-optical up to 100 TeV). From Yuan, Yin et al., http://arxiv.org/abs/1109.0075/arXiv:1109.0075

10.2.1.3 Supernova Remnants and Particle Acceleration

Supernova remnants (SNRs) are characterized by expanding ejected material interacting with ambient gas through shock fronts, with the generation of turbulent magnetic fields, of the order of $B \sim 10\,\mu$G to 1 mG. Typical velocities for the expulsion of the material out of the core of the explosion are of the order of 3000–10 000 km/s for a young (< 1000 yr) SNR. The shock slows down over time as it sweeps up the ambient medium, but it can expand over tens of thousands of years and over tens of parsecs before its speed falls below the local sound speed.[3]

Based on their emission and morphology (which are actually related), SNRs are generally classified under three categories: shell-type, pulsar wind nebulae (PWN), and composite (a combination of the former, i.e., a shell-type SNR containing a PWN). The best known case of a PWN is the Crab Nebula, powered by the central young ($\sim$1000 year) pulsar B0531+21. Crab Nebula emits radiation across a large part of the electromagnetic spectrum, as seen in Fig. 10.13 – and qualitatively one can see in this figure the SSC mechanism at work with a transition at $\sim$30 GeV between the synchrotron and the IC emissions. One can separate the contribution of the pulsar itself to the photon radiation from the contribution of the PWN (Fig. 10.12).

Note that sometimes in the literature shell-type supernova remnants are just called SNRs and distinguished from PWN, but this is not the convention used in this book.

[3]The speed of shock is the speed at which pressure waves propagate, and thus it determines the rate at which disturbances can propagate in the medium.

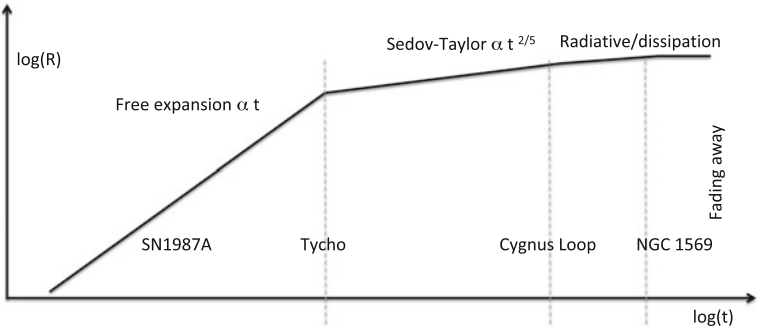

Fig. 10.14 Phases in the life of a supernova remnant

The evolution of a SNR can be described by a free expansion phase, an adiabatic phase, a radiative phase and a dissipation phase (Fig. 10.14).

1. In the free expansion phase, lasting up to few hundred years depending on the density of the surrounding gas, the shell expands at constant velocity and acts like an expanding piston, sweeping up the surrounding medium.
2. When the mass of the swept-up gas becomes comparable to the ejected mass, the Sedov-Taylor (adiabatic) phase starts. The ISM produces a strong pressure on the ejecta, reducing the expansion velocity, which remains supersonic for some 10^4 years, until all the energy is transferred to the swept-out material. During this phase, the radius of the shock grows as $t^{2/5}$. Strong X-ray emission traces the strong shock waves and hot shocked gas.
3. As the expansion continues, it forms a thin ($\lesssim$ 1 pc), dense (1–100 million atoms per cubic metre) shell surrounding the $\sim 10^4$K hot interior. The shell can be seen in optical emission from recombining ionized hydrogen and ionized oxygen atoms. Radiative losses become important, and the expansion slows down.
4. Finally, the hot interior starts cooling. The shell continues to expand from its own momentum, and $R \propto t^{1/4}$. This stage can be seen in the radio emission from neutral hydrogen atoms.

When the supernova remnant slows to the speed of the random velocities in the surrounding medium, after roughly 30 000 years, it merges into the general turbulent flow, contributing its remaining kinetic energy to the turbulence, and spreading around heavy atoms which can be recycled in the ISM.

A young supernova remnant has the ideal conditions for the Fermi 1st order acceleration. The maximum energy that a charged particle could achieve is given by the rate of energy gain, multiplied by the time spent in the shock. In the Fermi first-order model,

$$\frac{dE}{dt} \simeq \beta \frac{E}{T_{cycle}} \tag{10.35}$$

(Sect. 10.1.1); $\lambda_{cycle} \sim r_L \simeq E/(ZeB)$ is of the order of the Larmor radius (see Sect. 10.2).

$$T_{cycle} \simeq \frac{E}{ZeB\beta c} \Longrightarrow \frac{dE}{dt} \simeq (\beta^2 c) ZeB\,. \tag{10.36}$$

Finally

$$E_{\max} \simeq T_S \frac{dE}{dt} \simeq ZeBR_S\beta\,. \tag{10.37}$$

Inserting in Eq. 10.37 4 μG as a typical value of the magnetic field B, and assuming $T_e \simeq R_S/(\beta c)$, where R_S is the radius of the supernova remnant, we obtain:

$$E_{\max} \simeq \beta\, Ze\, B\, R_S \simeq 300\, Z\, \text{TeV}\,. \tag{10.38}$$

The shock acceleration of interstellar particles in SNR explains the spectrum of cosmic ray protons up to few hundreds of TeV, close to the region where the knee begins (see Fig. 10.1).

An important consequence of (10.38) is that the maximum energy is proportional to the charge Z of the ion, and it is thus higher for multiply ionized nuclei with respect to a single-charged proton. In this model, the knee is explained as a structure due to the different maximum energy reached by nuclei with different charge Z (Fig. 10.15). Note that the proportion to Z is an underestimate of the actual proportion, since in addition to the acceleration efficiency growing with Z the escape probability from the galaxy decreases with Z.

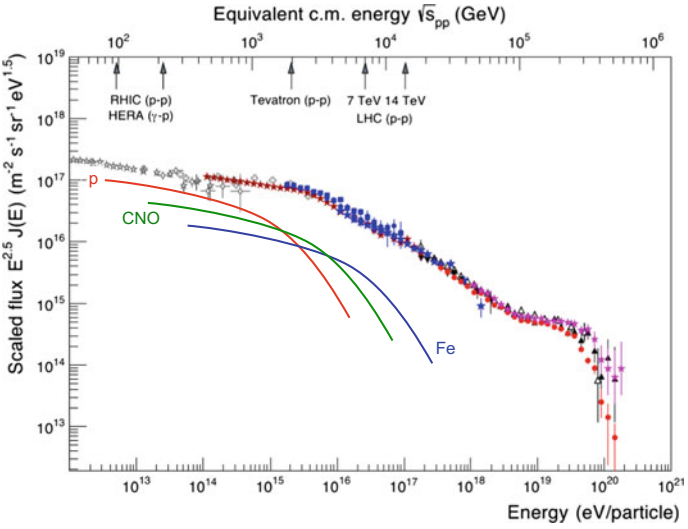

Fig. 10.15 The interpretation of the knee as due to the dependence of the maximum energy on the nuclear charge Z. The flux of each nuclear species decreases after a given cutoff. The behavior of hydrogen, CNO and iron ($Z = 26$) nuclei are depicted in figure. Adapted from R. Engel

10.2.2 Other Galactic Sources

Particle acceleration could be a more common phenomenon than indicated above, and be characteristic of many astrophysical objects. For example, we have seen that TeV emission has been found from binary sources.

The galactic zoo could be more varied at lower fluxes and energies; we shall discuss in the rest of the chapter some diffuse emitters up to ∼10 GeV. Next generation detectors will tell if other classes of emitters exist.

However, most of the galactic emitters of TeV gamma rays are SNRs at large. SNRs can, in principle, reach energies not larger than a few PeV, being limited by the product of radius time the magnetic field—see the Hillas plot. Photons above about 100 TeV have anyway never been observed, and the question is if this is due to the limited sensitivity of present detectors.

10.2.3 Extragalactic Acceleration Sites: Active Galactic Nuclei and Other Galaxies

Among the extragalactic emitters that may be observed from Earth, Active Galactic Nuclei (AGN) and Gamma Ray Bursts could fulfil the conditions (size, magnetic field, acceleration efficiency) to reach the highest energies.

Supermassive black holes of $\sim 10^6$–10^{10} solar masses ($M_\odot$) and beyond reside in the cores of most galaxies—for example, the center of our galaxy, the Milky Way, hosts a black hole of roughly 4 million solar masses, its mass having been determined by the orbital motion of nearby stars. The mass of BHs in the center of other galaxies has been calculated through its correlation to the velocity dispersion of the stars in the galaxy.[4]

In approximately 1% of the cases such black hole is active, i.e., it displays strong emission and has signatures of accretion: we speak of an active galactic nucleus (AGN). Despite the fact that AGN have been studied for several decades, the knowledge of the emission characteristics up to the highest photon energies is mandatory for an understanding of these extreme particle accelerators.

Infalling matter onto the black hole can produce a spectacular activity. An AGN emits over a wide range of wavelengths from γ ray to radio: typical luminosities can

[4]The so-called $M - \sigma$ relation is an empirical correlation between the stellar velocity dispersion σ of a galaxy bulge and the mass M of the supermassive black hole (SMBH) at its center:

$$\frac{M}{10^8 M_\odot} \simeq 1.9 \left(\frac{\sigma}{200\ \mathrm{km/s}} \right)^{5.1}$$

where $M_\odot$ is the solar mass. A relationship exists also between galaxy luminosity and black hole (BH) mass, but with a larger scatter.

be very large, and range from about 10^{37} to 10^{40} W (up to 10 000 times a typical galaxy). The energy spectrum of an AGN is radically different from an ordinary galaxy, whose emission is due to its constituent stars. The maximum luminosity (in equilibrium conditions) is set by requirement that gravity (inward) is equal to radiation pressure (outward); this is called the Eddington luminosity–approximately, the Eddington luminosity in units of the solar luminosity is 40 000 times the BH mass expressed in solar units. For short times, the luminosity can be larger than the Eddington luminosity.

Matter falling into the central black hole will conserve its angular momentum and will form a rotating accretion disk around the BH itself. In about 10% of AGN, the infalling matter turns on powerful collimated jets that shoot out in opposite directions, likely perpendicular to the disk, at relativistic speeds (see Fig. 10.16). Jets have been observed close to the BH having a transverse size of about 0.01 pc, orders of magnitude smaller than the radius of the black hole and a fraction 10^{-5} of the length of jets themselves.

Frictional effects within the disk raise the temperature to very high values, causing the emission of energetic radiation—the gravitational energy of infalling matter accounts for the power emitted. The typical values of the magnetic fields are of the order of 10^4 G close to the BH horizon, quickly decaying along the jet axis.

Many AGN vary substantially in brightness over very short timescales (days or even minutes). Since a source of light cannot vary in brightness on a timescale shorter than the time taken by light to cross it, the energy sources in AGN must be very compact, much smaller than their Schwarzschild radii—the Schwarzschild radius of the BH is $3\,\mathrm{km} \times (M/M_\odot)$, i.e., 20 AU (about 10^4 light seconds) for a supermassive black hole mass of $10^9 M_\odot$.

Broad emission lines are seen in many AGN, consistent with the emission from regions with typical speed of $\sim$5000 km/s, derived from the Doppler broadening. The general belief is that every AGN has a broad-line region (BLR), but in some cases our view of the BLR clouds is obscured by the dust torus, and thus broad lines do not appear in the spectrum. The clouds of the BLR, with typical radius of 10^{14} m, surround the central engine; at this distance from the BH, orbital speeds are several thousand kilometres per second. The clouds are fully exposed to the intense radiation from the engine and heated to a temperature $\sim 10^4$ K.

The so-called "unified model" accounts for all kinds of active galaxies within the same basic model. The supermassive black hole and its inner accretion disk are surrounded by matter in a toroidal shape, and according to the unified model the type of active galaxy we see depends on the orientation of the torus and jets relative to our line of sight. The jet radiates mostly along its axis, also due to the Lorentz enhancement—the observed energy in the observer's frame is boosted by a Doppler factor Γ which is obtained by the Lorentz transformation of a particle from the jet fluid frame into the laboratory frame; in addition the Lorentz boost collimates the jet.

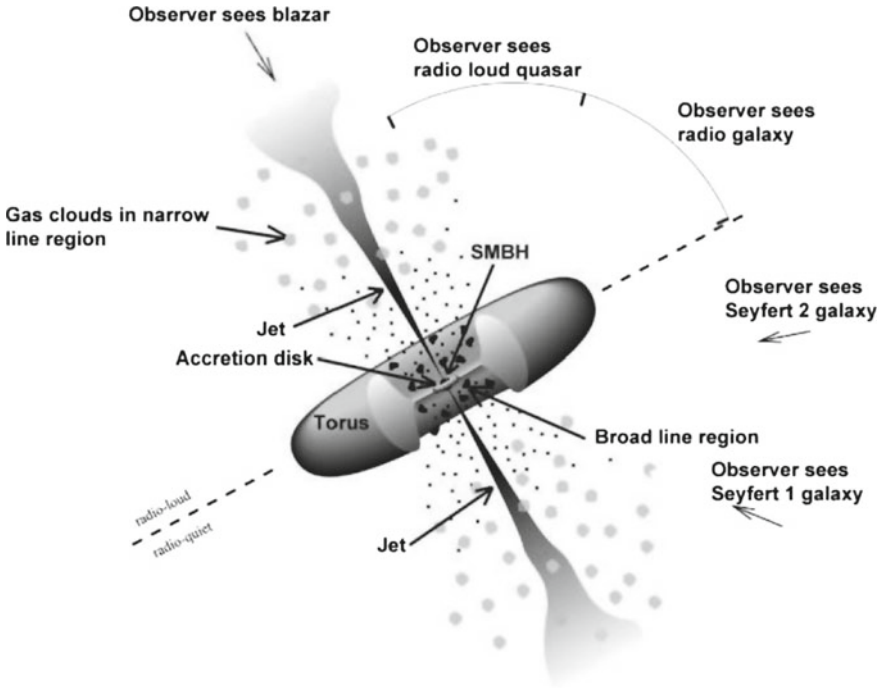

Fig. 10.16 Schematic diagram for the emission by an AGN. In the "unified model" of AGN, all share a common structure and only appear different to observers because of the angle at which they are viewed. Adapted from https://fermi.gsfc.nasa.gov/science

- An observer looking very close to the jet axis will observe essentially the emission from the jet, and thus will detect a (possibly variable) source with no spectral lines: this is called a blazar.
- As the angle of sight with respect to the jet grows, the observer will start seeing a compact source inside the torus; in this case we speak generically of a quasar.
- From a line of sight closer to the plane of the torus, the BH is hidden, and one observes essentially the jets (and thus, extended radio-emitting clouds); in this case, we speak of a radio galaxy (Fig. 10.16).

The class of jet dominated AGN corresponds mostly to radio-loud AGN. These can be blazars or nonaligned AGN depending on the orientation of their jets with respect to the line of sight. In blazars, emission is modified by relativistic effects due to the Lorentz boost. Due to a selection effect, most AGN we observe at high energies are blazars.

10.2.3.1 Blazars

Blazars accelerate particles to the highest observed energies, and are therefore of high interest.

Observationally, blazars are divided into two main subclasses depending on their spectral properties.

- Flat Spectrum Radio Quasars, or FSRQs, show broad emission lines in their optical spectrum.
- BL Lacertae objects (BL Lacs) have no strong, broad lines in their optical spectrum. Typically FSRQs have a synchrotron peak at lower energies than BL Lacs.
  BL Lacs are further classified according to the energies of the synchrotron peak $\hat{\nu}_S$ of their SED; they are called accordingly:
  - low-energy peaked BL Lacs (LBL) if $\hat{\nu}_S \lesssim 10^{14}$ Hz (about 0.4 eV);
  - intermediate-energy peaked BL Lacs (IBL);
  - high-energy peaked BL Lacs (HBL) if $\hat{\nu}_S \gtrsim 10^{15}$ Hz (about 4 eV).

  (note that the thresholds for the classification vary in the literature).

Blazar population studies at radio to X-ray frequencies indicate a redshift distribution for BL Lacs peaking at $z \sim 0.3$, with only few sources beyond $z \sim 0.8$, while the FSRQ population is characterized by a rather broad maximum at $z \sim 0.6$–1.5.

10.2.3.2 Non-AGN Extragalactic Gamma Ray Sources

At TeV energies, the extragalactic γ ray sky is completely dominated by blazars. At present, more than 50 objects have been discovered and are listed in the online TeV Catalog. Only 3 radio galaxies have been detected at TeV energies (Centaurus A, M87 and NGC 1275).

The two most massive closeby starburst (i.e., with an extremely large rate of star formation) galaxies NGC 253 and M82 are the only extragalactic sources detected at TeV energies for which the accretion disk-jet structure is not evidenced.

At GeV energies, a significant number (about 1/3 ot the total sample) of unidentified extragalactic objects has been detected by the *Fermi*-LAT (emitters that could not be associated to any known object), and few non-AGN objects have been discovered. Among non-AGN objects, there are several local group galaxies (LMC, SMC, M31) as well as galaxies in the star formation phase (NGC 4945, NGC 1068, NGC 253, and M82).

CRs might be accelerated by SNRs or other structures related to star formation activity.

10.2.3.3 The Gamma Ray Yield from Extragalactic Objects

The observed VHE spectra at high energies are usually described by a power law $dN/dE \propto E^{-\Gamma}$. The spectral indices Γ need to be fitted from a distribution deconvoluted from absorption in the Universe, since the transparency of the Universe depends on energy; they typically range in the interval from 2 to 4, with some indications for spectral hardening with increasing activity. Emission beyond 10 TeV has been established, for close galaxies like Mrk 501 and Mrk 421. Some sources are usually detected during high states (flares) only, with low states falling below current sensitivities.

Observed VHE flux levels for extragalactic objects range typically from 1 % of the Crab Nebula steady flux (for the average/steady states) up to 10 times as much when the AGN are in high activity phases. Since TeV instruments are now able to detect sources at the level of 1 % of the Crab, the variability down to few minute scale of the near and bright TeV-emitting blazars (Mrk 421 and Mrk 501) can be studied in detail. Another consequence of the sensitivity of Cherenkov telescopes is that more than one extragalactic object could be visible in the same field of view.

The study and classification of AGN and their acceleration mechanisms require observations from different instruments. The spectral energy distributions (SEDs) of blazars can span almost 20 orders of magnitude in energy, making simultaneous multiwavelength observations a particularly important diagnostic tool to disentangle the underlying nonthermal processes. Often, SEDs of various objects are obtained using nonsimultaneous data—which limits the accuracy of our models.

In all cases, the overall shape of the SEDs exhibits the typical broad double-hump distribution, as shown in Fig. 10.17 for three AGN at different distances. The SEDs of all AGN considered show that there are considerable differences in the position of the peaks of the two components and in their relative intensities. According to current models, the low-energy hump is interpreted as due to synchrotron emission from highly relativistic electrons, and the high-energy bump is related to inverse Compton emission of various underlying radiation fields, or π^0 decays, depending on the production mechanism in action (Sect. 10.1.2). Large variability is present, especially at optical/UV and X-ray frequencies.

Variability is also a way to distinguish between hadronic and leptonic acceleration modes. In a pure leptonic mode, one expects that in a flare the increase of the synchrotron hump is fully correlated to the increase of the IC hump; in a hadronic mode, vice versa, one can have a "orphan flare" of the peak corresponding to π^0 decay.

Studies on different blazar populations indicate a continuous spectral trend from FSRQ to LBL to IBL to HBL, called the "blazar sequence." The sequence is characterized by a decreasing source luminosity, increasing synchrotron peak frequency, and a decreasing ratio of high- to low-energy component (Fig. 10.17).

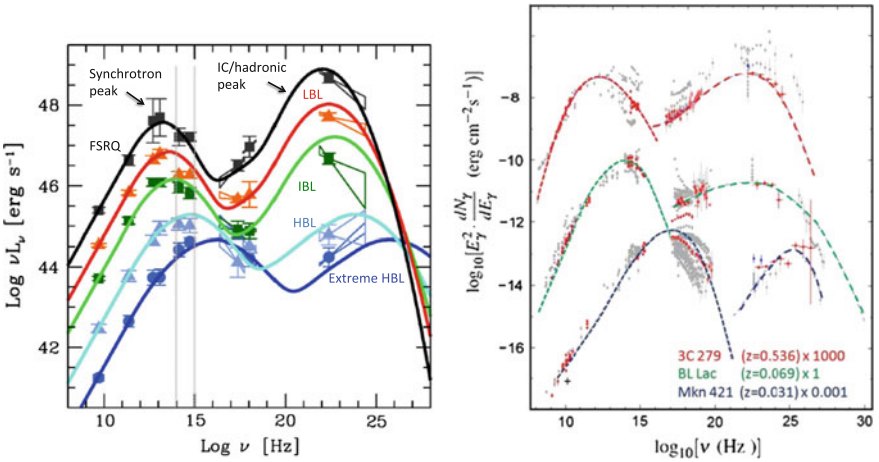

Fig. 10.17 Left: The blazar sequence. From G. Fossati et al., Mon. Not. Roy. Astron. Soc. 299 (1998) 433. Right: The SED of three different AGN at different distance from the Earth and belonging to different subclasses. To improve the visibility of the spectra, the contents of the farthest (3C 279) have been multiplied by a factor 1000, while that of the nearest (Mrk 421) by a factor 0.001. The dashed lines represent the best fit to the data assuming leptonic production. From D. Donato et al., Astron. Astrophys. 375 (2001) 739

10.2.4 Extragalactic Acceleration Sites: Gamma Ray Bursts

Gamma ray bursts (GRBs) are another very important possible extragalactic acceleration site. GRBs are extremely intense and fast shots of gamma radiation. They last from fractions of a second to a few seconds and sometimes up to a thousand seconds, often followed by "afterglows" orders of magnitude less energetic than the primary emission after minutes, hours, or even days. GRBs are detected once per day in average, typically in X-rays and soft gamma rays. They are named GRByymmdd after the date on which they were detected: the first two numbers after "GRB" correspond to the last two digits of the year, the second two numbers to the month, and the last two numbers to the day. A progressive letter ("A," "B," ...) might be added—it is mandatory if more than one GRB was discovered in the same day, and it became customary after 2010. A historical curiosity: the first GRB was discovered in 1967 by one of the US satellites of the Vela series, but the discovery has been kept secret for six years. The Vela satellites had been launched to verify if Soviet Union was respecting the nuclear test ban treaty imposing non-testing of nuclear devices in space. After the observation of the GRB, it took some time to be sure that the event was of astrophysical origin. Unfortunately, we do not know anything about possible similar discoveries by the Soviet Union.

GRBs are of extragalactic origin. The distribution of their duration is bimodal (Fig. 10.18), and allows a first phenomenological classification between "short" GRBs (lasting typically 0.3 s; duration is usually defined as the time T90 during

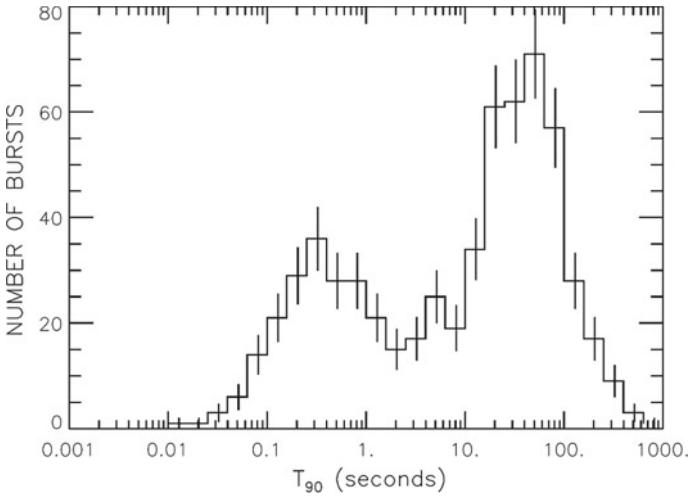

Fig. 10.18 Time distribution of GRBs detected by the BATSE satellite as a function of the time T90 during which 90 % of the photons are detected. It is easy to see "short" and "long" GRBs. Credit: NASA

which 90 % of the photons are detected) and "long" GRBs (lasting more than 2 s, and typically 40 s). Short GRBs are on average harder than long GRBs.

- Short GRBs have been associated to the coalescence of pairs of massive objects, neutron star-neutron star (NS-NS) or neutron star-black hole (NS-BH). The system loses energy due to gravitational radiation, and thus spirals closer and closer until tidal forces disintegrate it providing an enormous quantity of energy before the merger. This process can last only a few seconds, and has been recently proven by the simultaneous observation of gravitational waves and gamma rays in a NS-NS merger.
- For long GRBs in several cases the emission has been associated with a supernova from a very high mass progenitor, a "hypernova" (Sect. 10.2.4). The connection between large mass supernovae (from the explosion of hypergiants, stars with a mass of between 100 and 300 times that of the Sun) and long GRBs is proven by the observation of events coincident both in time and space, and the energetics would account for the emission—just by extrapolating the energetics from a supernova. During the abrupt compression of such a giant star the magnetic field could be squeezed to extremely large values, of the order of 10^{12}–10^{14} G, in a radius of some tens of kilometers.

Although the two families of GRBs have different progenitors, the acceleration mechanism that gives rise to the γ rays themselves (and possibly to charged hadrons one order of magnitude more energetic, and thus also to neutrinos) can be the same.

The fireball model is the most widely used theoretical framework to describe the physics of GRBs. In this model, first the black hole formed (or accreted) starts to

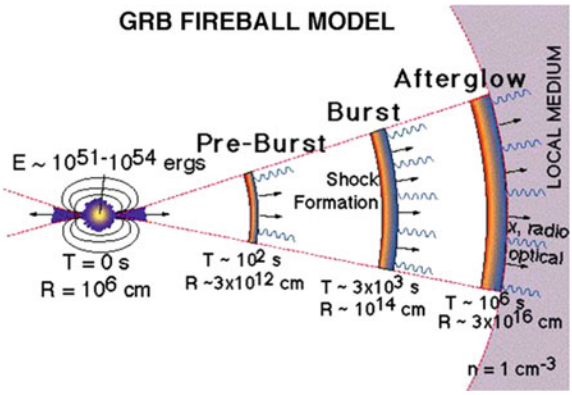

Fig. 10.19 The fireball model. Credit: http://www.swift.ac.uk/about/grb.php

pull in more stellar material; quickly an accretion disk forms, with the inner portion spinning around the BH at a relativistic speed. This creates a magnetic field which blasts outward two jets of electrons, positrons and protons at ultrarelativistic speed in a plane out of the accretion disk. Photons are formed in this pre-burst.

Step two is the fireball shock. Each jet behaves in its way as a shock wave, plowing into and sweeping out matter like a "fireball". Gamma rays are produced as a result of the collisions of blobs of matter; the fireball medium does not allow the light to escape until it has cooled enough to become transparent—at which point light can escape in the direction of motion of the jet, ahead of the shock front. From the point of view of the observer, the photons first detected are emitted by a particle moving at relativistic speed, resulting in a Doppler blueshift to the highest energies (i.e., gamma rays). This is the gamma ray burst.

An afterglow results when material escaped from the fireball collides with the interstellar medium and creates photons. The afterglow can persist for months as the energies of photons decrease.

Figure 10.19 shows a scheme of the fireball shock model.

10.2.5 Gamma Rays and the Origin of Cosmic Rays: The Roles of SNRs and AGN

10.2.5.1 Gamma Rays and the Origin of Cosmic Rays from SNRs

Among the categories of possible cosmic ray accelerators, several have been studied in an effort to infer the relation between gamma rays and charged particles. In the Milky Way in particular, SNRs are, since the hypothesis formulated by Baade and Zwicky in 1934, thought to be possible cosmic ray accelerators; according to the Hillas plot, this acceleration can go up to energies up to the order the PeV. The

particle acceleration in SNRs is likely to be accompanied by production of gamma rays due to interactions of accelerated protons and nuclei with the ambient medium.

The conjecture has a twofold justification. From one side, SNRs are natural places in which strong shocks develop and such shocks can accelerate particles. On the other side, supernovae can easily account for the required energetics. In addition, there are likely molecular clouds and photon fields which allow the reprocessing of accelerated protons–thus one can expect sizable gamma-ray and neutrino emission. Nowadays, as a general remark, we can state that there is no doubt that SNR accelerate (part of the) galactic CR, the open questions being: which kind of SNR; in which phase of their evolution SNR really do accelerate particles; and if the maximum energy of these accelerated particles can go beyond $\sim$1 PeV, and thus get insights on the nature, the energy and the composition of the knee.

A very important step forward in this field of research was achieved in the recent years with an impressive amount of experimental data at TeV energies, by Cherenkov telescopes (H.E.S.S., MAGIC, VERITAS), and at GeV energies, by the *Fermi*-LAT and AGILE satellites.

In SNRs with molecular clouds, in particular, a possible mechanism involves a source of cosmic rays illuminating clouds at different distances, and generating hadronic showers by pp collisions. This allows to spot the generation of cosmic rays by the study of photons coming from π^0 decays in the hadronic showers.

Recent experimental results support the "beam dump" hypothesis of accelerated protons on molecular clouds or photon fields from the imaging of the emitter. An example is the SNR IC443. In Fig. 10.20, a region of acceleration at GeV energies is seen by the *Fermi*-LAT. It is significantly displaced from the centroid of emission detected at higher energies by the MAGIC gamma ray telescope–which, in turn, is

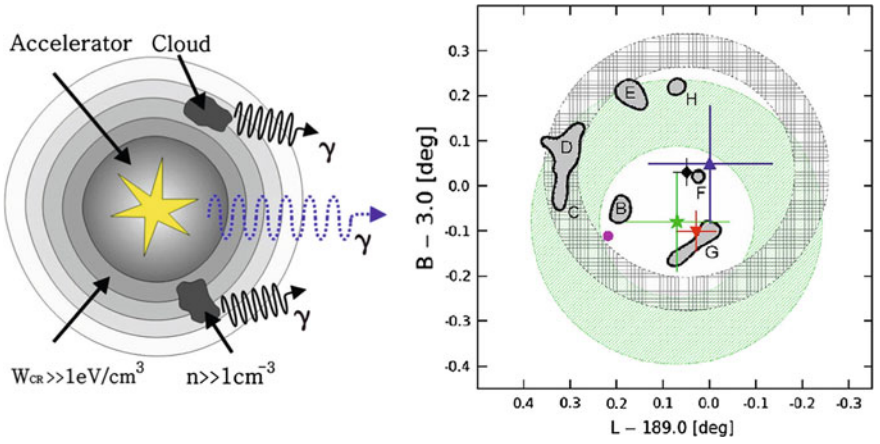

Fig. 10.20 On the left: Scheme of the generation of a hadronic cascade in the dump of a proton with a molecular cloud. On the right, IC443: centroid of the emission from different gamma detectors. The position measured by *Fermi*-LAT is marked as a diamond, that by MAGIC as a downwards oriented triangle; the latter is consistent with the molecular cloud G

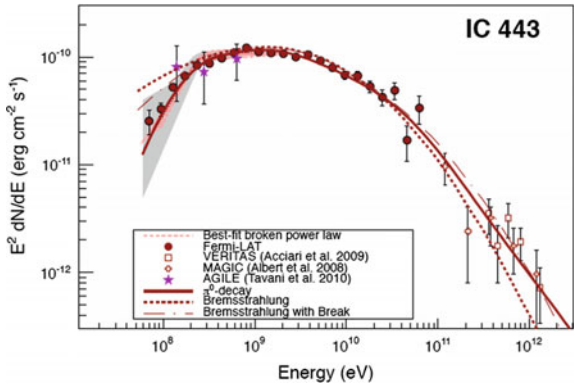

Fig. 10.21 Spectral energy distribution of photons emitted by the SNR IC443. The fit requires on top of photons coming from a leptonic acceleration mechanism also photons from π^0 decay. From *Fermi*-LAT Collaboration (M. Ackermann et al.), Science 339 (2013) 807

positionally consistent with a molecular cloud. The spectral energy distribution of photons also supports a two-component emissions, with a rate of acceleration of primary electrons approximately equal to the rate of production of protons. Such a 2-region displaced emission morphology has been also detected in several other SNRs (W44 and W82 for example).

A characteristics of hadroproduction of gamma rays is the presence of a "pion bump" at $\simeq m_\pi/2 \simeq 67.5$ MeV in the spectral energy distribution, which can be related to π^0 decay; this feature has been observed in several SNRs, see for example Fig. 10.21. Unfortunately, present gamma-ray detectors are not very sensitive in the region of few tens of MeV, and the reconstruction of the pion bump is not very accurate.

Besides indications from the studies of the morphology and from the shape of the SED, the simple detection of photons of energies of the order of 100 TeV and above could be a direct indication of production via π^0 decay, since the emission via leptonic mechanisms should be strongly suppressed at those energies where the inverse Compton scattering cross section enters the Klein–Nishina regime. A cosmic-ray accelerator near the PeV has likely been found in the vicinity of the GC.

10.2.5.2 Where Are the Galactic PeVatrons?

We saw that cosmic rays up to the knee are accelerated in the galaxy; this implies that our galaxy contains petaelectronvolt accelerators, often called PeVatrons.

Cosmic ray acceleration has been proven in particular in some stellar endproducts, as we have just seen; however, these sources display an exponential-like cutoff, or an index break, significantly below 100 TeV. This implies that none of these can be identified as a PeVatron. Now the question is: where are the PeVatrons?

Recent measurements of the galactic center region by H.E.S.S. have shown that gamma-ray emission is compatible with a steady source accelerating CRs up to

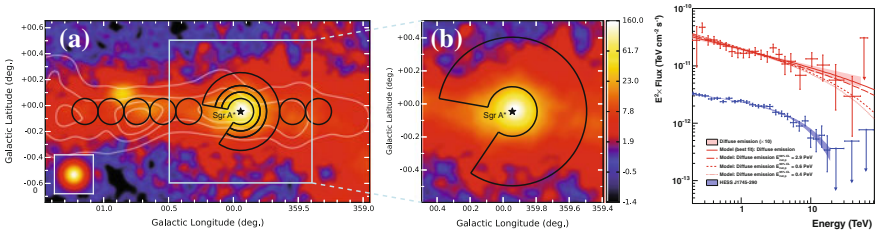

Fig. 10.22 Left: VHE γ-ray image of the GC region. The black lines show the regions used to calculate the CR energy density throughout the central molecular zone. White contour lines indicate the density distribution of molecular gas. The inset shows the simulation of a point-like source. The inner $\sim$70 pc and the contour of the region used to extract the spectrum of the diffuse emission are zoomed. Right: VHE γ-ray spectra of the diffuse emission and of the source HESS J1745-290, positionally consistent with the Galectic Center. The Y axis shows fluxes multiplied by a factor E^2, in units of TeV cm^{-2}s^{-1}. Arrows represent 95% C.L. flux upper limits. The red lines show the numerical computations assuming that γ-rays result from the decay of neutral pions produced by proton-proton interactions. The fluxes of the diffuse emission spectrum and models are multiplied by 10

PeV energies within the central 10 pc of the galaxy. The supermassive black hole Sagittarius A* could be linked to this possible PeVatron.

From an annulus centered at Sagittarius (Sgr) A* (see Fig. 10.22, left) the energy spectrum of the diffuse γ-ray emission (Fig. 10.22, right) has been extracted. The best fit to the data is found for a spectrum following a power law extending with a photon index $\simeq$2.3 to energies up to tens of TeV, without any indication of a cutoff. Since extremely-high energy γ-rays might result from the decay of neutral pions produced by pp interactions, the derivation of such hard power-law spectrum implies that the spectrum of the parent protons should extend to energies close to 1 PeV. The best fit of a γ-ray spectrum from neutral pion decays is found for a proton spectrum following a pure power-law with index $\approx$2.4. In the future, with larger and more sensitive neutrino detectors, pp interactions of 1 PeV protons could also be studied by the observation of emitted neutrinos.

Although its current rate of particle acceleration is not sufficient to provide a substantial contribution to galactic CR, Sagittarius A* could have plausibly been more active over the last $\gtrsim 10^{6-7}$ years, and therefore should be considered as a sizable source of PeV galactic cosmic rays. However, the hypothesis is speculative; moreover, the identification of the source remains unclear, since the GC region is very confused, and several other VHE gamma-ray sources exist.

Crab Nebula is a PWN currently showing no clear cutoff, and the gamma-ray emission reaches some 100 TeV and beyond, as shown by HEGRA, MAGIC and H.E.S.S.. Although there is no direct indication that it is a hadron accelerator from the morphology or from the SED, the fact itself that photon energies are so high disfavors a purely leptonic origin of gamma rays, due to Klein–Nishina suppression: Crab could likely be a PeVatron as well.

10.2.5.3 Testing if Cosmic Rays Originate from AGN

As the energetics of SNRs might explain the production of galactic CR, the energetics of AGN might explain the production of CR up to the highest energies. In the Hillas relation, the magnetic field and the typical sizes are such that acceleration is possible (Table 10.1).

Where molecular clouds are not a likely target, as, for example, in the vicinity of supermassive black holes, proton–photon interactions can start the hadronic shower.

Although the spatial resolution of gamma ray telescopes is not yet good enough to study the morphology of extragalactic emitters, a recent study of a flare from the nearby galaxy M87 (at a distance of about 50 Mly, i.e., a redshift of 0.0004) by the main gamma telescopes plus the VLBA radio array has shown, based on the VLBA imaging power, that this AGN accelerates particles to very high energies in the immediate vicinity (less than 60 Schwarzschild radii) of its central black hole. This galaxy is very active: its black hole, of a mass of approximately 7 billion solar masses, accretes by 2 or 3 solar masses per year. A jet of energetic plasma originates at the core and extends outward at least 5000 ly.

Also Centaurus A, the near AGN for which some weak hint of correlation with the Auger UHE data exists, has been shown to be a VHE gamma emitter.

The acceleration of hadrons above 1 EeV has been proven very recently to correlate with the position of AGN, and in particular one blazar has been identified as a hadron accelerator at some tens of PeV. These two evidences will be discussed in detail later, in Sect. 10.4.1.7 and in Sect. 10.4.3.2 respectively.

10.2.6 Sources of Neutrinos

Neutrinos play a special role in particle astrophysics. Their cross section is very small and they can leave production sites without interacting. Differently from photons, neutrinos can carry information about the core of the astrophysical objects that produce them. Different from photons, they practically do not suffer absorption during their cosmic propagation.

1. Neutrinos can be produced in the nuclear reactions generating energy in stars. For example, the Sun emits about 2×10^{38} neutrinos/s. The first detection of neutrinos from the Sun happened in the 1960s. The deficit of solar neutrinos with respect to the flux expected from the energy released by the Sun paved the way to the discovery of neutrino oscillations and thus, ultimately, of a nonzero neutrino mass (see Chaps. 4 and 9).
2. Neutrinos should be produced in the most violent phenomena, including the Big Bang, supernovae, and the accretion of supermassive black holes. The burst of neutrinos produced in a galactic core-collapse supernova is detectable with detectors like Super-Kamiokande and SNO; however, this has been detected only once up to now. On February 23, 1987, a neutrino burst from a supernova in the LMC, some

0.2 Mly from Earth, was observed in the proton-decay detectors Kamiokande and IMB (see Sect. 10.4.3).

3. Neutrinos are the main output of the cooling of astrophysical objects, including neutron stars and red giants.
4. Neutrinos are produced as secondary by-products of cosmic ray collisions:
   (a) with photons or nuclei near the acceleration regions (these are "astrophysical" neutrinos, like the ones at items 2. and 3.);
   (b) with the CMB in the case of ultrahigh-energy cosmic rays suffering the GZK effect (these are called cosmogenic neutrinos, or also "GZK neutrinos," although the mechanism was proposed by Berezinsky and Zatsepin in 1969);
   (c) and also with the Earth atmosphere (they are called atmospheric neutrinos). When primary cosmic protons and nuclei hit the atmosphere, the hadronic reactions with atmospheric nuclei can produce in particular secondary pions, kaons and muons. Atmospheric neutrinos are generated then by the decay of these secondaries. The dominating processes are:

$$\begin{aligned} \pi^{\pm}(K^{\pm}) &\rightarrow \mu^{\pm} + \nu_{\mu}(\overline{\nu}_{\mu}), \\ \mu^{\pm} &\rightarrow e^{\pm} + \nu_{e}(\overline{\nu}_{e}) + \overline{\nu}_{\mu}(\nu_{\mu})\,. \end{aligned} \tag{10.39}$$

   For cases (a) and (b), coming gamma-rays and neutrinos both from pion decay, the gamma and neutrino fluxes are of the same order of magnitude at production – of course, the flux at the Earth might be different due to the absorption of gamma rays.

5. Finally, they are likely to be present in the decay chain of unstable massive particles, or in the annihilation of pairs of particles like dark matter particles.

Sources 2., 4. and 5. in the list above are also common to photons. However, detection of astrophysical neutrinos could help constraining properties of the primary cosmic ray spectrum more effectively than high-energy photons. Neutrinos produced by reactions of ultrahigh-energy cosmic rays can provide information on otherwise inaccessible cosmic accelerators.

Neutrino sources associated with some of nature's most spectacular accelerators however exist similar to photon sources. The program of experiments to map out the high-energy neutrino spectrum is now very active, guided by existing data on cosmic ray protons, nuclei, and γ rays, which constrain possible neutrino fluxes. In 2013, the IceCube Collaboration discovered a flux of astrophysical neutrinos with estimated energies above 1 PeV. They are the highest energy neutrinos ever observed, and they must come, directly or indirectly, from extra solar sources; at the present status, however, these events do not appear to cluster to a common source (see Sect. 10.4.3.2).

The neutrino sources just discussed are displayed in Fig. 10.23, left, according to their contributions to the terrestrial flux density. The figure includes low-energy sources, such as the thermal solar neutrinos of all flavors, and the terrestrial neutrinos—i.e., neutrinos coming from the Earth's natural radioactivity—not explic-

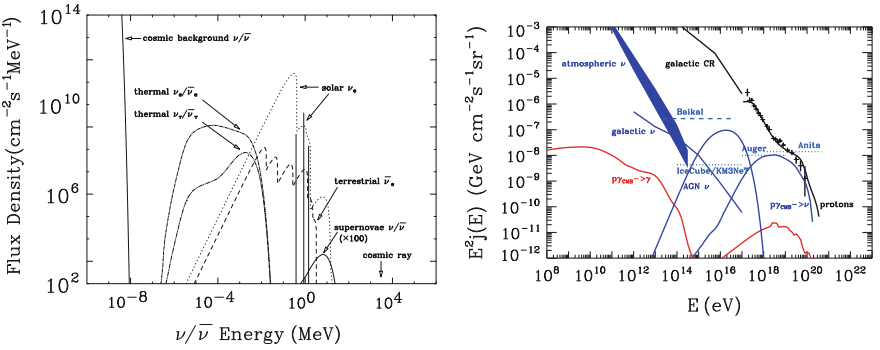

Fig. 10.23 Left: Sources of neutrinos with energies below 1 TeV. From W.C. Haxton, http://arxiv.org/abs/1209.3743/arXiv:1209.3743, to appear in Wiley's Encyclopedia of Nuclear Physics. Right: A theoretical model of high-energy neutrino sources. The figure includes experimental data, limits, and projected sensitivities to existing and planned telescopes. From G. Sigl, http://arxiv.org/abs/0612240/arXiv:0612240

itly discussed here. Beyond the figure's high-energy limits there exist neutrino sources associated with some of nature's most energetic accelerators.

Very high energy cosmic ray protons should be, as discussed above, a source of very energetic neutrinos (10^{17}–10^{19} eV) by, namely, its interaction with CMB photons. Theoretical predictions of the fluxes of such neutrinos as well as projected sensitivities of relevant experiments are shown in Fig. 10.23, right. Energetic nuclei may be also a source of neutrinos by its photo-desintegration ($A + \gamma \rightarrow A^{`} + p$) followed by the interaction of the resulting protons with again the IR/optical/UV photon background. Existing data on the high-energy particle spectrum is thus one of the frontiers of neutrino astronomy.

10.2.6.1 Testing if Ultra-High-Energy Cosmic Rays Originate from GRBs

IceCube has been searching for neutrinos arriving from the direction and at the time of a gamma-ray burst. After more than one thousand follow-up observations, none was found, resulting in a limit on the neutrino flux from GRBs of less than one per cent. This focuses to an alternative explanation for the sources of extragalactic cosmic rays: active galactic nuclei.

10.2.7 Sources of Gravitational Waves

The equations of Einstein's General Relativity (see Chap. 8) couple the metric of space–time with the energy and momentum of matter and radiation, thus providing the

mechanism to generate gravitational waves as a consequence of radially asymmetric acceleration of masses at all scales. At the largest scales (extremely low frequencies 10^{-15}–10^{-18}Hz) the expected sources are the fluctuations of the primordial Universe. At lower scales (frequencies 10^{-4}–10^{4}Hz) the expected sources are:

- Stellar mass black hole binaries, of the type detected already by LIGO.
- Neutrons star binaries.
- Supernova, gamma-ray bursts, mini-mountains on neutron stars (caused by phase transitions on the crust, for example).
- Supermassive black hole binaries, formed when galaxies merge.
- Extreme mass-ratio inspirals, when a neutron stars or stellar-mass black hole collides with a supermassive black hole.

Gravitational waves are ripples in space-time propagating in free space at the velocity of light. In the weak-field approximation (linearized gravity), the local metric is deformed by the addition of a dynamical tensor term $h_{\mu\nu}$ fulfilling the equation

$$\Box h_{\mu\nu} = 0\,. \tag{10.40}$$

This is a wave equation whose simplest solutions are transverse plane waves propagating along light rays at the speed of light. The effects of this wave in the space axes transverse to the propagation are opposite: while one expands, the other contracts and vice-versa. A gravitational wave changes the distance L between two masses placed on a transverse axis by an amount $\delta L = L\,h$, oscillating in time. The amplitude of the effect is quite tiny if the source is far (h is proportional to $1/R$ where R is the distance to the source). The relative change of the distance between two tests masses at Earth, the *strain*, which is the variable measured by gravitational wave detectors (see Sect. 4.6), is of the of the order of 10^{-23} for the Hulse-Taylor binary pulsar and of 10^{-21} for the coalescence of a binary stellar-mass black hole system (see Sect. 10.4.4).

The first gravitational wave signal (see Sect. 10.4.4), observed in 2015, was attributed to the coalescence of a stellar-mass binary black hole system. Before this detection and the following, the probability of formation of BH binaries with such masses (tens of solar masses) from the stellar collapse was believed to be quite small.

10.3 The Propagation

The propagation of cosmic messengers is influenced by the presence of magnetic fields in the Universe, and by the possible interaction with background photons and matter. The density of background photons, and of matter, can be extremely variable: it is larger within galaxies and even larger closer to acceleration sites than in the intergalactic space. We expect the same behavior for the magnetic field.

10.3.1 Magnetic Fields in the Universe

We know from studies of the Faraday rotation of polarization that the galactic magnetic fields are of the order of a few μG; the structure is highly directional and maps exist.

Although these values may appear quite small, they are large enough to not allow galactic "charged particle astronomy". Indeed, since the Larmor radius of a particle (note that this is the same formula we previously used to compute the maximum energy reachable by a cosmic accelerator) of unit charge in a magnetic field can be written as (see Sect. 10.2),

$$\frac{R_L}{1\text{kpc}} \simeq \frac{E/1\text{EeV}}{B/1\mu G}\,, \tag{10.41}$$

In order to "point" to the GC, which is about 8 kpc from the Earth, for a galactic field of 1μG one needs protons of energy of at least 10^{19} eV. The flux is very small at this energy; moreover, Galactic accelerators are not likely to accelerate particles up to this energy (remind the Hillas plot). There is thus a need to use neutral messengers to study the emission of charged cosmic rays. Unfortunately, the yield of photons at an energy of 1 TeV is only 10^{-3} times the yield of protons, and the yield of neutrinos is expected to be of the same order of magnitude or smaller. In addition, the detection of neutrinos is experimentally very challenging, as discussed in Chap. 4.

Different from galactic magnetic fields, the origin and structure of cosmic (i.e., extragalactic) magnetic fields remain elusive. Observations have detected the presence of nonzero magnetic fields in galaxies, clusters of galaxies, and in the bridges between clusters. The determination of the strength and topology of large-scale magnetic fields is crucial also because of their role in the propagation of ultrahigh-energy cosmic rays and, possibly, on structure formation.

Large-scale magnetic fields are believed to have a cellular structure. Namely, the magnetic field B is supposed to have a correlation length λ, randomly changing its direction from one domain to another but keeping approximately the same strength. Correspondingly, a particle of unit charge and energy E emitted by a source at distance $d \gg \lambda$ performs a random walk and reaches the Earth with angular spread

$$\theta \simeq 0.25^\circ \left(\frac{d}{\lambda}\right)^{1/2} \left(\frac{\lambda}{1\,\text{Mpc}}\right) \left(\frac{B}{1\,\text{nG}}\right) \left(\frac{10^{20}\,\text{eV}}{E}\right)\,. \tag{10.42}$$

The present knowledge of the extragalactic magnetic fields (EGMF), also called intergalactic magnetic field (IGMF), allows setting the following constraints:

$$B \simeq 10^{-9}\text{G} - 10^{-15}\text{G}\;;\;\; \lambda \simeq 0.1\,\text{Mpc} - 100\,\text{Mpc}\,. \tag{10.43}$$

This estimate is consistent with various intergalactic magnetic field generation scenarios, including in particular generated outflows from the galaxies, and, from the experimental side, with the negative results of the search for the secondary gamma-

ray emission from the e^+e^- pairs produced by the interaction of gamma rays from AGN with background photons in the Universe. In the presence of large magnetic fields, this would blur the image of distant galaxies.

10.3.2 Photon Background

The photon background in the Universe has the spectrum in Fig. 10.2. The maximum photon density corresponds to the CMB, whose number density is about 410 photons per cubic centimeter.

A region of particular interest is the so-called extragalactic background light (EBL), i.e., the light in the visible and near infrared regions. It is mainly composed by ultraviolet, optical, and near-infrared light emitted by stars throughout the whole cosmic history, and its re-emission to longer wavelengths by interstellar dust, which produces its characteristic double peak spectral energy distribution. This radiation is redshifted by the expansion of the Universe by a factor $(1 + z)$, and thus, the visible light from old sources is detected today as infrared. Other contributions to the EBL may exist such as those coming from the accretion on super-massive black holes, light from the first stars, or even more exotic sources such as products of the decay of relic dark matter particles.

The density of EBL photons in the region near the visible can be derived by direct deep field observations, and by constraints on the propagation of VHE photons (see later). A plot of the present knowledge on the density of photons in the EBL region is shown in Fig. 10.24, left. Figure 10.24, right, shows a summary of the estimated photon number density of the background photons as composed by the radio background, the CMB, and the infrared/optical/ultraviolet background (EBL).

10.3.3 Propagation of Charged Cosmic Rays

The presence of magnetic fields in the Universe limits the possibility to investigate sources of emission of charged cosmic rays, as they are deflected by such fields. The propagation is affected as well by the interaction with background photons and matter.

10.3.3.1 Propagation of Galactic Cosmic Rays and Interaction with the Interstellar Medium

Cosmic rays produced in distant sources have a long way to cross before reaching Earth. Those produced in our galaxy (Fig. 10.25) suffer diffusion in magnetic fields

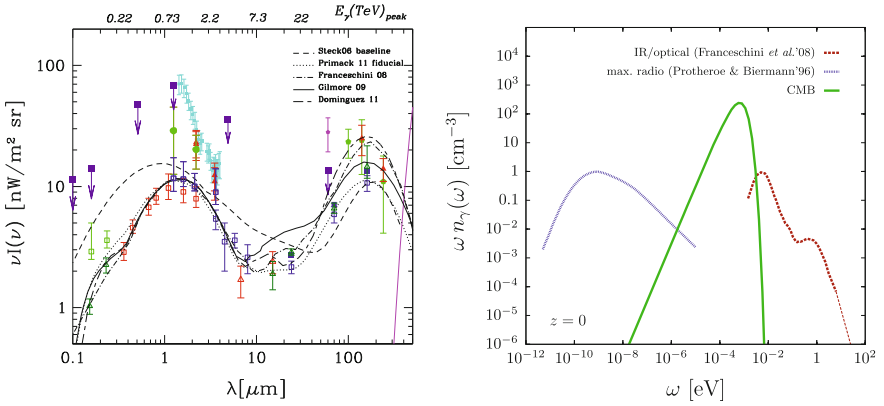

Fig. 10.24 Left: Spectral energy distribution of the EBL as a function of the wavelength and energy. Open symbols correspond to lower limits from galaxy counts while filled symbols correspond to direct estimates. The curves show a sample of different recent EBL models, as labeled. On the upper axis the TeV energy corresponding to the peak of the $\gamma\gamma$ cross section is plotted. From L. Costamante, IJMPD 22 (2013) 1330025. Right: A summary of our knowledge about the density of background photons in intergalactic space, from the radio region to the CMB, to the infrared/optical/ultraviolet region. From M. Ahlers et al., Astropart. Phys. 34 (2010) 106

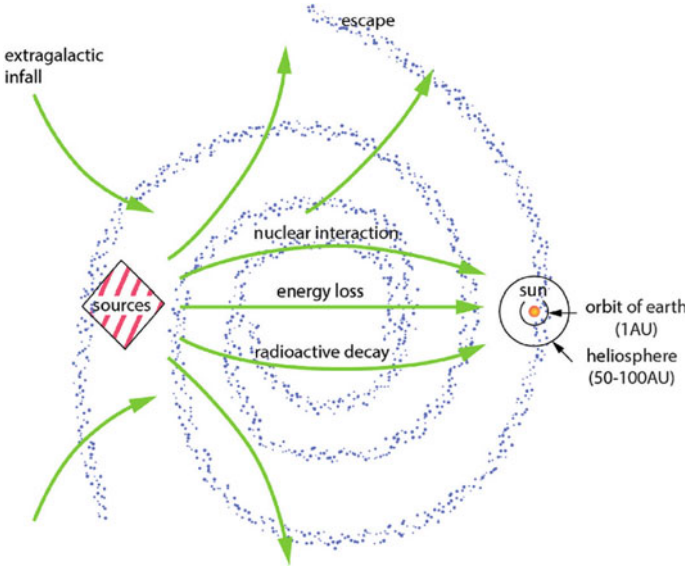

Fig. 10.25 Galactic cosmic ray propagation

of the order of a μG, convection by galactic winds, spallation[5] in the interstellar medium, radioactive decays, as well as energy losses or gains (reacceleration). At some point they may arrive to Earth or just escape the galaxy. Low-energy cosmic rays stay within the galaxy for quite long times. Typical values of confinement times of 10^7 years are obtained measuring the ratios of the abundances of stable and unstable isotopes of the same element (for instance ^{7}Be/^{10}Be, see below).

All these processes must be accounted in coupled transport equations involving the number density N_i of each cosmic ray species of atomic number Z_i and mass number A_i as a function of position, energy and time. These differential equations, can, for instance, be written as:

$$\begin{aligned}\frac{\partial N_i}{\partial t} &= C_i + \boldsymbol{\nabla}\cdot(D\boldsymbol{\nabla}N_i - \mathbf{V}N_i) + \frac{\partial}{\partial E}\left(b\left(E\right)N_i\right) + \\ &- \left(n\beta_i c\sigma_i^{\text{spall}} + \frac{1}{\gamma_i \tau_i^{\text{decay}}} + \frac{1}{\hat{\tau}_i^{\text{esc}}}\right) N_i + \\ &+ \sum_{j>i}\left(n\beta_j c\sigma_{ji}^{\text{spall}} + \frac{1}{\gamma_j \tau_{ji}^{\text{decay}}}\right) N_j \,. \end{aligned} \tag{10.44}$$

In the above equation:

- The term C_i on the right side accounts for the sources (injection spectrum).
- The second term accounts for diffusion and convection:
  - $\boldsymbol{\nabla}\cdot(D\boldsymbol{\nabla}N)$ describes diffusion: when at a given place N is high compared to the surroundings (a local maximum of concentration), particles will diffuse out and their concentration will decrease. The net diffusion is proportional to the Laplacian of the number density through a parameter D called diffusion coefficient or diffusivity, whose dimensions are a length squared divided by time;
  - $(\boldsymbol{\nabla}\cdot\mathbf{V})N$ describes convection (or advection), which is the change in density because of a flow with velocity $\mathbf{V}$.
- The third term accounts for the changes in the energy spectrum due to energy losses or reacceleration – we assume that energy is lost, or gained, at a rate $dE/dt = -b(E)$.
- The fourth term accounts for the losses due to spallation, radioactive decays, and probability of escaping the galaxy. n is the number density of the interstellar medium (ISM).
- The fifth term accounts for the gains due to the spallation or decays of heavier elements.

These equations may thus include all the physics process and all spatial and energy dependence but the number of parameters is large and the constraints from experi-

[5]The spallation (or fragmentation) process is the result of a nucleus-nucleus collision, in which the beam fragments into lighter nuclei.

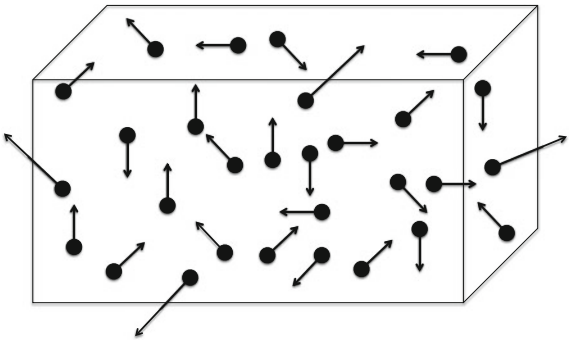

Fig. 10.26 The leaky box model: a sketch

mental data (see below) are not enough to avoid strong correlations between them. The solutions can be obtained in a semi-analytical way or numerically using sophisticated codes (e.g., GALPROP), where three-dimensional distributions of sources and the interactions with the ISM can be included.

Simpler models, like for example "leaky box" models, are used to cope with the main features of the data. In the simplest version the leaky box model consists in a volume (box) where there are sources uniformly distributed and charged cosmic rays freely propagate with some probability of escaping from the walls (see Fig. 10.26). Diffusion and convection effects are incorporated in the escape probability (lifetime). The stationary equation of the leaky box can be written as:

$$0 \simeq C_i - N_i \left(n\beta_i c\sigma_i^{\text{spall}} + \frac{1}{\gamma_i \tau_i^{\text{decay}}} + \frac{1}{\tau_i^{\text{esc}}} \right) + \sum_{j>i} N_j \left(n\beta_j c\sigma_{ji}^{\text{spall}} + \frac{1}{\gamma_j \tau_{ji}^{\text{decay}}} \right) . \tag{10.45}$$

Here once again the first term on the right side accounts for the sources and the second and the third, respectively, for the losses (due to spallation, radioactive decays, and escape probability) and the gains (spallation or decays of heavier elements). In a first approximation, the dependence of the escape time on the energy and the charge of the nucleus can be computed from the diffusion equations, the result being $\tau_i^{\text{esc}} \propto E^{-\delta}/Z_i$. For the values of size and magnetic field typical of the Milky Way, $\delta \sim 0.6$.

All these models are adjusted to the experimental data and in particular to the energy dependence of the ratios of secondary elements (produced by spallation of heavier elements during their propagation) over primary elements (produced directly at the sources) as well as the ratios between unstable and stable isotopes of the same element (see Fig. 10.27). Basically all nuclei heavier than He (at primordial nucleosynthesis only H and He nuclei were present, with a ratio 3:1) are produced by nuclear fusion inside stars, generating energy to support them. Nuclear fusion proceeds up to the formation of nuclei with $A < 60$; stellar nucleosynthesis, while producing carbon, nitrogen and oxygen, does not increase the abundance of light nuclei (lithium, beryllium, and boron). Heavier elements up to iron are only synthe-

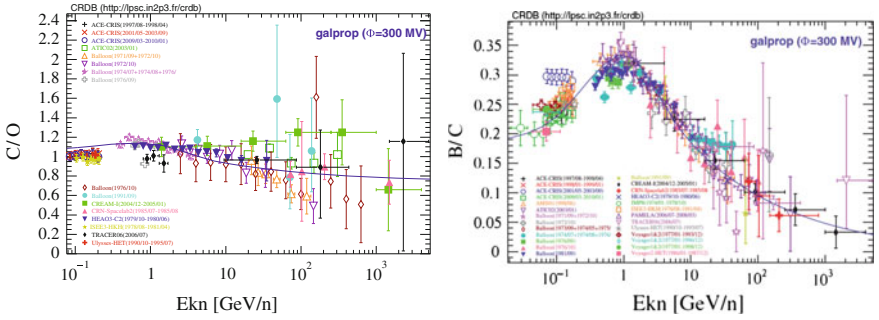

Fig. 10.27 Left: The C/O ratio (primary/primary) as a function of energy. Right: B/C (secondary over primary) as a function of the energy. Data points are taken from the Cosmic Ray database by Maurin et al. (2014) [http://arxiv.org/abs/1302.5525/arXiv:1302.5525]. The full lines are fits using the GALPROP model with standard parameters. Reference: http://galprop.stanford.edu

sized in massive stars with $M > 8M_{\odot}$. Once Fe becomes the primary element in the core of a star, further compression does not ignite nuclear fusion anymore; the star is unable to thermodynamically support its outer envelope and initiates its gravitational collapse and its eventual explosion; nuclei formed during stellar nucleosynthesis are released in the galaxy and can be recycled for the formation of new stars. The secondary abundances are tracers of spallation processes of primary CRs with the ISM. The unstable secondary nuclei that live long enough to be useful probes of CRs propagation are ^{10}Be ($\tau \sim 2.2$ Myr), ^{26}Al ($\tau \sim 1.2$ Myr), ^{36}Cl ($\tau \sim 0.4$ Myr), and ^{54}Mn ($\tau \sim 0.9$ Myr). The most used probe is ^{10}Be which has a lifetime similar to the escape time of 10^7 years from the galaxy and which is produced abundantly in the fragmentation of C, N, and O.

We can further simplify the last equation depending if we are dealing with primary or secondary CR: for primaries we can neglect spallation feed-down (i.e., they are not produced by heavier CR), while for secondaries we can neglect production by sources ($C_i = 0$). For example, let us assume now a primary cosmic nucleus P at speed β and energy E, assumed stable (most nuclei are stable, one exception being Be which is unstable through beta decay). The equation can be written as:

$$\frac{N_P(E)}{\tau^{\rm esc}(E)} \simeq C_P(E) - \frac{\beta c \rho_H N_P(E)}{\lambda_P(E)} \Longrightarrow N_P(E) \simeq \frac{C_P(E)}{1/\tau^{\rm esc}(E) + \beta c \rho_H / \lambda_P(E)}$$

where $\rho_H = n m_H$ is the density of targets and λ_P is the mean free path in g/cm^2.

While $\tau^{\rm esc}$ is the same for all nuclei with same rigidity at the same energy, λ depends on the mass of the nucleus. The equation suggests that at low energies the spectra for different primary nuclei can be very different (e.g. for Fe interaction losses dominate over escape losses), but ratios should be approximately constant at high energies if particles come from the same source.

For high-energy protons with interaction lengths λ_p much larger than the escape length, the equation can be even further simplified to

$$N_p(E) \simeq C_p(E)\tau^{\rm esc}(E)$$

and if $C_p(E) \propto E^{-2}$ (first order Fermi acceleration mechanism) we expect $N_p(E) \propto E^{-2.6}$.

Secondary/primary ratios (Fig. 10.27, right) show a strong energy dependence at high energies as a result of the increase of the escape probability, while primary/primary ratios (Fig. 10.27, left) basically do not depend on energy. By measuring primary/primary and secondary/primary ratios as a function of energy we can infer the propagation and diffusion properties of cosmic rays.

One should note that in the propagation of electrons and positrons the energy losses are much higher (dominated by synchrotron radiation and inverse Compton scattering) and the escape probability much higher. Thus leaky box models do not apply to electrons and positrons. Primary TeV electrons lose half their total energy within a distance smaller than few hundreds parsec from the source.

10.3.3.2 The SNR Paradigm

The energy density of CRs, extrapolated outside the reach of the solar wind (i.e., above 1–2 GeV), is

$$\rho_{\rm CR} = \int dE\ E_k n(E) = 4\pi \int dE\ \frac{E_k}{v}\, I(E) \sim 1\,{\rm eV/cm^3}\,.$$

The luminosity $L_{\rm CR}$ of galactic CR sources must provide this energy density, taking into account a residence time $\tau^{\rm esc} \sim 10^7$ yr of CR in the galactic disk (note that the product of the residence time to the ISM density in the galaxy is constrained by the B/C ratio). With $V_D = \pi R^2 h \sim 4 \times 10^{66}$ cm^3 (for $R = 15$ kpc and $h = 200$ pc) as volume of the galactic disc, the required luminosity is $L_{\rm CR} = V_D \rho_{\rm CR}/\tau^{\rm esc} \sim 6 \times 10^{40}$ erg/s. In a core-collapse SN, the average energy output is $E_{\rm SN} \sim 10^{51}$ erg. Taking into account a rate of a supernova every 30 years, a SNR efficiency $\mathcal{O}(0.01)$ in particle acceleration could explain all galactic cosmic rays.

10.3.3.3 Extragalactic Cosmic Rays: The GZK Cutoff and the Photodisintegration of Nuclei

Extragalactic cosmic rays might cross large distances (tens or hundreds of Mpc) in the Universe. Indeed the Universe is full of CMB photons ($n_\gamma \sim 410$ photons/cm^3—see Chap. 8) with a temperature of $T \sim 2.73$ K ($\sim 2 \times 10^{-4}$ eV). Greisen and Zatsepin, and Kuzmin, realized independently early in 1966 that for high-energy protons the inelastic interaction

$$p\ \gamma_{CMB} \rightarrow \Delta^+ \rightarrow p\ \pi^0\ (n\ \pi^+)$$

is likely leading to a strong decrease of the proton interaction length. The proton threshold energy for the process is called the "GZK cutoff"; its value is given by relativistic kinematics:

$$\left(p_p + p_\gamma\right)^2 = \left(m_p + m_\pi\right)^2 \Longrightarrow E_p = \frac{m_\pi^2 + 2m_p m_\pi}{4\, E_\gamma} \simeq 6 \times 10^{19}\ \text{eV}\ . \quad (10.46)$$

The pion photoproduction cross section, $\sigma_{\gamma p}$, reaches values as large as $\sim$500 μb just above the threshold (with a plateau for higher energies slightly above $\sim$100 μb). The mean free path of the protons above the threshold is thus:

$$\lambda_p \simeq \frac{1}{n_\gamma\, \sigma_{\gamma p}} \simeq 10\ \text{Mpc}\,. \quad (10.47)$$

In each GZK interaction the proton looses on average around 20 % of its initial energy.

A detailed computation of the effect of such cutoff on the energy spectrum of ultrahigh-energy cosmic ray at Earth would involve not only the convolution of the full CMB energy spectrum with the pion photoproduction cross section but also the knowledge of the sources, their location and energy spectrum as well as the exact model of expansion of the Universe (CMB photons are redshifted). An illustration of the energy losses of protons as a function of their propagation distance is shown in Fig. 10.28 without considering the expansion of the Universe. Typically, protons with energies above the GZK threshold energy after 50–100 Mpc loose the memory of their initial energy and end up with energies below the threshold.

The decay of the neutral and charged pions produced in these GZK interactions will originate, respectively, high-energy photons and neutrinos which would be a distinctive signature of such processes.

At a much lower energy ($E_p \sim 2\ 10^{18}$ eV) the conversion of a scattered CMB photon into an electron–positron pair may start to occur, what was associated by Hillas and Berezinsky to the existence of the ankle (this is the so-called "dip model", Sect. 10.4.1).

Heavier nuclei interacting with the CMB and Infrared Background (IRB) photons may disintegrate into lighter nuclei and typically one or two nucleons. The photo-disintegration cross section is high (up to $\sim$100 mb) and is dominated by the Giant Dipole resonance with a threshold which is a function of the nuclei binding energy per nucleon (for Fe the threshold of the photon energy in the nuclei rest frame is $\sim$10 MeV). Stable nuclei thus survive longer. The interaction length of Fe, the most stable nucleus, is, at the GZK energy, similar to the proton GZK interaction length. Lighter nuclei have smaller interaction lengths and thus the probability of interaction during their way to Earth is higher.

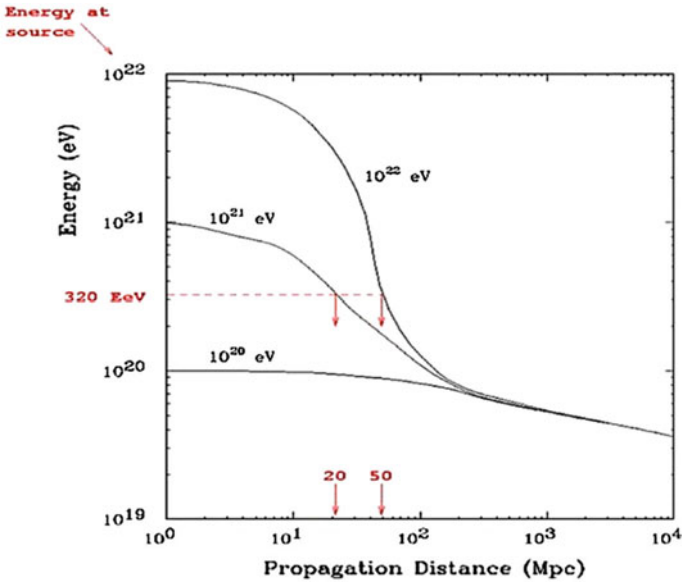

Fig. 10.28 Proton energy as a function of the propagation distance. From J.W. Cronin, Nucl. Phys. B Proc. Suppl. 28B (1992) 213

10.3.4 Propagation of Photons

Once produced, VHE photons must travel towards the observer. Electron–positron ($e^- e^+$) pair production in the interaction of VHE photons off extragalactic background photons is a source of opacity of the Universe to γ rays whenever the corresponding photon mean free path is of the order of the source distance or smaller.

The dominant process for the absorption is pair-creation

$$\gamma + \gamma_{\text{background}} \rightarrow e^+ + e^- ;$$

the process is kinematically allowed for

$$\epsilon > \epsilon_{\text{thr}}(E, \varphi) \equiv \frac{2\, m_e^2\, c^4}{E\,(1 - \cos\varphi)} , \tag{10.48}$$

where φ denotes the scattering angle, m_e is the electron mass, E is the energy of the incident photon and ϵ is the energy of the target (background) photon. Note that E and ϵ change along the line of sight in proportion of $(1 + z)$ because of the cosmic expansion. The corresponding cross section, computed by Breit and Wheeler in 1934, is

$$\sigma_{\gamma\gamma}(E,\epsilon,\varphi) = \frac{2\pi\alpha^2}{3m_e^2} W(\beta) \simeq 1.25 \cdot 10^{-25}\, W(\beta)\,\mathrm{cm}^2\,, \tag{10.49}$$

with

$$W(\beta) = \left(1-\beta^2\right)\left[2\beta\left(\beta^2-2\right) + \left(3-\beta^4\right)\,\ln\left(\frac{1+\beta}{1-\beta}\right)\right].$$

The cross section depends on E, ϵ and φ only through the speed β—in natural units—of the electron and of the positron in the center-of-mass

$$\beta(E,\epsilon,\varphi) \equiv \left[1 - \frac{2\,m_e^2\,c^4}{E\epsilon\,(1-\cos\varphi)}\right]^{1/2}\,, \tag{10.50}$$

and Eq. 10.48 implies that the process is kinematically allowed for $\beta^2 > 0$. The cross section $\sigma_{\gamma\gamma}(E,\epsilon,\varphi)$ reaches its maximum $\sigma_{\gamma\gamma}^{\max} \simeq 1.70 \cdot 10^{-25}\,\mathrm{cm}^2$ for $\beta \simeq 0.70$. Assuming head-on collisions ($\varphi = \pi$), it follows that $\sigma_{\gamma\gamma}(E,\epsilon,\pi)$ gets maximized for the background photon energy

$$\epsilon(E) \simeq \left(\frac{500\,\mathrm{GeV}}{E}\right)\,\mathrm{eV}\,, \tag{10.51}$$

where E and ϵ correspond to the same redshift. For an isotropic background of photons, the cross section is maximized for background photons of energy:

$$\epsilon(E) \simeq \left(\frac{900\,\mathrm{GeV}}{E}\right)\,\mathrm{eV}\,. \tag{10.52}$$

Explicitly, the situation can be summarized as follows:

- For $10\,\mathrm{GeV} \leq E < 10^5\,\mathrm{GeV}$ the EBL plays the leading role in the absorption. In particular, for $E \sim 10\,\mathrm{GeV}$ $\sigma_{\gamma\gamma}(E,\epsilon)$—integrated over an isotropic distribution of background photons—is maximal for $\epsilon \sim 90\,\mathrm{eV}$, corresponding to far-ultraviolet soft photons, whereas for $E \sim 10^5\,\mathrm{GeV}$ $\sigma_{\gamma\gamma}(E,\epsilon)$ is maximal for $\epsilon \sim 9 \cdot 10^{-3}\,\mathrm{eV}$, corresponding to soft photons in the far-infrared.
- For $10^5\,\mathrm{GeV} \leq E < 10^{10}\,\mathrm{GeV}$ the interaction with the CMB becomes dominant.
- For $E \geq 10^{10}\,\mathrm{GeV}$ the main source of opacity of the Universe is the radio background.

The upper x-axis of Fig. 10.24, left, shows the energy of the incoming photon for which the cross section of interaction with a photon of the wavelength as in the lower x-axis is maximum.

From the cross section in Eq. 10.49, neglecting the expansion of the Universe, one can compute a mean free path (Fig. 10.29); for energies smaller than some 10 GeV this is larger than the Hubble radius, but it becomes comparable with the distance of observed sources at energies above 100 GeV.

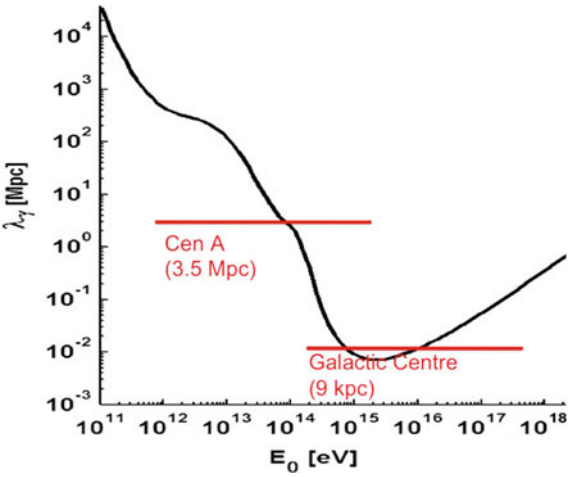

Fig. 10.29 Mean free path as a function of the photon energy, at $z = 0$. Adapted from A. de Angelis, G. Galanti, M. Roncadelli, MNRAS 432 (2013) 3245

The attenuation suffered by observed VHE spectra can thus be used to derive constraints on the EBL density. Specifically, the probability P for a photon of observed energy E to survive absorption along its path from its source at redshift z to the observer plays the role of an attenuation factor for the radiation flux, and it is usually expressed in the form:

$$P = e^{-\tau(E,z)} \,. \tag{10.53}$$

The coefficient $\tau(E, z)$ is called *optical depth*.

To compute the optical depth of a photon as a function of its observed energy E and the redshift z of its emission one has to take into account the fact that the energy E of a photon scales with the redshift z as $(1+z)$; thus when using Eq. 10.49 we must treat the energies as function of z and evolve $\sigma\big(E(z), \epsilon(z), \theta\big)$ for $E(z) = (1+z)E$ and $\epsilon(z) = (1+z)\epsilon$, where E and ϵ are the energies at redshift $z = 0$. The optical depth is then computed by convoluting the photon number density of the background photon field with the cross section between the incident γ ray and the background target photons, and integrating the result over the distance, the scattering angle and the energy of the (redshifted) background photon:

$$\begin{aligned}\tau(E, z) = &\int_0^z dl(z) \int_{-1}^{1} d\cos\theta \frac{1-\cos\theta}{2} \times \\ &\times \int_{\frac{2(m_e c^2)^2}{E(1-\cos\theta)}}^{\infty} d\epsilon(z)\, n_\epsilon\big(\epsilon(z), z\big)\, \sigma(E(z), \epsilon(z), \theta)\end{aligned} \tag{10.54}$$

where θ is the scattering angle, $n_\epsilon\big(\epsilon(z), z\big)$ is the density for photons of energy $\epsilon(z)$ at the redshift z, and $l(z) = c\, dt(z)$ is the distance as a function of the redshift, defined by

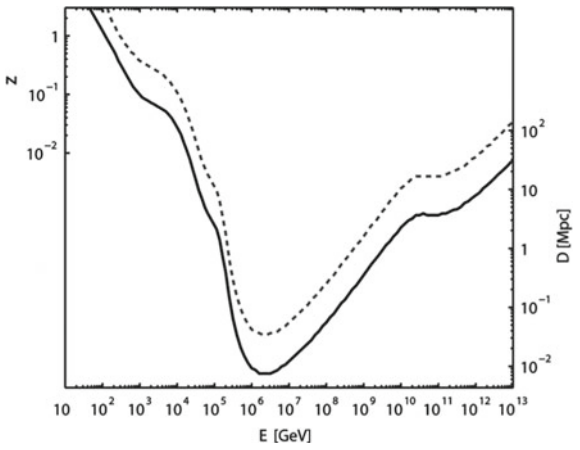

Fig. 10.30 Curves corresponding to the gamma ray horizon $\tau(E, z) = 1$ (lower) and to a survival probability of $e^{-\tau(E,z)} = 1\,\%$ (upper). Adapted from A. de Angelis, G. Galanti, M. Roncadelli, MNRAS 432 (2013) 3245

$$\frac{dl}{dz} = \frac{c}{H_0} \frac{1}{(1+z)\left[(1+z)^2(\Omega_M z + 1) - \Omega_\Lambda z(z+2)\right]^{\frac{1}{2}}} . \tag{10.55}$$

In the last formula (see Chap. 8) H_0 is the Hubble constant, Ω_M is the matter density (in units of the critical density, ρ_c) and Ω_Λ is the "dark energy" density (in units of ρ_c); therefore, since the optical depth depends also on the cosmological parameters, its determination constrains the values of the cosmological parameters if the cosmological emission of galaxies is known.

The energy dependence of τ leads to appreciable modifications of the observed source spectrum (with respect to the spectrum at emission) even for small differences in τ, due to the exponential dependence described in Eq. 10.53. Since the optical depth (and consequently the absorption coefficient) increases with energy, the observed flux results steeper than the emitted one.

The *horizon* or *attenuation edge* for a photon of energy E is defined as the distance corresponding to the redshift z for which $\tau(E, z) = 1$, that gives an attenuation by a factor $1/e$ (see Fig. 10.30).

Other interactions than the one just described might change our picture of the attenuation of γ rays, and they are presently subject of intense studies, since the present data on the absorption of photons show some tension with the pure QED picture: from the observed luminosity of VHE photon sources, the Universe appears to be more transparent to γ rays than expected. One speculative explanation could be that γ rays might transform into sterile or quasi-sterile particles (like, for example, the axions which have been described in Chap. 8); this would increase the transparency by effectively decreasing the path length. A more detailed discussion will be given at the end of this chapter.

Mechanisms in which the absorption is changed through violation of the Lorentz invariance are also under scrutiny; such models are particularly appealing within scenarios inspired by quantum gravity (QG).

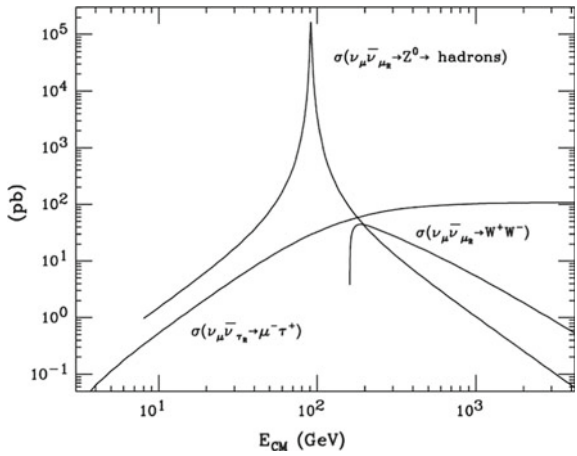

Fig. 10.31 $\nu\nu_c$ inelastic cross section as a function of the interaction center of mass. From D. Fargion and B. Mele, http://arxiv.org/abs/astro-ph/9902024/arXiv:astro-ph/9902024

10.3.5 Propagation of Neutrinos

The neutrino cross section is the lowest among elementary particles. Neutrinos can thus travel with the smallest interaction probability and are the best possible astrophysical probe.

Neutrinos of energies up to 10^{16} eV (which is the largest possible detectable energy, given the hypothesis of fluxes comparable with the photon fluxes, and the maximum size of neutrino detectors, of the order of a cubic kilometer) in practice travel undisturbed to the Earth.

On the other hand extremely high energetic neutrinos, if ever they exist in the Universe, will suffer a GZK-like interaction with the cosmological neutrinos ν_c. Indeed, the $\nu\nu_c$ cross section increases by several orders of magnitude whenever the center-of-mass energy of this interaction is large enough to open the inelastic channels as it is shown in Fig. 10.31. For instance, at $E_\nu \sim 10^{21}(4eV/m_\nu)$ the s-channel $\nu\nu_c \to Z$ is resonant. Thus, the Universe for these neutrinos of extreme energies becomes opaque.

10.3.6 Propagation of Gravitational Waves

Gravitational waves are oscillations of the space–time metrics which, accordingly to general relativity, propagate in the free space with the speed of light in the vacuum. Their coupling with matter and radiation is extremely weak and they propagate without significant attenuation, scattering, or dispersion in their way through the Universe. By energy conservation their amplitude follows a $1/R$ dependence where R is the distance to the source. A very good reference for a detailed discussion is [F10.4]] by K. S. Thorne.

Note that the speed of gravitational waves is not the speed of the gravitational field in the case, e.g., of a planet orbiting around the Sun. The speed of the propagation of the information on physical changes in the gravitational (or electromagnetic) field should not be confused with changes in the behavior of static fields that are due to pure observer effects. The motion of an observer with respect to a static charge and its extended static field does not change the field, which extends to infinity, and does not propagate. Irrespective of the relative motion the field points to the "real" direction of the charge, at all distances from the charge.

10.4 More Experimental Results

10.4.1 Charged Cosmic Rays: Composition, Extreme Energies, Correlation with Sources

Charged cosmic rays arrive close to the solar system after being deflected from the galactic magnetic fields (about 1 μG in intensity) and possibly by extragalactic magnetic fields, if they are of extragalactic origin; when getting closer to the Earth they start interacting with stronger magnetic fields—up to $\mathcal{O}(1\text{G})$ at the Earth's surface, although for shorter distances. Fluxes of charged particles at lower energies, below 1 GeV, can thus be influenced, e.g., by the solar cycle which affects the magnetic field from the Sun.

Cosmic rays are basically protons (∼90 %) and heavier nuclei. The electron/positron flux at the top of the atmosphere is small (a few per mil of the total cosmic ray flux) but extremely interesting as it may be a signature of unknown astrophysical or Dark Matter sources (see Chap. 8). Antiprotons fluxes are even smaller (about four orders of magnitude) and so far compatible with secondary production by hadronic interactions of primary cosmic rays with the interstellar medium. Up to now there is no evidence for the existence of heavier anti-nuclei (in particular anti-deuterium and anti-helium) in cosmic rays.

10.4.1.1 Energy Spectrum

The energy spectrum of charged cosmic rays reaching the atmosphere spans over many decades in flux and energy, as we have seen in the beginning of this Chapter (Fig. 10.1).

At low energies, $E \lesssim 1$ GeV, the fluxes are high (thousands of particles per square meter per second) while there is a strong cutoff at about $10^{19.5}$ eV–at the highest energies ever observed, $E \gtrsim 10^{11}$ GeV, there is less than one particle per square kilometer per century. The cosmic rays at the end of the known spectrum have energies well above the highest beam energies attained in any human-made accelerator and their interactions on the top of the Earth atmosphere have center-of-

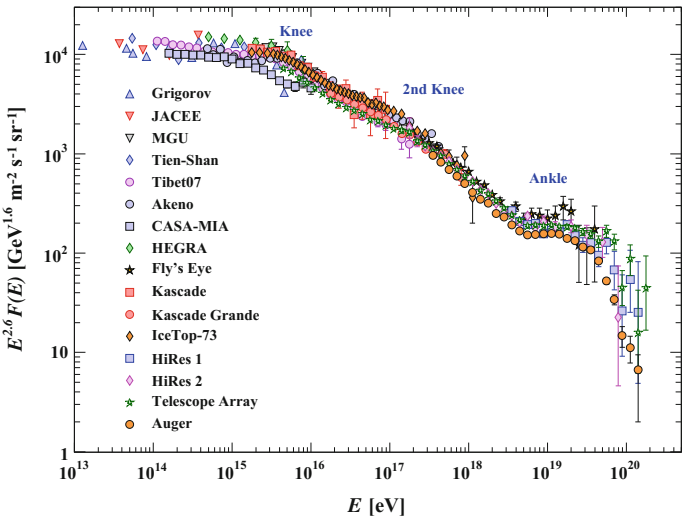

Fig. 10.32 Cosmic-ray spectrum coming from experimental measurements by different experiments; the spectrum has been multiplied by $E^{+2.6}$. The anthropomorphic interpretation should be evident. From Beatty, Matthews, and Wakely, "Cosmic Rays", in Review of Particle Physics, 2018

mass energies of a few hundred TeV (the design LHC beam energy is $E = 7 \times 10^3$ GeV); at these energies, however, the flux of cosmic rays is highly suppressed. This fact affects the choice of experiments to detect cosmic rays: one can study the energies up to the knee with satellites, while above the knee one must rely on ground-based detectors. Above a few GeV the intensity of the cosmic rays flux follows basically a power law,

$$I(E) \propto E^{-\gamma}$$

with the differential spectral index γ being typically between 2.7 and 3.3. Below a few GeV, the flux is modulated by the solar activity and in particular by the magnetic field from the Sun–notice that these effects are variable in time.

The small changes in the spectral index can be clearly visualized multiplying the flux by some power of the energy. Figure 10.32 shows a suggestive anthropomorphic representation of the cosmic ray energy spectrum obtained multiplying the flux by $E^{+2.6}$. Two clear features corresponding to changes in the spectral index are observed. The first, called the knee, occurs around $E \simeq 5 \times 10^{15}$ eV, and it is sometimes associated to the transition from galactic to extragalactic cosmic rays; it corresponds to a steepening from a spectral index of about 2.7 to a spectral index of about 3.1. The second clear feature, denominated the "ankle," occurs around $E \simeq 5 \times 10^{18}$ eV and its nature is still controversial. Another feature, called the second knee, marks a steepening to from about 3.1 to about 3.3, at an energy of about 400 PeV.

The number of primary nucleons per GeV from about 10 GeV to beyond 100 TeV is approximately

$$\frac{dN}{dE} \simeq 1.8 \times 10^4 E^{-2.7} \frac{\text{nucleons}}{\text{m}^2\,\text{s}\,\text{sr}\,\text{GeV}} \tag{10.56}$$

where E is the energy per nucleon in GeV.

A strong suppression at the highest energies, $E \simeq 5 \times 10^{19}$ eV, is nowadays clearly established (Fig. 10.32); it may result, as explained in Sect. 10.3.3.3, from the so-called GZK mechanism due to the interaction of highly energetic protons with the Cosmic Microwave Background (CMB). However, a scenario in which an important part of the effect is a change of composition (from protons to heavier nuclei, which undergo nuclear photodisintegration[6]) and the exhaustion of the sources is not excluded as it will be discussed in Sect. 10.4.1.6.

10.4.1.2 Composition

The composition and energy spectrum of cosmic rays is not a well-defined problem: it depends on where experiments are performed. One could try a schematic separation between "primary" cosmic rays—as produced by astrophysical sources—and "secondaries"—those produced in interactions of the primaries with interstellar gas or with nuclei in the Earth's atmosphere. Lithium, beryllium and boron, for example, are very rare products in stellar nucleosynthesis, and thus are secondary particles, as well as antiprotons and positrons—if some antimatter is primary is a question of primary interest.

The interaction with the Earth's atmosphere is particularly important since it changes drastically the composition of cosmic rays. In the cases in which the flux of cosmic rays has to be measured at ground (for example, high-energy cosmic rays, at energies above hundreds GeV, where the low flux makes the use of satellites ineffective) one needs nontrivial unfolding operations to understand the primary composition. What one observes is a cascade shower generated by a particle interacting with the atmosphere, and the unfolding of the fundamental properties (nature and energy of the showering particle) requires the knowledge of the physics of the interaction at energies never studied at accelerators: experimental data are thus less clear.

Accessing the composition of cosmic rays can be done, in the region below a few TeV, at the top or above the Earth atmosphere by detectors placed in balloons or satellites able, for example, of combining the momentum measurement with the information from Cherenkov detectors, or transition radiation detectors.

The absolute and relative fluxes of the main hadronic components of cosmic rays measured directly is shown in Fig. 10.33, and compared to the relative abundances existing in the solar system. To understand this figure, one should take into account

[6] In the case of nuclei, the spallation cross section is enhanced due to the giant dipole resonance, a collective excitation of nucleons in nuclei due to the interaction with photons. For all nuclei but iron the corresponding mean free paths are, at these energies, much smaller than the proton GZK mean free path.

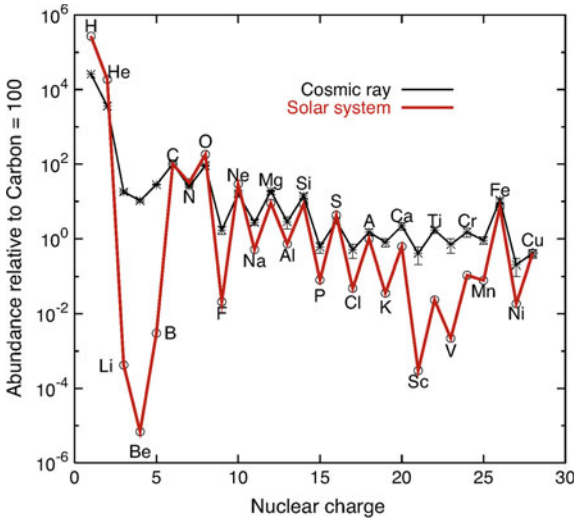

Fig. 10.33 Relative abundance of the main nuclear species present in galactic cosmic rays and in the solar system. Both are normalized to the abundance of C= 100, and the relevant energy range is a few hundred MeV/nucleon. From J.A. Aguilar, lectures at the Université Libre Bruxelles, 2016

the fact that nuclei with even number of nucleons are more stable, having higher binding energy because of pairing effects.

Besides a clear deficit of hydrogen and helium in the cosmic rays compared to the composition of the solar system, the main features from this comparison are the agreement on the "peaks" (more tightly bounded even-Z nuclei) and higher abundances for cosmic rays on the "valleys." These features can be explained within a scenario where primary cosmic rays are produced in stellar end-products, being the "valley" elements mainly secondaries produced in the interaction of the primaries cosmic rays with the interstellar medium ("spallation").

Direct composition measurements are not possible above a few hundred GeV. For extensive air shower (EAS, see Chap. 4) detectors, effective at higher energies, being able to distinguish between a shower generated by a proton or by a heavier particle is a more difficult task. Variables which may allow the disentangling between protons and heavier nuclei, as it will be discussed in Sect. 10.4.1.6, are: in ground sampling detectors, the muonic contents of the air shower; at high energies in shower detectors, the depth of the maximum of the shower (the so-called $X_{\max}$). A summary plot including these higher energy is shown in Fig. 10.34.

There is experimental evidence that the chemical composition of cosmic rays changes after the knee region with an increasing fraction of heavy nuclei at higher energy, at least up to about 10^{18} eV (see Sect. 10.4.1.6).

10.4.1.3 Electrons and Positrons

High-energy electrons and positrons have short propagation distances (less than a few hundred parsec, as seen before) as they lose energy through synchrotron and

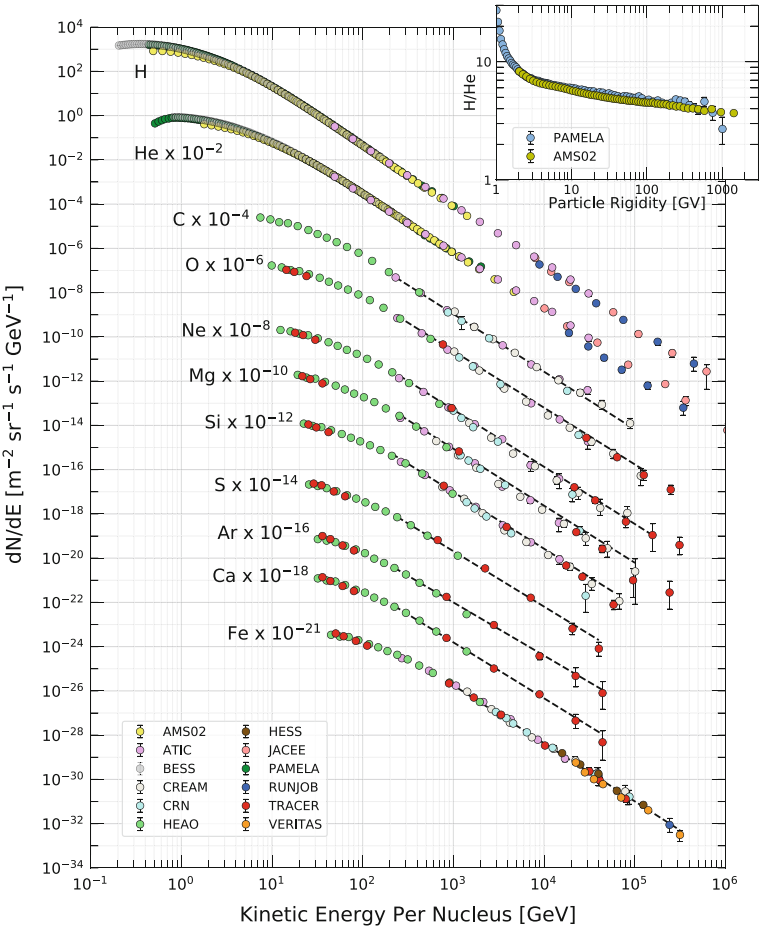

Fig. 10.34 Fluxes of nuclei of the primary cosmic radiation in particles per energy-per-nucleus plotted versus energy-per-nucleus. The inset shows the H/He ratio at constant rigidity. From Beatty, Matthews, and Wakely, "Cosmic Rays", in Review of Particle Physics, 2018

inverse Compton processes while propagating through the galaxy. Their spectra, which extend up to several TeV, are therefore expected to be dominated by local electron accelerators or by the decay/interactions of heavier particles nearby. Positrons in particular could be the signature of the decay of dark matter particles.

The experimental data on the flux of electrons plus positrons suggested in a recent past the possible evidence a bump-like structure (ATIC balloon experiment results) at energies between 250 and 700 GeV. These early results were not confirmed by later and more accurate instruments like the *Fermi* satellite Large Area Tracker (*Fermi*-LAT), AMS-02 and DAMPE, as it is shown in Fig. 10.35. However, either in the individual flux of positrons or in its fraction with respect to the total flux of electrons

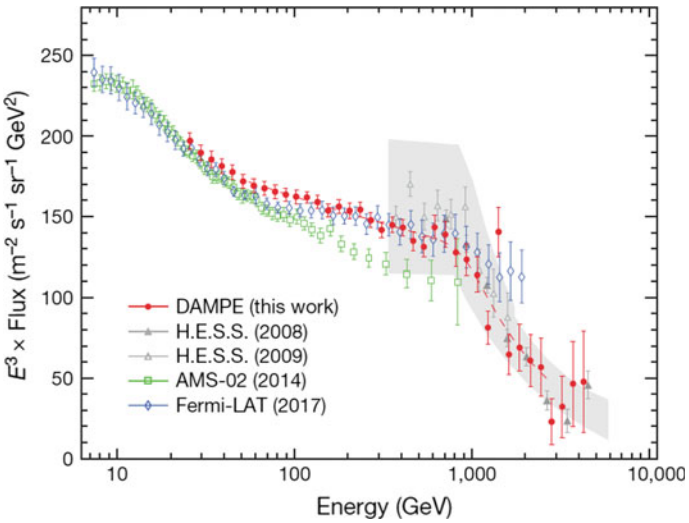

Fig. 10.35 Energy spectrum of e^+ plus e^-, multiplied by E^3. The dashed line represents a smoothly broken power-law model that best fits the DAMPE data in the range from 55 GeV to 2.63 TeV. The grey band represents the systematic error from HESS. From DAMPE Collaboration, Nature 2017, doi:10.1038/nature24475

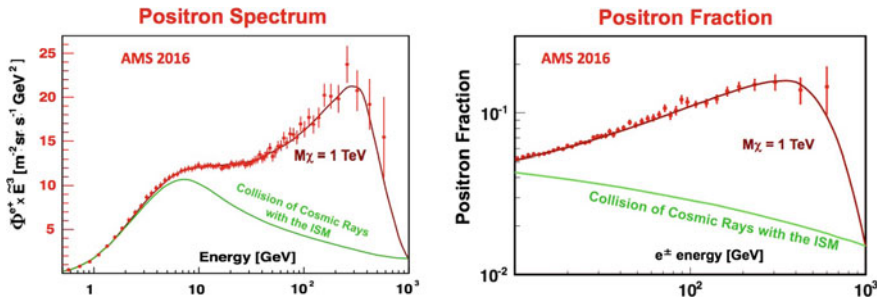

Fig. 10.36 Left: Energy spectrum of e^+ (multiplied by E^3) from AMS-02. Right: positron fraction in high-energy cosmic rays of the flux of positrons with respect to the total flux of electrons plus positrons measured from AMS-02

plus positrons (Fig. 10.36), an excess in the high-energy positron fraction with respect to what expected from known sources (basically the interactions of cosmic rays with the interstellar medium), first observed by PAMELA and thus called the PAMELA effect, was clearly confirmed by AMS-02.

This is indeed quite intriguing: in a matter-dominated Universe, one would expect this ratio to decrease with energy, unless specific sources of positrons are present nearby. If these sources are heavy particles decaying into final states involving positrons, one could expect the ratio to increase, and then steeply drop after reaching half of the mass of the decaying particle. If an astrophysical source of high-energy

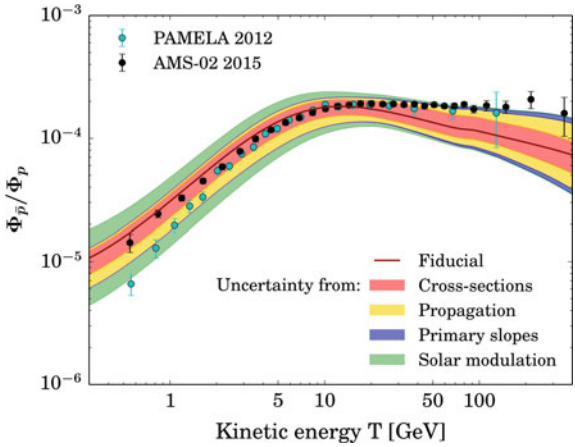

Fig. 10.37 Antiproton to proton ratio measured by AMS-02 and PAMELA. From G. Giesen et al., JCAP 1509 (2015) 023

positrons is present, a smooth spectrum is expected, while in the case of the origin from DM, a steep fall comes from kinematics. The present data is compatible both with the presence of nearby astrophysical sources, though not fully known, and with a hypothetical dark-matter particle with a mass of around 1 TeV, but there is not a definite answer yet. The most recent data on the abundance of high-energy pulsars nearby might justify an astrophysical explanation of this excess but not the results in antiproton observed also by AMS-02 as discussed in the next section.

10.4.1.4 Antiprotons

Data are shown in Fig. 10.37. The antiproton to proton ratio stays constant from 20 to 400 GeV. This behavior cannot be explained by secondary production of antiprotons from ordinary cosmic ray collisions. In contrast with the excess of positrons, the excess of antiprotons cannot be easily explained from pulsar origin. More study is needed, and this is certainly one of the next frontiers.

10.4.1.5 Cosmic Rays at the Earth's Surface: Muons

Most charged particles on the top of the atmosphere are protons; however, the interaction with the atoms of the atmosphere itself has the effect that the nature of particles reaching ground does not respect the composition of cosmic rays. Secondary muons, photons, electrons/positrons and neutrinos are produced by the interaction of charged cosmic rays in air, in addition to less stable particles. Note that the neutron/proton ratio changes dramatically in such a way that neutrons, which are 10 % of the total at the atmosphere's surface, become roughly 1/3 at the Earth's surface.

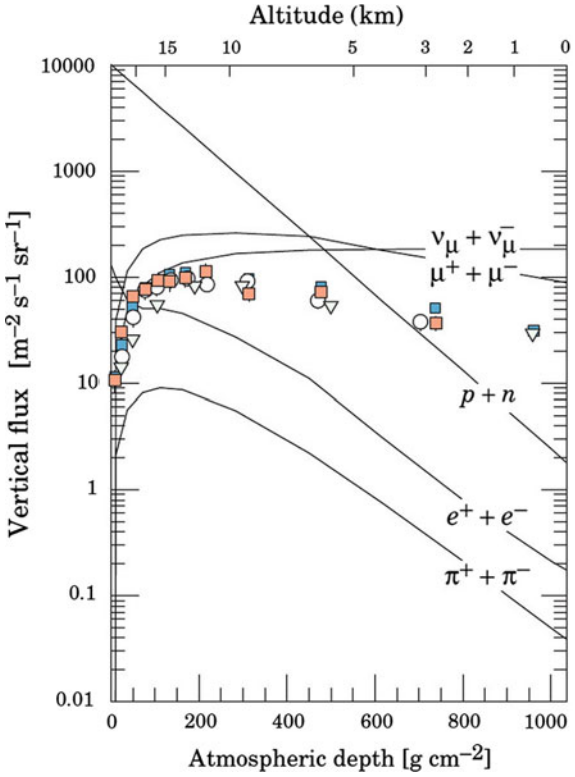

Fig. 10.38 Fluxes of cosmic rays with $E > 1$ GeV in the atmosphere as a function of height (simulation). The points show experimental measurements of negative muons. From K.A. Olive et al. (Particle Data Group), Chin. Phys. C 38 (2014) 090001

Astrophysical muons can hardly reach the Earth's atmosphere due to their lifetime ($\tau \sim 2\,\mu$s); this lifetime is however large enough, that secondary muons produced in the atmosphere can reach the Earth's surface, offering a wonderful example of time dilation: the space crossed on average by such particles is $L \simeq c\gamma\tau$, and already for $\gamma \sim 50$ (i.e., an energy of about 5 GeV) they can travel 20, 30 km, which roughly corresponds to the atmospheric depth. Muons lose some 2 GeV by ionization when crossing the atmosphere.

Charged particles at sea level are mostly muons (see Fig. 10.38), with a mean energy of about 4 GeV.

The flux of muons from above 1 GeV at sea level is about 60 m^{-2}s^{-1}sr^{-1}. A detector looking at the horizon sees roughly one muon per square centimeter per minute. The zenith angular distribution for muons of $E \sim 3$ GeV is $\propto \cos^2\theta$, being steeper at lower energies and flatter at higher energies: low energy muons at large angles decay before reaching the surface. The ratio between μ^+ and μ^- is due to the fact that there are more π^+ than π^- in the proton-initiated showers; there are about 30 % more μ^+ than μ^- at momenta above 1 GeV/c.

A fortiori, among known particles only muons and neutrinos reach significant depths underground. The muon flux reaches $10^{-2}\,\mathrm{m}^{-2}\,\mathrm{s}^{-1}\,\mathrm{sr}^{-1}$ under 1 km of water equivalent (corresponding to about 400 m of average rock) and becomes about $10^{-8}\,\mathrm{m}^{-2}\,\mathrm{s}^{-1}\,\mathrm{sr}^{-1}$ at 10 km of water equivalent.

10.4.1.6 Ultrahigh-Energy Cosmic Rays

Ultra-High-Energy Cosmic Rays (UHECR) are messengers from the extreme Universe and a unique opportunity to study particle physics at energies well above those reachable at the LHC. However, their limited flux and their indirect detection have not yet allowed to answer to the basic, and always present, questions: Where are they coming from? What is their nature? How do they interact?

The energy spectrum of the UHECR is nowadays well measured up to 10^{20}eV (see Fig. 10.39). The strong GZK-like suppression at the highest energies may be interpreted assuming different CR composition and source scenarios. Indeed, both pure proton and mixed composition scenarios are able to describe the observed features. In the case of a pure proton scenario, the ankle would be described by the opening, at that energy, of the pair production channel in the interaction of the incoming protons with the CMB photons ($p\,\gamma_{CMB} \rightarrow p\,e^+e^-$) (this is called the "dip model"), while the suppression at the highest energies would be described in terms of the predicted GZK effect. In the case of mixed composition scenarios such features may be described by playing with different source distributions and injection spectra, assuming that the maximum energy that each nucleus may attain, scales with its atomic number Z. An example of composition fit is given in Fig. 10.39, where

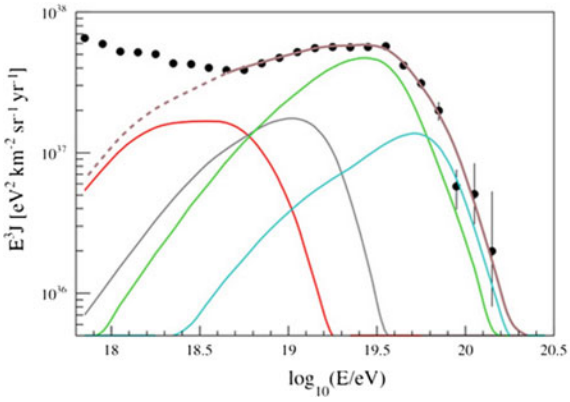

Fig. 10.39 UHECR Energy spectrum measured by the Pierre Auger Observatory (closed circles); the spectrum has been multiplied by E^3. Superposed is a fit to the sum of different components at the top of the atmosphere. The partial spectra are grouped as according to the mass number as follows: Hydrogen (red), Helium-like (grey), Carbon, Nitrogen, Oxygen (green), Iron-like (cyan), total (brown). Image credit: Pierre Auger Collaboration

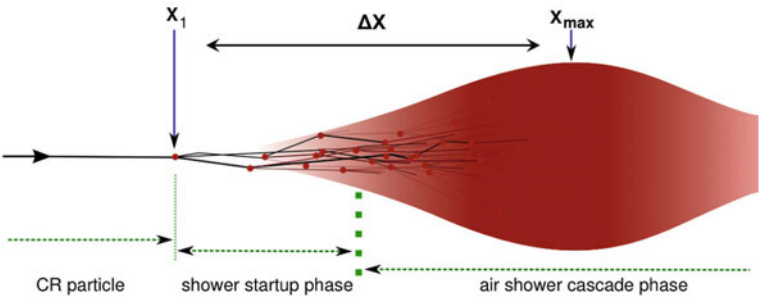

Fig. 10.40 Shower development scheme. Adapted from the Ph.D. thesis of R. Ulrich: "Measurement of the proton–air cross section using hybrid data of the Pierre Auger Observatory," http://bibliothek.fzk.de/zb/berichte/FZKA7389.pdf

the Pierre Auger Observatory data are fitted to a mixed composition scenario. The solution of such puzzle may only be found with the experimental determination of the cosmic ray composition from detailed studies on the observed characteristics of the extensive air showers.

The depth of the maximum number of particles in the shower, $X_{\max}$, schematically represented in Fig. 10.40), is sensitive to the cross-section of the primary cosmic ray interaction in the air. Thus it can be used either to measure the cross-section, if the composition is known, or, since the cross section for a nucleus grows with its atomic number, to determine the composition, if the nuclei-air interaction cross-sections at these energies are assumed to be described correctly by the model extrapolations of the cross-sections measured at lower energies from the accelerators. Indeed, $X_{\max}$ may be defined as the sum of the depth of the first interaction X_1 and a shower development length ΔX (see Fig. 10.40):

$$X_{\max} = X_1 + \Delta X \,.$$

The experimental $X_{\max}$ distribution is then the convolution of the X_1 distribution with the ΔX distribution (which has a shape similar to the $X_{\max}$ distribution) and a detector resolution function (see Fig. 10.41). The distribution of X_1, in the case of a single component composition, should be just a negative exponential, $\exp\left(-X_1/\Lambda_\eta\right)$, where Λ_η is the interaction length which is proportional to the inverse of the cosmic ray–air interaction cross section. Thus, the tail of the observed $X_{\max}$ distribution reflects the X_1 exponential distribution of the lighter cosmic ray component (smaller cross-section, deeper penetration).

The measured $X_{\max}$ distribution by the Pierre Auger collaboration in the energy bin 10^{18}–$10^{18.5}$eV for the 20 % of the most deeply penetrating showers is shown in Fig. 10.42. It follows the foreseen shape with a clear exponential tail. The selection of the most deeply penetrating showers strongly enhances the proton contents in the data sample since the proton penetrate deeply in the atmosphere than any other nuclei.

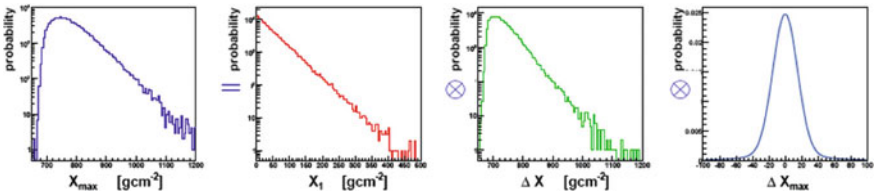

Fig. 10.41 Ingredients of the experimental $X_{\max}$ distribution. Adapted from the Ph.D. thesis of R. Ulrich: "Measurement of the proton–air cross section using hybrid data of the Pierre Auger Observatory," http://bibliothek.fzk.de/zb/berichte/FZKA7389.pdf

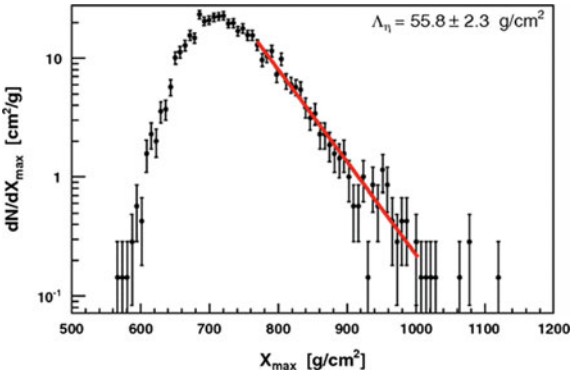

Fig. 10.42 $X_{\max}$ distribution expressed in g/cm^2 measured by the Pierre Auger Observatory in the energy interval 10^{18}–$10^{18.5}$eV. The line represents the likelihood fit performed to extract Λ_η. From P. Abreu et al., Phys. Rev. Lett. 109 (2012) 062002

The conversion of the exponential index of the distribution tail to a value of proton-air cross section is performed using detailed Monte Carlo simulations. The conversion to proton–proton total and inelastic cross section is then done using the Glauber model which takes into account the multi-scattering probability inside the nuclei (Sect. 6.4.7). The Auger result is shown in Fig. 10.43 together with accelerator data–namely with the recent LHC results, as well as with the expected extrapolations of several phenomenological models. The experimental results confirm the evolution of the proton–proton cross section as a function of the energy observed so far, and give a strong indication that the fraction of protons in the cosmic ray "beam" is important at least up to 10^{18} eV.

The study of the first two momenta of the $X_{\max}$ distribution ($\langle X_{\max} \rangle$ and the RMS) is nowadays the main tool to constrain hadronic interactions models and hopefully access the cosmic ray composition. The mean and the RMS of the $X_{\max}$ distributions measured by the Pierre Auger collaboration as a function of the energy are shown in Fig. 10.44 and compared to the prediction for pure p, He, N and Fe. A fit to extract the fractions of each of these components as a function of the energy was then performed assuming several different hadronic interaction models. The results indicate evidence of a change of the cosmic ray composition from light elements (with a large fraction of protons) at lower energies to heavier elements (He or N depending on the hadronic model) but a negligible abundance of Fe at least until $10^{19.4}$ eV. However, none of the current simulation models fits perfectly the data.

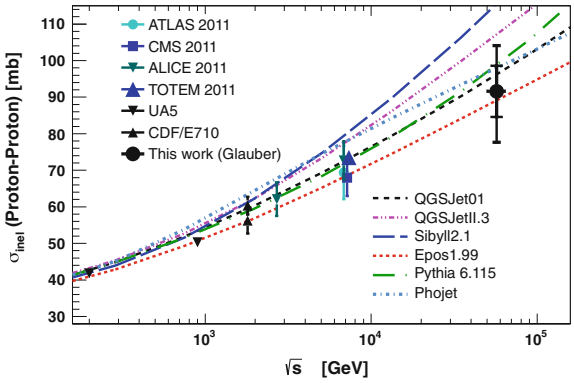

Fig. 10.43 Comparison of the inelastic proton–proton cross section derived by the Pierre Auger Observatory in the energy interval 10^{18}–$10^{18.5}$ eV to phenomenological model predictions and results from accelerator experiments at lower energies. From P. Abreu et al., Phys. Rev. Lett. 109 (2012) 062002

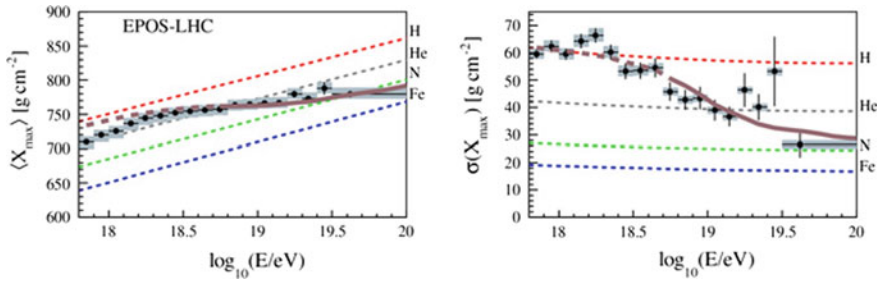

Fig. 10.44 Energy evolution of the mean (Left:) and the RMS (Right:) of the $X_{\max}$ distribution measured by the Pierre Auger Observatory. The lines from top to bottom represent the expectations for pure proton, helium, nitrogen and iron from a simulation model tuned at the LHC energies. Credit: Auger Collaboration

Only qualitative and quantitative improvements in the understanding of the shower development, for example, accessing direct experimental information on the muon contents and improving the modelling of hadronic interactions in Monte Carlo simulations, may clarify this striking open question. The scenario in which the strong GZK-like suppression at the highest energies is due to the exhaustion of the sources and that the higher number of muons in the shower are due to bad modelling of the hadronic interactions is nowadays the most widely accepted. "New physics" scenarios providing, for instance, a sudden increase of the proton-proton cross section (related to the access of a new scale of interaction below the parton scale) are however not excluded.

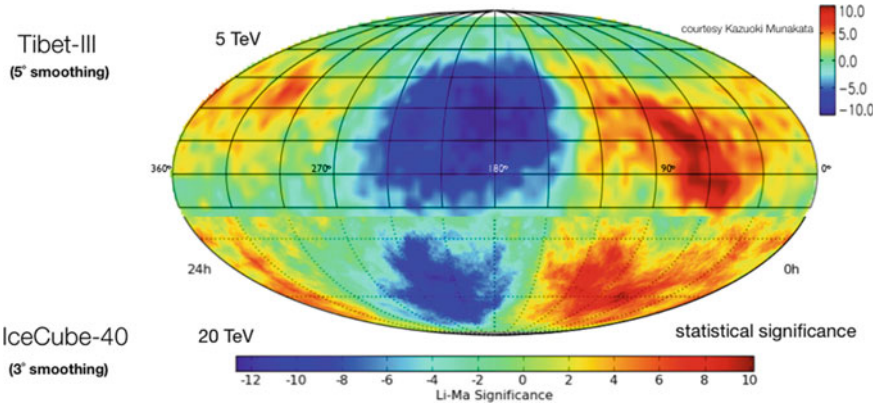

Fig. 10.45 Skymap in equatorial coordinates showing the relative intensity of multi-TeV cosmic rays arrival directions: the northern hemisphere data is from Tibet-III Air Shower Array, Amenomori M. et al., Science 314, 439, 2006, (map courtesy of Kazuoki Munakata); the southern hemisphere data is from the IceCube-40 string configuration from http://icecube.wisc.edu/~desiati/activity/anisotropy/large

10.4.1.7 Correlation of Charged Cosmic Rays with Sources

When integrating over all energies, say, above a few GeV, the arrival direction of charged cosmic rays is basically isotropic—a fact which can find explanation in the effect of the Galactic magnetic field smearing the directions–the Compton-Getting effect, a dipole anisotropy of about 0.6% resulting from the proper motion of Earth in the rest frame of cosmic ray sources, has to be subtracted. However, Milagro, IceCube, HAWC, ARGO-YBJ and the Tibet air shower array have observed additional small large-scale anisotropies (at the level of 10^{-3}), and small small-scale anisotropies (at the level of about $10^{-4}-10^{-5}$) in an energy range from a few tens of GeV to a few hundreds of TeV (see Fig. 10.45). Its origin is still under debate; the disentangling of its probable multiple causes is not easy. There is no simple correlation of anisotropies with known astrophysical objects.

At extremely high energies, instead, statistically significant anisotropies have been found – and their interpretation is straightforward.

To accelerate particles up to the ultra-high-energy region above the EeV, 10^{18} eV, one needs conditions that are present in astrophysical objects such as the surroundings of SMBHs in AGN, or transient high-energy events such as the ones generating gamma ray bursts. Galactic objects are not likely to be acceleration sites for particles of such energy, and coherently we do not observe a concentration of UHECRs in the galactic plane; in addition, the galactic magnetic field cannot confine UHECRs above 10^{18} eV within our Galaxy.

Under the commonly accepted assumptions of a finite horizon (due to a GZK-like interaction) and of extragalactic magnetic fields in the range (1 nG–1 fG), the number of sources is relatively small and thus some degree of anisotropy could be

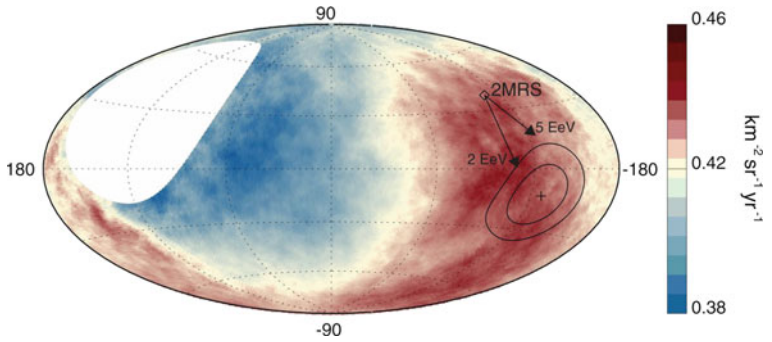

Fig. 10.46 Sky map in galactic coordinates showing the cosmic-ray flux for $E > 8$ EeV. The cross indicates the measured dipole direction; the contours denote the 68 and 95% confidence level regions. The dipole in the 2MRS galaxy distribution is indicated. Arrows show the deflections expected due to the galactic magnetic field on particles with $E/Z = 5$ and 2 EeV. Image credit: Pierre Auger collaboration

found studying the arrival directions of the cosmic rays at the highest energies. Such searches have been performed extensively in the last years either by looking for correlations with catalogs of known astrophysical objects or by applying sophisticated self-correlation algorithms at all angular scales. Indication for intermediate-scale anisotropy, namely correlated to Active Galactic Nuclei and Star-forming or Starburst Galaxies catalogs, have been reported by the Pierre Auger Observatory. At large scales,

- In about 30 000 cosmic rays with energies above 8 EeV recorded over a period of 12 years, corresponding to a total exposure of 76 800 km^2 sr year, the Pierre Auger Observatory has evidenced at more than 5.2σ a dipole anisotropy of about 6.5% towards $(\ell, b) \simeq (233°, -13°)$ (see Fig. 10.46).
  If ultrahigh-energy cosmic rays originate from an inhomogeneous distribution of sources and then diffuse through intergalactic magnetic fields, one can expect dipole amplitudes growing with energy, reaching 5–20% at 10 EeV. If the sources were distributed like galaxies, the distribution of which has a significant dipolar component, a dipolar cosmic-ray anisotropy would be expected in a direction similar to that of the dipole associated with the galaxies. For the infrared-detected galaxies in the 2MRS catalog,[7] the flux-weighted dipole points in galactic coordinates in the direction $(\ell, b) \simeq (251°, 38°)$, about 55° away from the dipole direction found by Auger. However, as shown in Fig. 10.46, the effect of galactic magnetic fields is to get the two directions closer; in addition, the correlation between the visible flux and the cosmic ray flux is just qualitative.
  The conclusion is that the anisotropy seen by Auger strongly supports, and prob-

[7] The 2MASS Redshift Survey (2MRS) maps the distribution of galaxies out to a redshift of $z \simeq 0.03$ (about 115 Mpc).

ably demonstrates, the hypothesis of an extragalactic origin for large part of the highest-energy cosmic rays; the origin is in particular related to AGN.
- In 2007 the Pierre Auger collaboration claimed with a significance larger than 3σ a hot spot near the Centaurus A AGN, at a distance of about 5 Mpc. Cen A is also a VHE gamma-ray emitter. However, the data collected after 2007 have not increased the significance of the detection.
- the Telescope Array Project observes at energies above 57 EeV a hot spot, with best circle radius: 25°, near the region of the Ursa Major constellation.

10.4.2 Photons: Different Source Types, Transients, Fundamental Physics

High-energy astrophysical processes generate photon radiation over a large range of wavelengths. Such photon radiation can be easily associated to the emitters, which is an advantage with respect to charged cosmic rays. In addition, photon radiation, besides being interesting per itself, can give insights on the acceleration of charged particles, being photons secondary products of accelerated charged particles. In addition, they are likely to be present in the decay chain of unstable massive particles, or in the annihilation of pairs of particles like dark matter particles.

The experimental data on the diffuse cosmic photon radiation span some 30 energy decades; a compilation of the data is shown in Fig. 10.2. A bump is visible corresponding to the CMB, while the general behavior of the yield of gamma rays at high energies can be approximated by an energy dependence as a power law $E^{-2.4}$ (Fig. 10.47). A cutoff at energies close to 1 TeV might be explained by the absorption of higher energy photons by background photons near the visible populating the intergalactic medium—through creation of e^+e^- pairs.

There is little doubt on the existence of the so-called ultra- and extremely-high-energy photons (respectively in the PeV-EeV and in the EeV-ZeV range), but so far cosmic gamma rays have been unambiguously detected only in the low (MeV), high (GeV) and very high-energy (TeV) domains. The behavior above some 30 TeV is extrapolated from data at lower energies and constrained by experimental upper limits.

In Chap. 4 we have defined as high energy (HE) the photons above 30 MeV—i.e., the threshold for the production of e^+e^- pairs plus some phase space; as very high energy (VHE) the photons above 30 GeV. The HE—and VHE in particular—regions are especially important related to the physics of cosmic rays and to fundamental physics. One of the possible sources of HE gamma rays is indeed the generation as a secondary product in conventional scenarios of acceleration of charged particles; in this case cosmic gamma rays are a probe into cosmic accelerators. The VHE domain is sensitive to energy scales important for particle physics. One is the 100 GeV – 1 TeV scale expected for cold dark matter and for the lightest supersymmetric particles. A second scale is the scale of possible superheavy particles, at $\sim 10^{20}$ eV. Finally, it

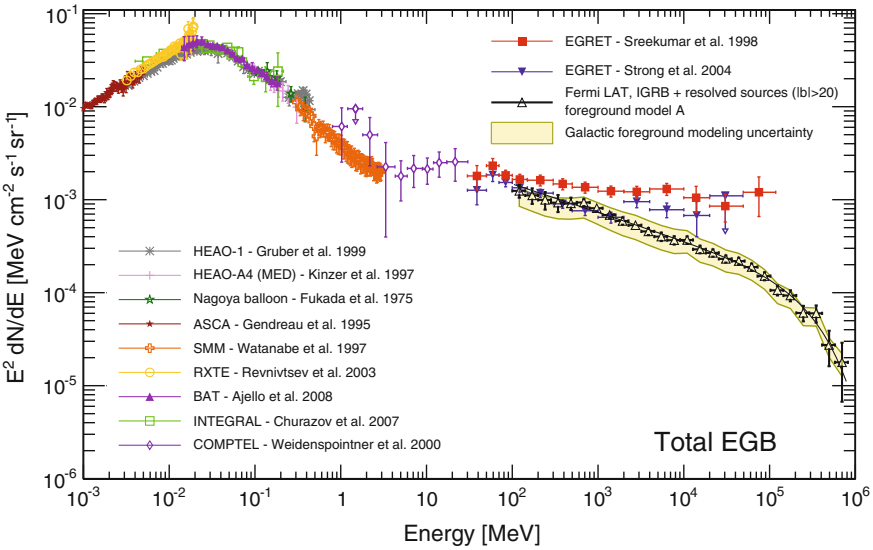

Fig. 10.47 Spectrum of the total extragalactic gamma ray emission measured by the *Fermi*-LAT. From M. Ackermann et al., The Astrophysical Journal 799 (2015) 86

might be possible to access the GUT scale and the Planck scale, at energies $\sim 10^{24}$ eV – $\sim 10^{19}$ GeV. This last scale corresponds to a mass $\sqrt{\hbar c/G}$—which is, apart from factors of order 1, the mass of a black hole whose Schwarzschild radius equals its Compton wavelength.

Gamma rays provide at present the best window into the nonthermal Universe, being the "hottest" thermalized processes observed up to now in the accretion region of supermassive black holes at a temperature scale of the order of 10 keV, in the X-ray region. Tests of fundamental physics with gamma rays are much beyond the reach of terrestrial accelerators.

Besides the interest for fundamental physics, the astrophysical interest of HE and VHE photons is evident: for some sources such as the AGN—supermassive black holes in the center of galaxies, powered by infalling matter—the total power emitted above 100 MeV dominates the electromagnetic dissipation.

10.4.2.1 Hunting Different Sources and Source Types

The study of the galactic sources continues and their morphology and the SED of the emitted photons are telling us more and more, also in the context of multiwavelength analyses; in the future, the planned Cherenkov Telescope Array (CTA) will give the possibility to explore the highest energies, and to contribute, together with high-energy CR detectors and possibly with neutrino detectors, to the final solution of the CR problem.

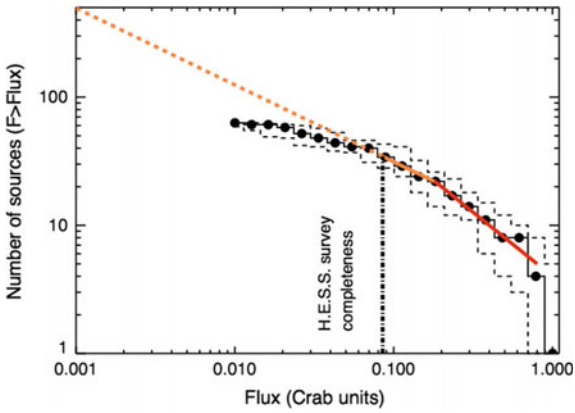

Fig. 10.48 "($\log N - \log S$)" diagram of the VHE galactic sources. From M. Renaud, http://arxiv.org/abs/0905.1287

One of the main results from the next-generation detectors will probably be the discovery of new classes of CR sources. The key probably comes from dedicating effort to surveys, which constitute an unbiased, systematic exploratory approach. Surveys of different extents and depths are amongst the scientific goals of all major planned facilities.

The key for such surveys are today gamma detectors (and in the future neutrino detectors as well).

More than half of the known VHE gamma-ray sources are located in the Galactic plane. Galactic plane surveys are well suited to Cherenkov telescopes given the limited area to cover, as well as their low-energy thresholds and relatively good angular resolution (better than 0.1° to be compared to ∼1° for EAS detectors). CTA, investing 250 h (3 months) of observation, can achieve a 3 mCrab sensitivity (being the flux limit on a single pointing roughly proportional to $1/\sqrt{t_{obs}}$, where t_{obs} is the observation time) on the galactic plane. More than 300 sources are expected at a sensitivity based on an extrapolation of the current "($\log N - \log S$)" diagram[8] for VHE galactic sources (Fig. 10.48).

All-sky VHE surveys are well suited to EAS arrays that observe the whole sky with high duty cycles and large field of view. MILAGRO and the Tibet air shower arrays have carried out a survey for sources in the Northern hemisphere down to an average sensitivity of 600 mCrab above 1 TeV; HAWC has a sensitivity of 50 mCrab in a year, at median energy around 1 TeV. EAS detectors like HAWC can then "guide" the CTA. A combination of CTA and the EAS can reach sensitivities better than 30 mCrab in large parts of the extragalactic sky. The survey could be correlated with maps obtained by UHE cosmic ray and high-energy neutrino experiments.

Roughly, 5500 HE emitters above 100 MeV have been identified up to now, mostly by the *Fermi*-LAT, and some 200 of them are VHE emitters as well (Fig. 10.3).

[8]The number of sources as a function of flux "($\log N - \log S$)" is an important tool for describing and investigating the statistical properties of various types of source populations. It is defined as the cumulative distribution of the number of sources brighter than a given flux density S, and it is based on some regularity properties like homogeneity and isotropy.

About half of the gamma ray emitters are objects in our galaxy; at TeV energies most of them can be associated to different kinds of supernova remnants (SNR), while at MeV to GeV energies they are mostly pulsars; the remaining half are extragalactic, and the space resolution of present detectors (slightly better than 0.1°) is not good enough to associate them with particular points in the host galaxies; we believe, however, that they are produced in the vicinity of supermassive black holes in the centers of the galaxies (see Sect. 10.2 and 10.4.1.7).

The strongest steady emitters are galactic objects; this can be explained by the fact that, being closer, they suffer a smaller attenuation. The observed strongest steady emitter at VHE is the Crab Nebula. The energy distribution of the photons from Crab Nebula is typical for gamma sources (see the explanation of the "double-hump" structure in Sect. 10.1.2.1), and it is shown in Fig. 10.13.

10.4.2.2 Transient Phenomena and Gamma Ray Bursts; Quasiperiodical Emissions

Among cosmic rays, gamma rays are important not only because they point to the sources, but also because the sensitivity of present instruments is such that transient events (in jargon, "transients") can be recorded. Sources of HE and VHE gamma rays (some of which might likely be also sources of charged cosmic rays, neutrinos and other radiation) were indeed discovered to exhibit transient phenomena, with timescales from few seconds to few days.

The sky exhibits in particular transient events from steady emitters ("flares") and burst of gamma rays from previously dark regions ("gamma ray bursts"). The phenomenology of such events is described in the rest of this section.

Short timescale variability has been observed in the gamma emission at high energies for several astrophysical objects, both galactic and extragalactic, in particular binary systems, and AGN. For binary systems the variability is quasiperiodical and can be related to the orbital motion, while for AGN it must be related to some cataclysmic events; this is the phenomenon of flares. Flares observed from Crab Nebula have, as today, no universally accepted interpretation.

Flares. Flares are characteristic mostly of extragalactic emitters (AGN). Among galactic emitters, the Crab Nebula, which was for longtime used as a "standard candle" in gamma astrophysics, has been recently discovered to be subject to dramatic flares on timescales of ∼10 h. The transient emission briefly dominates the flux from this object with a diameter of 10 light-years—which is the diameter of the shell including the pulsar remnant of the imploded star, and corresponds to roughly 0.1° as seen from Earth.

Very short timescale emission from blazars have also been observed in the TeV band, the most prominent being at present the flare from the AGN PKS 2155-304 shown in Fig. 10.49: a flux increase by a factor larger than ten with respect to the quiescent state, with variability on timescales close to 1 min. Note that the Schwarzschild radius of the black hole powering PKS2155 is about 10^4 light seconds (correspond-

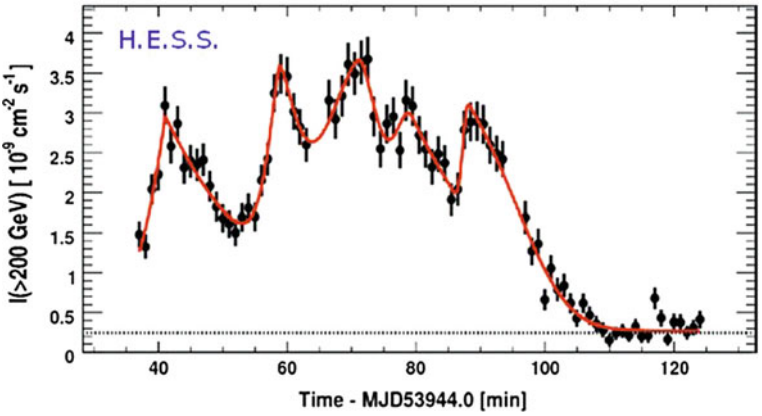

Fig. 10.49 Variability in the very-high-energy emission of the blazar PKS 2155-304. The dotted horizontal line indicates the flux from the Crab Nebula (from the H.E.S.S. experiment, http://www.mpi-hd.mpg.de/hfm/HESS

ing to 10^9 solar masses), which has implications on the mechanisms of emission of gamma rays (see later).

Indeed the gamma ray sky looks like a movie rather than a picture, the most astonishing phenomenon being the explosion of gamma ray bursts.

Gamma Ray Bursts. Gamma Ray Bursts (GRBs) are extremely intense and fast shots of gamma radiation. They last from fractions of a second to a few seconds and sometimes up to a thousand seconds, often followed by "afterglows" orders of magnitude less energetic than the primary emission after minutes, hours, or even days. GRBs are detected once per day on average, typically in X-rays and soft gamma rays. They are named GRByymmdd after the date on which they were detected: the first two numbers after "GRB" correspond to the last two digits of the year, the second two numbers to the month, and the last two numbers to the day. A progressive letter ("A," "B," ...) might be added—it is mandatory if more than one GRB was discovered in the same day, and it became customary after 2010.

Their position appears random in the sky (Fig. 10.50), which suggests that they are of extragalactic origin. A few of them per year have energy fluxes and energies large enough that the *Fermi*-LAT can detect them (photons of the order of few tens of GeV have been detected in a few of them). Also in this case the sources appear to be isotropic.

The energy spectrum is nonthermal and varies from event to event, peaking at around a few hundred keV and extending up to several GeV. It can be roughly fitted by phenomenological function (a smoothly broken power law) called "Band spectrum" (from the name of David Band who proposed it). The change of spectral slope from a typical slope of -1 to a typical slope of -2 occurs at a break energy E_b which, for the majority of observed bursts, is in the range between 0.1 and 1 MeV. Sometimes HE photons are emitted in the afterglows.

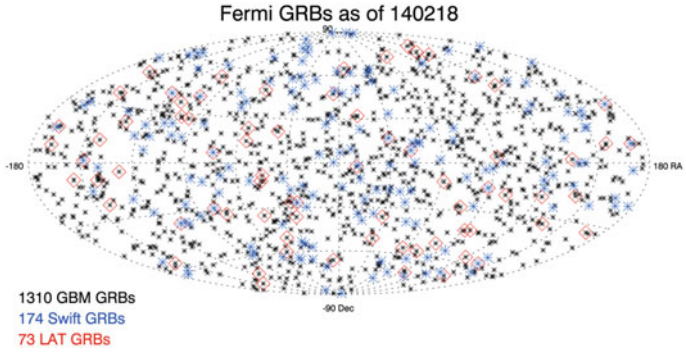

Fig. 10.50 Skymap of the GRBs located by the GRB monitor of *Fermi* and by the *Fermi*-LAT. Some events also seen by the Swift satellite are also shown. Credit: NASA

During fractions of seconds, their energy emission in the gamma ray band exceeds in some cases the energy flux of the rest of the Universe in the same band. The time integrated fluxes range from about 10^{-7} to about 10^{-4} erg/cm^2. If the emission were isotropic, the energy output would on average amount to a solar rest-mass energy, about 10^{54} erg; however, if the mechanism is similar to the one in AGN the emission should be beamed,[9] with a typical jet opening angle of a few degrees. Thus the actual average energy yield in γ rays should be $\sim 10^{51}$ erg. This value can be larger than the energy content of a typical supernova explosion, of which only 1 % emerges as visible photons (over a time span of thousands of years).

The distribution of their duration is bimodal (Fig. 10.18), and allows a first phenomenological classification between "short" GRBs (lasting typically 0.3 s; duration is usually defined as the time T90 during which 90 % of the photons are detected) and "long" GRBs (lasting more than 2 s, and typically 40 s). Short GRBs are on average harder than long GRBs.

GRBs are generally very far away, typically at $z \sim 1$ and beyond (Fig. 10.51). The farthest event ever detected is a 10-s long GRB at $z \simeq 8.2$, called GRB090423, observed by the Swift satellite (the burst alert monitor of Swift being sensitive to energies up to 0.35 MeV).

Short GRBs have been associated to the merging of pairs of compact objects. For long GRBs in several cases the emission has been associated with a formation of a supernova, presumably of very high mass (a "hypernova"). Possible mechanisms for GRBs will be discussed in Sect. 10.2.4.

[9] Nuclear regions of AGN produce sometimes two opposite collimated jets, with a fast outflow of matter and energy from close to the disc. The direction of the jet is determined by the rotational axis of the accreting structure. The resolution of astronomical instruments is in general too poor, especially at high energies, to resolve jet morphology in gamma rays, and as a consequence observations cannot provide explanations for the mechanism yet. The limited experimental information available comes from the radio waveband, where very-long-baseline interferometry can image at sub-parsec scales the emission of synchrotron radiation near the black hole—but radiation should be present from the radio through to the gamma ray range.

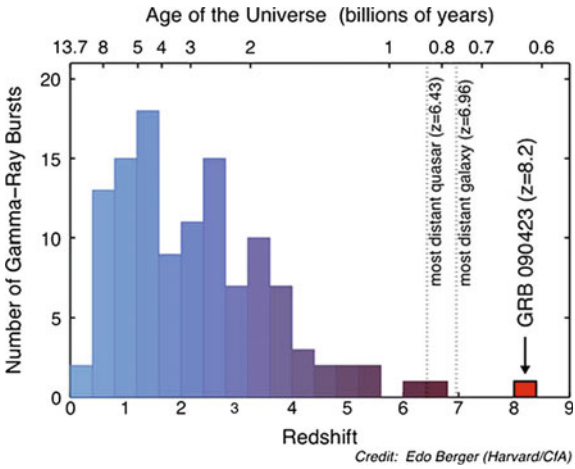

Fig. 10.51 Distribution of redshifts and corresponding age of the Universe for gamma ray bursts detected by NASA's Swift satellite. Credit: Edo Berger (Harvard), 2009

Binary Systems. Binary stars (i.e., pairs of stars bound by gravitational interaction) are frequent in the Universe: most solar-size and larger stars reside in binaries. Binary systems in which one object is compact (a pulsar, a neutron star, or a black hole) have been observed to be periodical emitters of gamma radiation.

Finally, binary systems in which one object is compact (a pulsar, a neutron star, or a black hole) have been observed to be periodical emitters of gamma radiation.

A particular class of binary systems are microquasars, binary systems comprising a black hole, which exhibit relativistic jets (they are morphologically similar to the AGN). In quasars, the accreting object is a supermassive (millions to several billions of solar masses) BH; in microquasars, the mass of the compact object is only a few solar masses.

10.4.2.3 Diffuse Regions of Photon Emission; the *Fermi* Bubbles

As the space resolution of the *Fermi*-LAT and of the Cherenkov telescopes are of the order of 0.1°, we can image diffuse structure only in the Milky Way: the other galaxies will mostly appear like a point. Morphology studies at VHE are basically limited to structures within our Galaxy.

Morphology of SNR is in particular one of the keys to understand physics in the vicinity of matter at high density—and one of the tools to understand the mechanism of acceleration of cosmic rays. Sometimes SNRs and the surrounding regions are too large to be imaged by Cherenkov telescopes, which typically have fields of view of 3°–4°. A large field of view is also essential to understand the nature of primary accelerators in pulsar wind nebulae (PWN), as discussed in Sect. 10.2.1.3: it would be important to estimate the energy spectrum as a function of the angular distance to the center of the pulsar to separate the hadronic acceleration from the leptonic

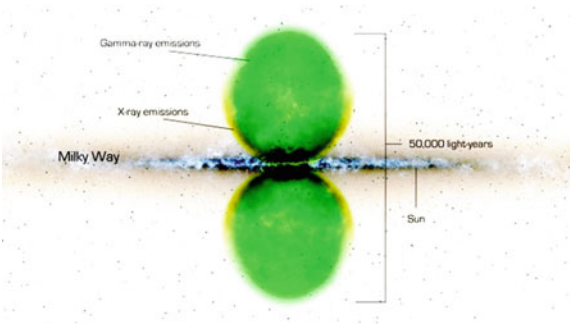

Fig. 10.52 The *Fermi* bubbles (smoothed). Credit: NASA

acceleration. The highest energy electrons lose energy quickly as they propagate away from the source; this is not true for protons.

Intermediate emission structures, a few degrees in radius, have been observed by MILAGRO and ARGO, which can be attributed to diffusion of protons within the interstellar medium.

A surprising discovery by *Fermi*-LAT was the existence of a giant structure emitting photons in our galaxy, with size comparable to the size of the galaxy itself: the so-called *Fermi* bubbles. These two structures, about 50 000-light-years across (Fig. 10.52), have quite sharp boundaries and emit rather uniformly in space with an energy spectrum peaking at a few GeV but yielding sizable amount of energy still up to 20 GeV.

Although the parts of the bubbles closest to the Galactic plane shine in microwaves as well as gamma rays, about two-thirds of the way out the microwave emission fades and only X- and gamma rays are detectable.

Possible explanations of such a large structure are related to the past activity of the black hole in the center of the Milky Way. A large-scale structure of the magnetic field in the bubble region might indicate an origin from the center of the galaxy, where magnetic fields are of the order of 100 μG, and might also explain the mechanism of emission as synchrotron radiation from trapped electrons. However, this explanation is highly speculative, and as of today the reason for the emission is unknown.

10.4.2.4 Results on WIMPs

WIMPs are mostly searched in final states of their pair annihilation or decay involving antimatter and gamma rays. We shall refer in the following, unless explicitly specified, to a scenario in which secondary particles are produced in the annihilation of pairs of WIMPs.

Dark matter particles annihilating or decaying in the halo of the Milky Way could produce an excess of antimatter, and thus, an observable flux of cosmic positrons and/or antiprotons. This could explain the so-called PAMELA anomaly, i.e., the excess of positron with respect to models just accounting for secondary production

(Fig. 10.36). Most DM annihilation or decay models can naturally reproduce the observed rise of the positron fraction with energy, up to the mass of the DM candidate (or half the mass, depending if the self-annihilation or the decay hypothesis is chosen). This flux is expected not to be directional. The measured antiproton flux also shows unexpected features with respect to the hypothesis of pure secondary production.

It is plausible that both the positron excess and the excess observed in the electron/positron yield with respect to current models (see Sect. 10.4.1) can be explained by the presence of nearby sources, in particular pulsars, which have indeed been copiously found by the *Fermi*-LAT (Sect. 10.2.1.1). AMS-02 is steadily increasing the energy range over which positrons and electrons are measured, as well as the statistics. If the positron excess is originated from a few nearby pulsars, it would probably give an anisotropy in the arrival direction of cosmic rays at the highest energies—there is a tradeoff here between distance and energy, since synchrotron losses are important; in addition, the energy spectrum should drop smoothly at the highest energies. A sharp cutoff in the positron fraction would instead be the signature of a DM origin of the positron excess; the present data do not demonstrate such a scenario, but they cannot exclude it, either: the attenuation of the positron/electron ratio observed by AMS-02 at several hundred GeV is consistent with the production from a particle at the TeV scale.

For what concerns photons, the expected flux from dark matter annihilation can be expressed as

$$\frac{dN}{dE} = \frac{1}{4\pi} \underbrace{\frac{\langle \sigma_{\text{ann}} v \rangle}{2m_{DM}^2} \frac{dN_\gamma}{dE}}_{\text{Particle Physics}} \times \underbrace{\int_{\Delta\Omega - l.o.s.} dl(\Omega) \rho_{DM}^2}_{\text{Astrophysics}} . \tag{10.57}$$

The astrophysical factor, proportional to the square of the density, is also called the "boost factor". DM-induced gamma rays could present sharp spectral signatures, like for instance $\gamma\gamma$ or $Z\gamma$ annihilation lines, with energies strictly related to the WIMP mass. However, since the WIMP is electrically neutral, these processes are loop suppressed and therefore should be rare. WIMP-induced gamma rays are thus expected to be dominated by a relatively featureless continuum of by-products of cascades and decays (mostly from π^0) following the annihilation in pairs of quarks or leptons. The number of resulting gamma rays depends quadratically on the DM density along the line of sight of the observer. This motivates search on targets, where one expects DM density enhancements. Among these targets are the galactic center, galaxy clusters, and nearby dwarf spheroidal galaxies. Of course, an additional proof is given by proximity, to reduce the $1/d^2$ attenuation.

Unfortunately, as said before, dark matter densities are not known in the innermost regions of galaxies, where most of the signal should come from: data allow only the computation in the halos, and models helping in the extrapolation to the centers frequently disagree (Sect. 8.1.4). Observations of galaxy rotation curves favor constant density cores in the halos; unresolved "cusp" substructures can have a very large impact, but their existence is speculative—however, since they exist for baryonic

matter, they are also likely to exist for DM. This uncertainty is typically expressed by the so-called "boost factor," defined as the ratio of the true, unknown, line-of-sight integral to the one obtained when assuming a smooth component without substructure.

As a consequence of all uncertainties described above, the choice of targets is somehow related to guesses, driven by the knowledge of locations where one expects large ratios of gravitating to luminous mass. Remembering Chap. 8, the main targets are:

- *Galactic center.* The GC is expected to be the brightest source of dark matter annihilation. However, the many astrophysical sources of gamma rays in that region complicate the identification of DM. In the GeV region the situation is further complicated by the presence of a highly structured and extremely bright diffuse gamma ray background arising from the interaction of the pool of cosmic rays with dense molecular material in the inner galaxy. Finally, there is a huge uncertainty on the boost factor. To limit problems, searches for dark matter annihilation/decay are usually performed in regions 0.3°–1° away form the central black hole.
  At TeV energies, Cherenkov telescopes detected a point source compatible with the position of the supermassive black hole in the center of our galaxy and a diffuse emission coinciding with molecular material in the galactic ridge. The GC source has a featureless power law spectrum at TeV energies with an exponential cutoff at ∼10 TeV not indicating a dark matter scenario; the signal is usually attributed to the supermassive black hole Sgr A* or a to pulsar wind nebula in that region.
  Searches have been performed for a signal from the galactic dark matter halo close to the core; no signal has been found.
  There have been several claims of a signal in the Galactic center region. An extended signal coinciding with the center of the Milky Way, corresponding to a WIMP of mass about 40 GeV/c^2 was reported above the galactic diffuse emission—however, the interaction of freshly produced cosmic rays with interstellar material is a likely explanation. The second claimed signal was the indication of a photon line at ∼130 GeV in regions of interest around the GC, but this has not been confirmed.
- *Dwarf Spheroidal Galaxies.* Dwarf spheroidal galaxies (dSph) are a clean environment to search for dark matter annihilation: astrophysical backgrounds that produce gamma rays are expected to be negligible. The DM content can be determined from stellar dynamics and these objects have been found to be the ones with the largest mass-to-light ratios in the Universe, and uncertainties on the boost factor are within one order of magnitude. Some three-four dozens of dwarf satellite galaxies of the Milky Way are currently known and they are observed both by ground-based and by satellite-based gamma detectors. No signal has been found, and stringent limits have been calculated. In particular, a combined ("stacked") analysis of all known dwarf satellites with the *Fermi*-LAT satellite has allowed a limit to be set below the canonical thermal relic production cross section of $3 \times 10^{-26}\text{cm}^3\text{s}^{-1}$ for a range of WIMP masses (around 10 GeV) in the case of

the annihilation into $b\bar{b}$ (the $b\bar{b}$ is used as a template due to the result obtained in Sect. 8.4.2).

- *Galaxy clusters.* Galaxy clusters are groups of hundreds to thousands galaxies bound by gravity. Galaxy clusters nearby (10–100 Mpc) include the Virgo, Fornax, Hercules, and Coma clusters. A very large aggregation known as the Great Attractor, is massive enough to locally modify the trajectories in the expansion of the Universe.
  Galaxy clusters are much more distant than dwarf spheroidal galaxies or any of the other targets generally used for dark matter searches with gamma rays; however, like dwarf spheroidals, astrophysical dynamics shows that they are likely to be dark matter dominated—and if DM exists, one of the largest accumulators. The range of likely boost factors due to unresolved dark matter substructure can be large; however, when making conservative assumptions, the sensitivity to DM is several orders of magnitude away from the canonical thermal relic interaction rate.
- *Line Searches.* The annihilation of WIMP pairs into γX would lead to monochromatic gamma rays with $E_\gamma = m_\chi(1 - m_X^2/4m_\chi^2)$. Such a signal would provide a smoking gun since astrophysical sources could very hardly produce it, in particular if such a signal is found in several locations. This process is expected to be loop suppressed being possible only at $\mathcal{O}(\alpha^2)$.

A summary of the present results from searches in the photon channel is plotted in Fig. 10.53 together with extrapolation to the first three years of data collection by the next generation detector CTA, and with a collection of 10 years of data by *Fermi* (to be reached in 2019). Note that the *Fermi* discovery potential continues to extend linearly with time, being its background negligible.

Neutrinos. Equation (10.57) holds for neutrinos as well, but the branching fractions into neutrinos are expected to be smaller, due to the fact that the radiative production of neutrinos is negligible. In addition, experimental detection is more difficult. However, the backgrounds are smaller with respect to the photon case.

Balancing the pros and the cons, gamma rays are the best investigation tool in case the emission comes from a region transparent to photons. However, neutrinos are the best tool in case DM is concentrated in the center of massive objects, the Sun for example, which are opaque to gamma rays. Once gravitationally captured by such massive objects, DM particles lose energy in the interaction with nuclei and then settle into the core, where their densities and annihilation rates can be greatly enhanced; only neutrinos (and axions) can escape these dense objects. The centers of massive objects are among the places to look for a possible neutrino excess from DM annihilation using neutrino telescopes.

No signal has been detected up to now (as in the case of axions from the Sun). A reliable prediction of the sensitivity is difficult, depending on many uncertain parameters like the annihilation cross section, the decay modes and the capture rate. The first two uncertainties are common to the photon channels.

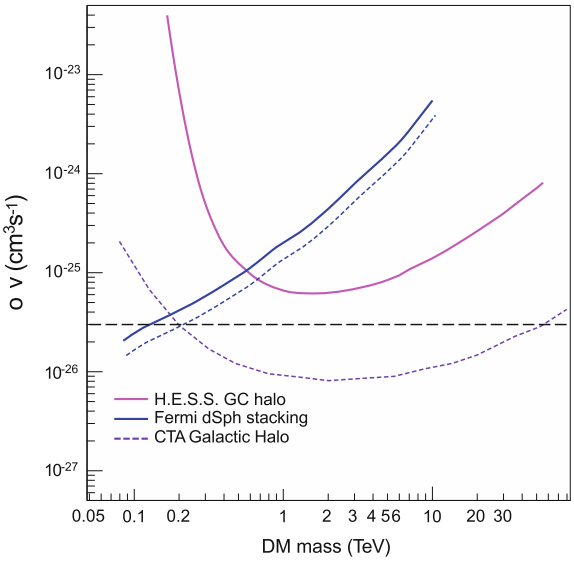

Fig. 10.53 Comparison of the sensitivities in terms of $< \sigma v >$ from the observation of the Milky Way galactic halo (present results from H.E.S.S., continuous line, and expected results from three years of operation of CTA South, dotted line), and from a stacked sample of dwarf spheroidal galaxies (*Fermi*-LAT). The *Fermi*-LAT lines are relative to 6 years of data analysis (continuous, upper line; this is the present result) and to an extrapolation to 10 years of analyzed data (dotted, lower). The sensitivity curves have been calculated assuming decays into an appropriate mixture $b\bar{b}$ and W^+W^- pairs, and the Einasto dark matter profile. The horizontal dashed line indicates the thermal velocity-averaged cross-section. From "Science with the CTA", September 2018, and from *Fermi*-LAT publications

10.4.2.5 Lorentz Symmetry Violation

Variable gamma-ray sources in the VHE region, and in particular AGN, can provide information about possible violations of the Lorentz invariance in the form of a dispersion relation for light expected, for example, in some quantum gravity (QG) models.

Lorentz invariance violation (LIV) at the n-th order in energy can be heuristically incorporated in a perturbation to the relativistic Hamiltonian:

$$E^2 \simeq m^2c^4 + p^2c^2 \left[1 - \xi_n \left(\frac{pc}{E_{\mathrm{LIV,n}}}\right)^n\right], \tag{10.58}$$

which implies that the speed of light ($m = 0$) could have an energy dependence. From the expression $v = \partial E/\partial p$, the modified dispersion relation of photons can be expressed by the leading term of the Taylor series as an energy-dependent light speed

$$v(E) = \frac{\partial E}{\partial p} \simeq c\left[1 - \xi_n \frac{n+1}{2}\left(\frac{E}{E_{\mathrm{LIV,n}}}\right)^n\right], \tag{10.59}$$

where n = 1 or n = 2 corresponds to linear or quadratic energy dependence, and $\xi_n = \pm 1$ is the sign of the LIV correction. If $\xi_n = +1$ ($\xi_n = -1$), high-energy photons travel in vacuum slower (faster) than low-energy photons.

The scale E_{LIV} at which the physics of space–time is expected to break down, requiring modifications or the creation of a new paradigm to avoid singularity problems, is referred to as the "QG energy scale", and is expected to be of the order of the Planck scale—an energy $E_P = M_P c^2 \simeq 1.2 \times 10^{19}$ GeV—or maybe lower, if new particles are discovered at an intermediate scale.

Because of the spectral dispersion, two GRB photons emitted simultaneously by the source would arrive on Earth with a time delay (Δt) if they have different energies. With the magnification of the cosmological distances of the GRBs and the high energies of these photons, the time delay (Δt) caused by the effect of Lorentz invariance violation could be measurable. Taking account of the cosmological expansion and using Eq. 10.59, we write the formula of the time delay as:

$$\Delta t = t_h - t_l = \xi_n \frac{1+n}{2H_0} \frac{E_h^n - E_l^n}{E_{LIV,n}^n} \int_0^z \frac{(1+z')^n dz'}{\sqrt{\Omega_m (1+z')^3 + \Omega_\Lambda}}. \tag{10.60}$$

Here, t_h is the arrival time of the high-energy photon, and t_l is the arrival time of the low-energy photon, with E_h and E_l being the photon energies measured at Earth.

For small z, and at first order,

$$t(E) \simeq d/c(E) \simeq \frac{z c_0}{H_0 c(E)} \simeq z T_H \left(1 - \xi_1 \frac{E}{E_P}\right)$$

where $T_H = 1/H_0 \simeq 5 \times 10^{17}$ s is Hubble's time.

AGN flares (Sect. 10.4.2.2) can be used as experimental tools: they are fast and photons arriving to us travel for long distances.

Mkn 501 (z = 0.034) had a spectacular flare between May and July 2005; it could be analyzed by the MAGIC telescope. The MAGIC data showed a negative correlation between the arrival time of photons and their energy (Fig. 10.54), yielding, if one assumes that the delay is due to linear QG effects, to an evaluation of $E_{\mathrm{LIV}} \sim 0.03\, E_P$. H.E.S.S. observations of the flare in PKS 2155 (Fig. 10.49), however, evidenced no effect, allowing to set a lower limit $E_{\mathrm{LIV}} > 0.04\, E_P$.

Lately, several GRBs observed by the *Fermi* satellite have been used to set more stringent limits. A problem, when setting limits, is that one does not know if photon emission at the source is ordered in energy; thus one has to make hypotheses—for example, that QG effects can only increase the intrinsic dispersion.

The *Fermi* satellite derived strong upper limits at 95 % C.L. from the total degree of dispersion, in the data of four GRBs:

$$E_{\mathrm{LIV},1} > 7.6 E_P\,.$$

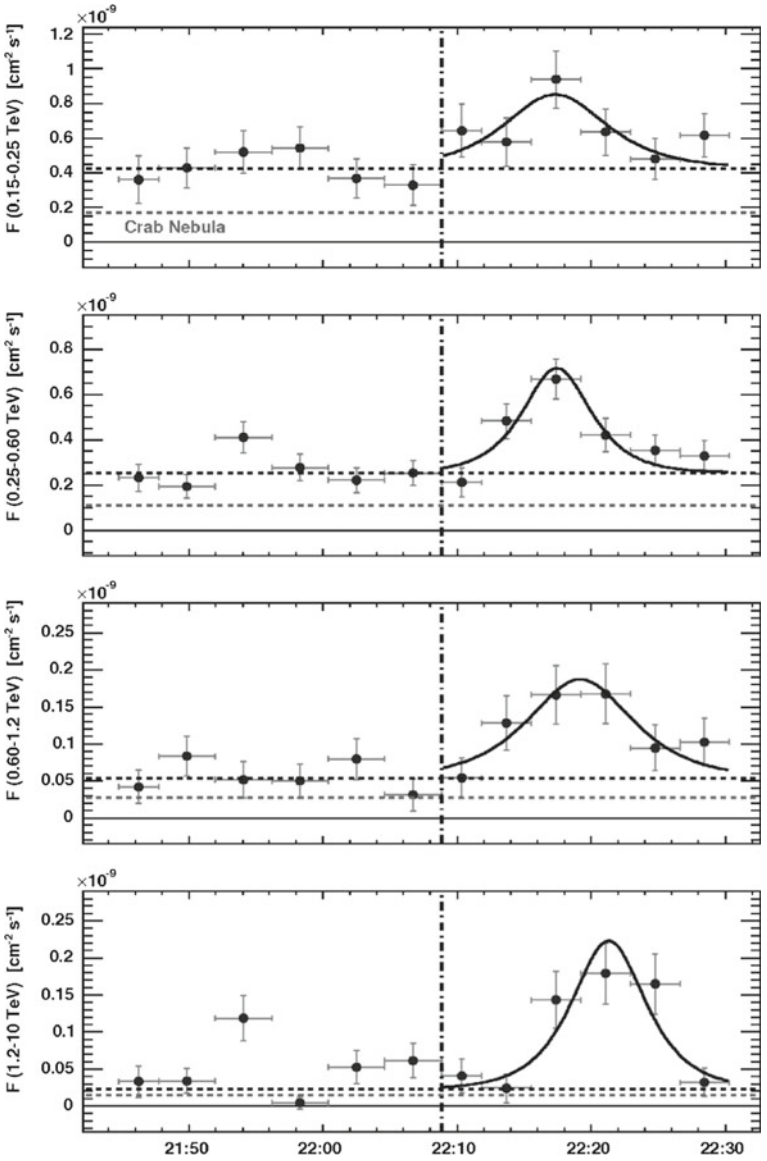

Fig. 10.54 Integral flux of Mkn 501 detected by MAGIC in four different energy ranges. From J. Albert et al., Phys. Lett. B668 (2008) 253

In most QG scenarios violations to the universality of the speed of light happen at order larger than 1: $\Delta t \simeq (E/E_{\rm LIV})^{\nu}$ with $\nu > 1$. In this case the VHE detectors are even more sensitive with respect to other instruments like *Fermi*; for $\nu = 2$ the data from PKS 2155 give $E_{\rm LIV} > 10^{-9}\ E_P$.

10.4.2.6 Possible Anomalous Photon Propagation Effects

Some experimental indications exist, that the Universe might be more transparent to gamma rays than computed in Sect. 10.3.4.

As discussed before, the existence of a soft photon background in the Universe leads to a suppression of the observed flux of gamma rays from astrophysical sources through the $\gamma\gamma \to e^+e^-$ pair-production process. Several models have been proposed in the literature to estimate the spectral energy density (SED) of the soft background (EBL); since they are based on suitable experimental evidence (e.g., deep galaxy counts), all models yield consistent results, so that the SED of the EBL is fixed to a very good extent. Basically, the latter reproduces the SED of star-forming galaxies, which is characterized by a visible/ultraviolet hump due to direct emission from stars and by an infrared hump due to the emission from the star-heated warm dust that typically hosts the sites of star formation.

However, the Universe looks more transparent than expected—this is called the "EBL crisis." Basically, two experimental evidences support this conjecture:

- When for each SED of high-z blazars, the data points observed in the optically thin low photon energy regime ($\tau < 1$) are used to fit the VHE spectrum in optically thick regions, points at large attenuation are observed (Fig. 10.55, left). This violates the current EBL models, strongly based on observations, at some 5σ.
- The energy dependence of the gamma opacity τ leads to appreciable modifications of the observed source spectrum with respect to the spectrum at emission, due to the exponential decrease of τ on energy in the VHE gamma region. One would expect naively that the spectral index of blazars at VHE would increase with distance: due to absorption, the SED of blazars should become steeper at increasing distance. This phenomenon has not been observed (Fig. 10.55, right).

Among the possible explanations, a photon mixing with axion-like particles (ALPs), predicted by several extensions of the standard model (Sect. 8.5.1), can fix the EBL crisis, and obtain compatibility on the horizon calculation. Since ALPs are characterized by a coupling to two photons, in the presence of an external magnetic field B photon-ALP oscillations can show up. Photons are supposed to be emitted by a blazar in the usual way; some of them can turn into ALPs, either in the emission region, or during their travel. Later, some of the produced ALPs can convert back into photons (for example, in the Milky Way, which has a relatively large magnetic field) and ultimately be detected. In empty space this would obviously produce a flux dimming; remarkably enough, due to the EBL such a double conversion can make the observed flux considerably larger than in the standard situation: in fact, ALPs do not undergo EBL absorption (Fig. 10.56).

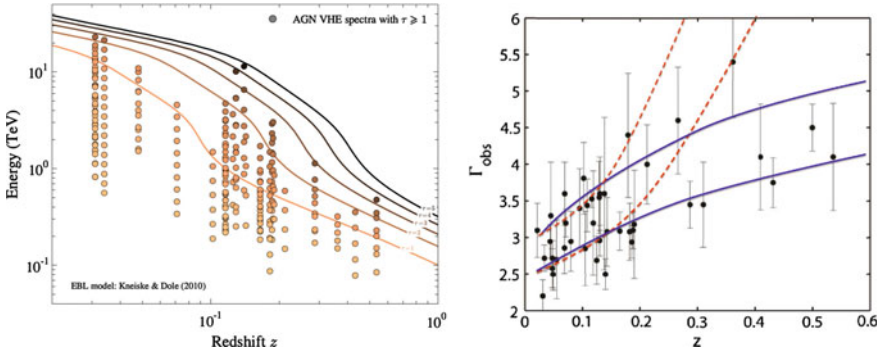

Fig. 10.55 Left: For each individual spectral measurement including points at $\tau > 1$, the corresponding value of z and E are marked in this diagram. The iso-contours for $\tau = 1, 2, 3, 4$ calculated using a minimum EBL model are overlaid. From D. Horns, M. Meyer, JCAP 1202 (2012) 033. Right: Observed values of the spectral index for all blazars detected in VHE; superimposed is the predicted behavior of the observed spectral index from a source at constant intrinsic spectral index within two different scenarios. In the first one (area between the two dotted lines) Γ is computed from EBL absorption; in the second (area between the two solid lines) it is evaluated including also the photon-ALP oscillation. Original from A. de Angelis et al., Mon. Not. R. Astron. Soc. 394 (2009) L21; updated

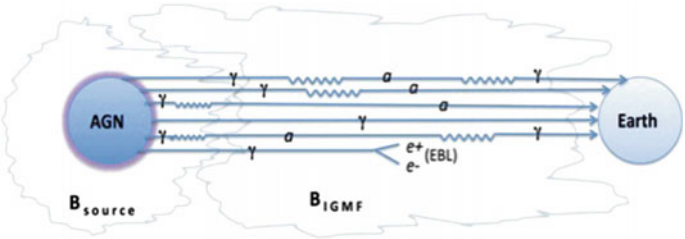

Fig. 10.56 Illustration of gamma ray propagation in the presence of oscillations between gamma rays and axion-like particles. From M.A. Sanchez-Conde et al., Phys. Rev. D79 (2009) 123511

We concentrate now on the photon transition to ALP in the intergalactic medium. The probability of photon-ALP mixing depends on the value and on the structure of the cosmic magnetic fields, largely unknown (see Sect. 10.3.1).

Both the strength and the correlation length of the cosmic magnetic fields do influence the calculation of the $\gamma \to a$ conversion probability. In the limit of low conversion probability, if s is the size of the typical region, the average probability $P_{\gamma\to a}$ of conversion in a region is

$$P_{\gamma\to a} \simeq 2 \times 10^{-3} \left(\frac{B_T}{1\,\mathrm{nG}} \frac{\lambda_B}{1\,\mathrm{Mpc}} \frac{g_{a\gamma\gamma}}{10^{-10}\,\mathrm{GeV}^{-1}} \right)^2 , \qquad (10.61)$$

where B_T is the transverse component of the magnetic field.

For a magnetic field of 0.1–1 nG, and a cellular size structure $\lambda_B \sim 1\text{Mpc} - 10$ Mpc, any ALP mass below 10^{-10} eV, with a coupling such that 10^{11} GeV $< M < 10^{13}$ GeV (well within the region experimentally allowed for mass and coupling) can explain the experimental results (Fig. 10.55).

Another possible explanation for the hard spectra of distant blazars, needing a more fine tuning, is that line-of-sight interactions of cosmic rays with CMB radiation and EBL generate secondary gamma rays relatively close to the observer.

LIV and Photon Propagation

A powerful tool to investigate Planck scale departures from Lorentz symmetry could be provided by a possible change in the energy threshold of the pair production process $\gamma_{VHE}\gamma_{EBL} \rightarrow e^+e^-$ of gamma rays from cosmological sources. This would affect the optical depth, and thus, photon propagation.

In a collision between a soft photon of energy ϵ and a high-energy photon of energy E, an electron–positron pair could be produced only if E is greater than the threshold energy E_{th}, which depends on ϵ and m_e^2.

Note that also the violation of the Lorentz invariance changes the optical depth. Using a dispersion relation as in Eq. 10.58, one obtains, for $n = 1$ and unmodified law of energy–momentum conservation, that for a given soft-photon energy ϵ, the process $\gamma\gamma \rightarrow e^+e^-$ is allowed only if E is greater than a certain threshold energy E_{th} which depends on ϵ and m_e^2. At first order:

$$E_{th}\epsilon + \xi(E_{th}^3/8E_p) \simeq m_e^2. \tag{10.62}$$

The $\xi \rightarrow 0$ limit corresponds to the special-relativistic result $E_{th} = m_e^2/\epsilon$. For $|\xi| \sim 1$ and sufficiently small values of ϵ (and correspondingly large values of E_{th}) the Planck scale correction cannot be ignored.

This provides an opportunity for tests based on dynamics. As an example, a 10 TeV photon and a 0.03 eV photon can produce an electron–positron pair according to ordinary special-relativistic kinematics, but they cannot produce a e^+e^- pair according to the dispersion relation in Eq. 10.58, with $n = 1$ and $\xi \sim -1$. The non-observation of EeV gamma rays has already excluded a good part of the parameter range of terms suppressed to first and second order in the Planck scale.

The situation for positive ξ is somewhat different, because a positive ξ decreases the energy requirement for electron–positron pair production.

A Win–Win Situation: Determination of Cosmological Parameters

If no indications of new physics (LIV, anomalous propagation) will be found after all, since the optical depth depends also on the cosmological parameters (Eq. 10.55), its determination constrains the values of the cosmological parameters if the EBL is known, and if only standard processes are at work.

A determination of Ω_M and Ω_Λ independent of the luminosity–distance relation currently used by the Supernovae 1 A observations can be obtained from the spectra of distant AGN.

10.4.3 Astrophysical Neutrinos

Experimental data on astrophysical neutrinos are scarce: their small cross section makes the detection difficult, and a detector with a sensitivity large enough to obtain useful information on astrophysical neutrinos sources should have an active volume larger than 1 km^3. We discussed in Chap. 4 the problems of such detectors.

Up to now we detected astrophysical neutrinos from the Sun, from the center of the Earth, from the supernova SN1987A, one extremely-high-energy neutrino from the blazar TXS 0506+056, and in addition diffuse very-high-energy astrophysical neutrinos for which we are unable to locate the origin.

The (low-energy) neutrino data from the Sun was discussed in Chap. 9, where we also shortly discussed neutrinos coming from the Earth; hereafter we review briefly the neutrinos produced in the flare of SN1987A and the (very-high-energy) neutrinos detected by IceCube.

10.4.3.1 Neutrinos from SN1987A

On February 23, 1987, a supernova was observed in the Large Magellanic Cloud (LMC), a galaxy satellite of the Milky Way (about 10^{10} solar masses, i.e., 1 % of the Milky Way) at a distance of about 50 kpc from the Earth. As it was the first supernova observed in 1987, it was called SN1987A; it was also the first supernova since 1604 visible with the naked eye. The event was associated with the collapse of the star Sanduleak-69202, a main sequence star of mass about 20 solar masses.

Three hours before the optical detection, a bunch of neutrinos was observed on Earth. SN1987A was the first (and the only up to now) unambiguous detection of neutrinos that can be localized from a source other from the Sun: three water Cherenkov detectors, Kamiokande, the Irvine–Michigan–Brookhaven (IMB) experiment, and the Baksan detector observed 12, 8, and 5 neutrino interaction events, respectively, over a 13 s interval (Fig. 10.57). Within the limited statistics achieved by these first-generation detectors, the number of events and the burst duration were consistent with standard estimates of the energy release and cooling time of a supernova. The energy of neutrinos can be inferred from the energy of the recoil electrons to be in the tens of MeV range, consistent with the origin from a collapse.

The optical counterpart reached an apparent magnitude of about 3. No very high-energy gamma emission was detected (in 1987 gamma detectors were not operating), but gamma rays at the intermediate energies characteristic of gamma transitions could be recorded.

SN1987A allowed also investigations on particle physics properties of neutrinos. The neutrino arrival time distribution sets an upper limit of 10 eV on the neutrino mass; the fact that they did not spread allows setting an upper limit on the magnetic moment $<10^{-12}\mu_B$, where μ_B is the Bohr magneton. A determination of the neutrino velocity can also be derived, being consistent with the speed of light within two parts in 10^{-9}.

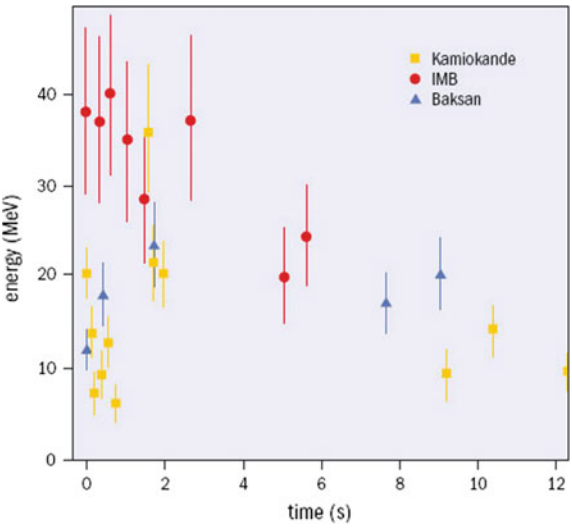

Fig. 10.57 Time-line of the SN1987a neutrino observation. From M. Nakahata, Cern Courier, September 2007

10.4.3.2 Very-High-Energy Neutrinos

The IceCube experiment at the South Pole reported for the first time in 2013 the detection of astrophysical neutrinos; after a few years the evidence is much stronger and tens of astrophysical neutrinos are collected every year. IceCube detects the Cherenkov radiation in the Antarctic ice generated by charged particles, mostly muons, produced by neutrino interactions.

The experimental problem is linked to the relatively large background from atmospheric muons, i.e., muons coming from interactions of cosmic rays with the atmosphere, which are recorded, even at a depth of 1450 m, at a rate of about 3000 per second. Two methods are used to identify genuine neutrino events:

1. Use the Earth as a filter to remove the huge background of cosmic-ray muons. i.e., look only to events originated "from the bottom". This limits the neutrino view to a single flavour (the muon flavor, since muons are the only charged particles which have a reasonably long interaction length) and half the sky.
2. Identify neutrinos interacting inside the detector. This method divides the instrumented volume of ice into an outer veto shield and a 500 megaton inner fiducial volume. The advantage of focusing on neutrinos interacting inside the instrumented volume of ice is that the detector functions as a total absorption calorimeter, and one can have an energy estimate. Also, neutrinos from all directions in the sky can be identified.

Both methods for selecting cosmic neutrinos harvest together about 1 event/month, twice that if one can tolerate a $\sim$25% background. Standard model physics allows one to infer the energy spectrum of the parent neutrinos – for the highest energy event the most likely energy of the parent neutrino is almost 10 PeV. Data indicate

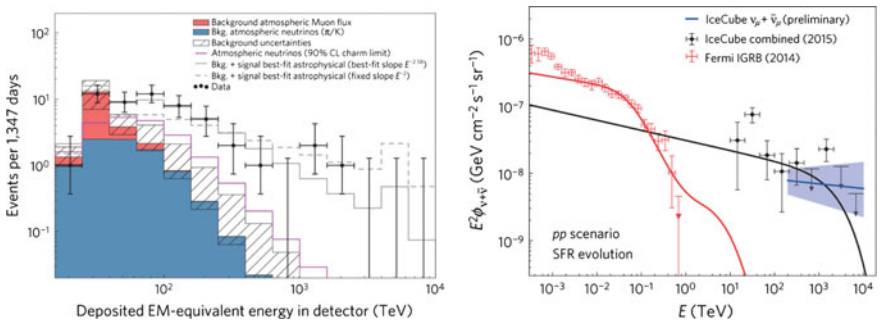

Fig. 10.58 Left: Deposited energies, by neutrinos interacting inside IceCube, observed in four years of data. The hashed region shows uncertainties on the sum of all backgrounds. The atmospheric muon flux (red) and its uncertainty is computed from simulation. The atmospheric neutrino flux is derived from previous measurements. Also shown are two illustrative power-law fits to the spectrum. Data measurements are shown by the black crosses. Right: The astrophysical neutrino flux (black line) observed by IceCube matches the corresponding cascaded gamma-ray flux (red line) observed by *Fermi*, see Fig. 10.47. From F. Halzen, Nature Physics 13 (2017) 232

an excess of neutrino events with respect to atmospheric neutrinos above 30 TeV. The cosmic flux above 100 TeV is well described by a power law

$$\Phi_\nu \simeq (0.9 \pm 0.3) \times 10^{-14} \left(\frac{E}{100\,\mathrm{TeV}} \right)^{-2.13 \pm 0.13} \mathrm{GeV}^{-1} \mathrm{m}^{-2} \mathrm{sr}^{-1} \,. \qquad (10.63)$$

To give an example, the ratio between the neutrino flux and the charged cosmic ray flux at 100 TeV is

$$\Phi_\nu / \Phi_{CR} \sim 2 \times 10^{-5} \,.$$

The energy and zenith angle dependence observed for completely contained events, shown in Fig. 10.58, is consistent with expectations for a flux of neutrinos produced by cosmic accelerators – a purely atmospheric component is excluded at more than 7σ.

Considerations based on the expected fluxes allow predicting that in a few years we shall reach the statistics required to identify their origin by matching arrival directions with astronomical maps.

Figure 10.59 shows in galactic coordinates the arrival directions of cosmic neutrinos for four years of events with interaction vertices inside the detector. The observed neutrino flux is consistent with an isotropic distribution of arrival directions and equal contributions of all neutrino flavours.

A variety of analyses suggest that the cosmic neutrino flux dominates the atmospheric background above an energy that may be as low as 30 TeV, with an energy spectrum that cannot be described as a single power, as was the case for the muon neutrino flux through the Earth for energies exceeding 220 TeV. This is reinforced

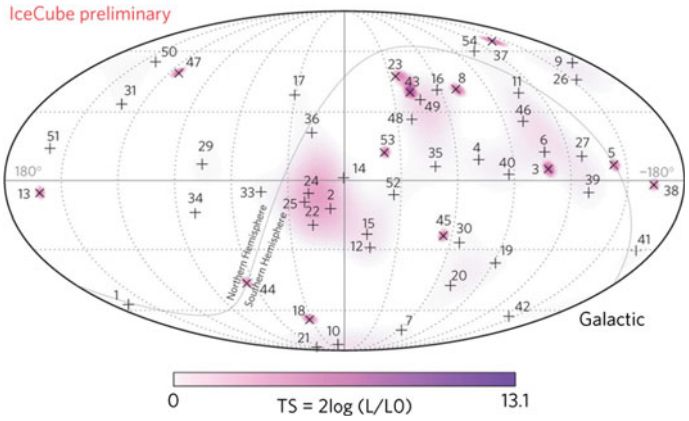

Fig. 10.59 Arrival directions of neutrinos in the four-year starting-event sample in galactic coordinates. Shower-like events (contained in the detector) are shown with "+" and those containing muon tracks with "x". The colour scale indicates the value of the test statistic (TS) of an unbinned maximum likelihood test searching for anisotropies of the event arrival directions. From F. Halzen, Nature Physics 13 (2017) 232

by the fact that fitting the excess flux in different ranges of energy yields different values for the power-law exponent.

Gamma rays at energies above some 100 TeV are likely to interact with background photons before reaching Earth. The resulting electromagnetic shower subdivides the initial photon energy, resulting in multiple photons in the GeV–TeV energy range by the time the shower reaches Earth. After accounting for the cascading of the PeV photons in cosmic radiation backgrounds between source and observation, a gamma-ray flux similar to the IceCube neutrino flux matches the extragalactic high-energy gamma-ray flux observed by the *Fermi* satellite as shown in Fig. 10.47, right.

10.4.3.3 The First Multimessenger Neutrino-Gamma Detection: EHE170922

On September 22, 2017, IceCube detected an extremely-high-energy neutrino event, consisting in a muon coming from the bottom of the detector through the Earth with an estimated energy between 100 TeV and 150 TeV, likely produced by a neutrino of energy of $E_\nu \sim 300$ TeV. Promptly alerted, the *Fermi* LAT and MAGIC detected at more than 5σ a flare from the blazar TXS 0506 +056, at a redshift $\sim$0.34, within the region of sky consistent with the 50% probability region of the IceCube neutrino (about one degree in size). The MAGIC detection allowed to determine that the electromagnetic emission had a cutoff at a few hundred GeV.

The simultaneous emission of gamma rays and neutrinos from the same source proves that the "hadronic mechanism" has been seen at work. The estimated energy

of a proton producing such a high energy neutrino in a "beam dump" is

$$E_p \gtrsim 20\, E_\nu \sim 10 - 20\,\mathrm{PeV}\,, \tag{10.64}$$

an energy above the knee and well appropriate for a blazar; blazar models prefer the target to be a photon gas.

This event opened the era of multimessenger astronomy with neutrinos. The present detection rate of astrophysical neutrinos is $\mathcal{O}$(1 event/month), and it is thus likely that such events will not be common in the future. It sets however a benchmark for the size of future IceCube-like detectors: a size ten times larger will almost certainly allow detecting clusters of neutrinos from astrophysical hadronic accelerators, as well as larger numbers of neutrinos from a flare like the one detected.

It is important to note that the cutoff energy in the gamma rays detected is much lower than the neutrino energy. This is a consequence of the fact that the energy of the gamma rays is degraded due to the interaction with photons and matter when traveling in the jet and during their cosmic voyage, and agrees qualitatively with the effect shown in Fig. 10.58, right.

10.4.4 Gravitational Radiation

The graviton, a massless spin 2 particle (this condition is required by the fact that gravity is attractive only), is the proposed mediator of any field theory of gravity. Indeed the coupling of the graviton with matter is predicted to be extremely weak and thus its direct detection is extremely difficult – Einstein had sentenced that it was "impossible to detect" experimentally. However, indirect and direct evidence of gravitational radiation have been clearly demonstrated.

The indirect evidence was firmly established in 1974 by Hulse and Taylor (Nobel Prize in Physics 1993). They observed that the orbital period of the binary pulsar PSR 1913+16, at a distance of about 6400 pc, was decreasing in agreement with the prediction of Einstein general theory of relativity (about 40 s in 30 years, see Fig. 10.60). In such system it was possible to deduce, from the time of arrival of the recorded pulses, the binary orbital parameters. The masses of the two neutron stars were estimated to be about 1.4 solar masses, the period to be 7.75 h and the maximum and the minimum separation to be 4.8 and 1.1 solar radii respectively. The gravitational waves produced by such a system induce a strain (see Chap. 4), when they now reach Earth, of the order of 10^{-23}; its direct observation is out of the reach of the present ground-based GW detectors but it will be detectable by future space detectors. The two neutron stars will merge in about 300 million years producing then a strain of the order of 10^{-18} at the Earth.

The direct evidence was firmly established in 2015 by the LIGO/Virgo collaboration detecting the collapse of pairs of black holes (Nobel Prize in Physics 2017 awarded to Rainer Weiss, Barry C. Barish and Kip S. Thorne). On September 14th, 2015, the two detectors of the LIGO collaboration observed simultaneously a large

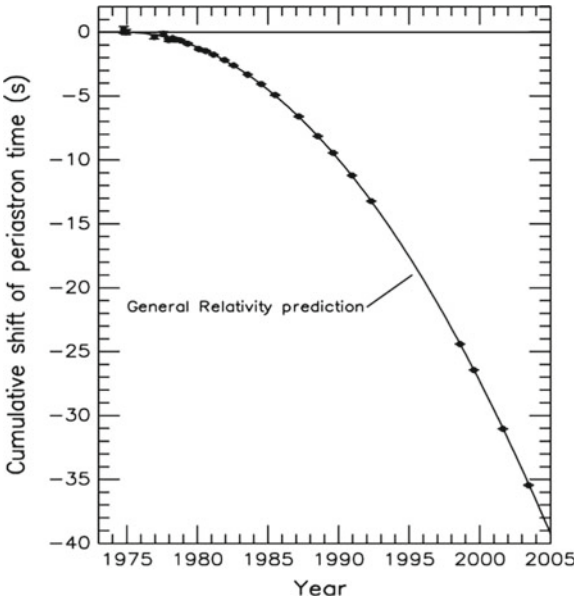

Fig. 10.60 Observed accumulated shifts of the times of periastron in the PSR 1913+16 compared with the general relativity prediction from gravitational radiation. From Joseph H. Taylor Jr.—©The Nobel Foundation 1993

and clear gravitational wave signal (labelled as GW150914) that matches the prediction of general relativity for the coalescence of a binary black hole system (see Fig. 10.61). The simulation of such merger is shown in Fig. 10.62 where three phases are well identified:

1. *Inspiral*: the approach of the two black holes; in this phase frequency and amplitude increase slowly;
2. *Merger*: the merging of the two black holes; frequency and amplitude increase rapidly;
3. *Ringdown*: the newly formed black hole is distorted and rings down to its final state by emitting characteristic radiation: the ringdown radiation. This radiation has a precise frequency and its amplitude decays exponentially as time goes by. The ringdown phase is similar to that of a church bell or a guitar string when plucked: black holes also have a characteristic sound! After this stage, there is only a single, quiet black hole, and no radiation is emitted.

The observed amplitudes (*strain* - see Chap. 8), are of the order of 10^{-21} and the frequencies are in the range 35–250 Hz. The masses of the initial black holes were estimated to be $36^{+5}_{-4}$and 29^{+4}_{-4} solar masses while the final black hole mass was estimated to be 62^{+4}_{-4} solar masses. The luminosity distance of such system was estimated to be 410^{+160}_{-180} Mpc.

Four more events were observed by LIGO respectively in December 2015, January 2017 (already during the second observation run), August 2017 (two events, one of which with a positive observation as well by Virgo), again interpreted as the coalescence of binary black hole system:

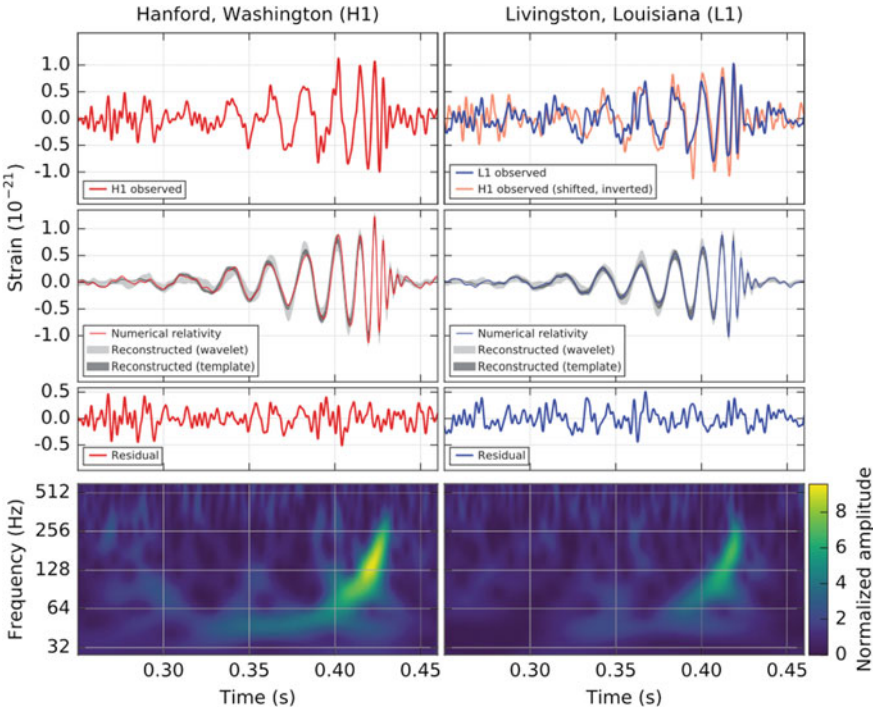

Fig. 10.61 The first gravitational-wave event (GW150914) observed by LIGO: left from the Hanford (H1) site; right from the Livingston (L1) site. From Phys. Rev. Lett. 116, 061102 (2016)

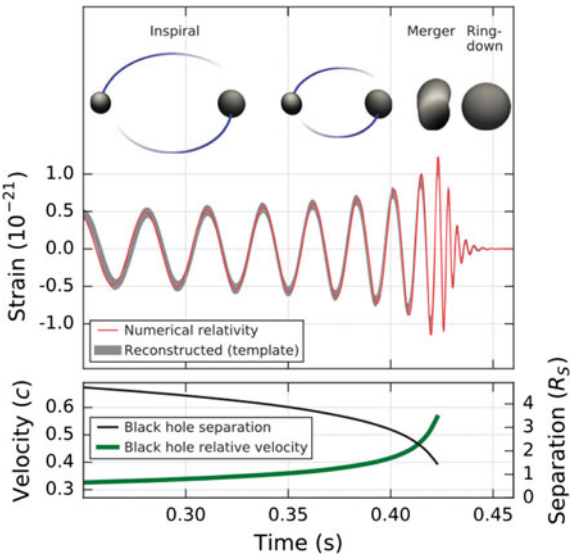

Fig. 10.62 Top: The waveform of the merger of a binary black hole system with the parameters measured from GW150914. Estimated gravitational-wave strain amplitude from GW150914 projected onto H1. Bottom: The BH separation in units of Schwarzschild radii and the relative velocity normalized to the speed of light c. From Phys. Rev. Lett. 116, 061102 (2016)

- In the event GW151226 the masses of the initial black holes were estimated to be $14.2^{+8.3}_{-3.7}$ and $7.5^{+2.3}_{-2.3}$ solar masses while the final BH mass was estimated to be $20.8^{+6.1}_{-1.7}$ solar masses. The luminosity distance of such system was estimated to be 440^{+180}_{-190} Mpc.
- In GW170104 the masses of the initial BHs were estimated to be $31.2^{+8.4}_{-6.0}$ and $19.4^{+5.3}_{-5.9}$ solar masses while the final BH mass was estimated to be $48.7^{+5.7}_{-4.6}$ solar masses. The luminosity distance of such system was estimated to be 340 ± 140 Mpc.
- In GW170608 the masses of the initial BHs were estimated to be 12^{+7}_{-2} and 7 ± 2 solar masses while the final BH mass was estimated to be $18^{+4.8}_{-0.9}$ solar masses. The luminosity distance of such system was estimated to be 880^{+450}_{-390} Mpc.
- GW170814 resulted from the inspiral and merger of a pair of black holes with $30.5^{+5.7}_{-3.0}$ and $25.3^{+2.8}_{-4.2}$ times the mass of the Sun, at a distance of 540^{+130}_{-210} Mpc from Earth. The resulting black hole had a mass of $53.2^{+3.2}_{-2.5}$ solar masses, 2.7 solar masses having been radiated away as gravitational energy. The peak luminosity was about 3.7×10^{49} W.

Contrary to what was previously believed there is thus a significant population of binary BH systems with component masses of tens of solar masses and merger rates that allow their regular detection by the present GW observatories. The study of these events has shown, so far, no evidence of any deviation from the General Relativity predictions. In Fig. 10.63 the masses of the initial and final BH detected mergers are compared to the BHs observed in X rays and to the known neutron star masses.

A special GW event, different in nature from the previous five, has been detected on August 17, 2017.

10.4.4.1 GW170817, the First Multimessenger Discovery of a Binary Neutron Star Merger

The first observation of a single astrophysical source through both gravitational and electromagnetic waves happened on August 17, 2017. LIGO/Virgo detected a gravitational wave signal possibly associated with the merger of two neutron stars (GW170817), and (1.75 ± 0.05) s later the *Fermi* Gamma-Ray Burst Monitor and the INTEGRAL SPI/ACS detector observed independently in the same sky region (Fig. 10.64) a short, ∼2 s long, GRB (GRB 170817A) whose time-averaged spectrum is well fit by a power law function with an exponential high-energy cutoff at ∼80 keV. The masses of the initial neutron stars were estimated to be in the range [1.36, 2.26] solar masses and [0.86, 1.36] solar masses respectively, while the final mass was estimated to be $2.82^{+0.47}_{-0.09} M_{\odot}$. These observations were followed by an extensive multimessenger campaign covering all the electromagnetic spectrum as well as the neutrino channel: a bright optical transient (SSS17a) was discovered in the NGC 4993 galaxy located at 40 Mpc of the Earth by the Swope Telescope in

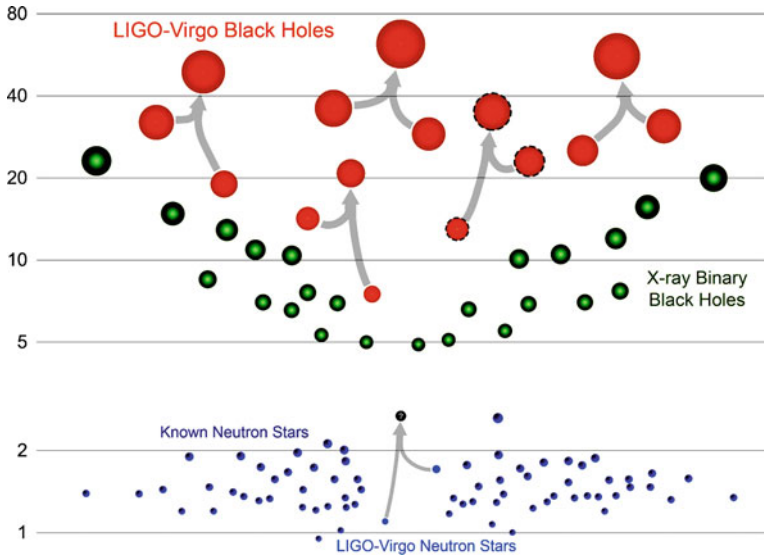

Fig. 10.63 The masses of the black holes and neutron stars measured through GW observations are shown together with those detected through electromagnetic observations. Adapted from LIGO-Virgo/Frank Elavsky/Northwestern University

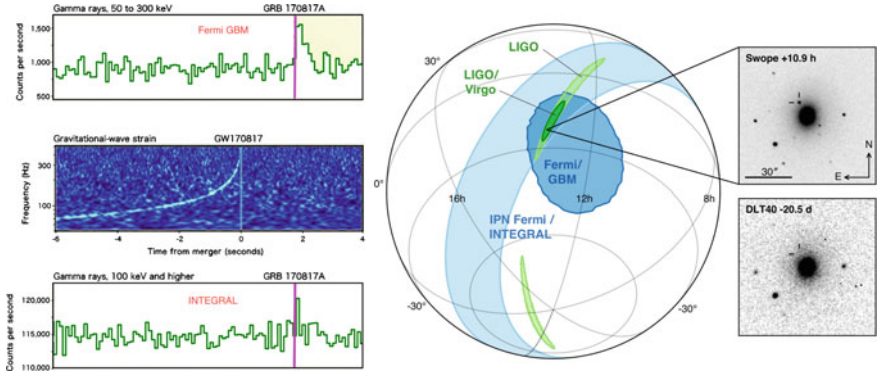

Fig. 10.64 The signals detected by *Fermi* GBM (top left), by LIGO/Virgo (center left), and by INTEGRAL (bottom left); the 90% location contour regions of the GW170817 / GRB 170817A / SSS17a event as determined by LIGO, LIGO-Virgo, INTEGRAL, *Fermi*. The insets show the location of the NGC 4993 galaxy in the images of the Swope (top right) and of the DLT40 (bottom right) optical telescopes respectively 10.9 hr after and 20.5 days before the GW observation. The perpendicular lines indicate the location of the transient in both images. Courtesy S. Ciprini, ASI

South America and shortly after by five more teams. The follow-up was then done by ground and space observatories all around the world: X-ray and radio counterparts were discovered respectively $\sim$9 days and $\sim$16 days after the merger, while no neutrino candidates were seen.

The neutron star merger event is thought to result in a "kilonova", characterized by a short GRB followed by a longer optical afterglow. A total of 16 000 times the mass of the Earth in heavy elements is believed to have formed; for some of them spectroscopical signatures have been observed.

The scientific importance of this event is huge. Just to quote two aspects:

- It provides strong evidence that mergers of binary stars are the cause of short GRBs.
- It provides a limit on the difference between the speed of light and that of gravity. Assuming the first photons were emitted between zero and ten seconds after peak gravitational wave emission, the relative difference between the speeds of gravitational and electromagnetic waves, $|v_{GW} - v_{EM}|/c$, is constrained to be smaller than $\sim 10^{-15}$.

Unlike all previous GW detections, corresponding to BH mergings and not expected to produce a detectable electromagnetic signal, the aftermath of this merger was seen by 70 observatories across the electromagnetic spectrum, marking a significant breakthrough for multi-messenger astronomy and opening a new era. Several events of this kind can be expected in the future.

10.5 Future Experiments and Open Questions

The field of astroparticle physics has been extremely successful: five Nobel Prizes (2002, 2006, 2011, 2015 and 2017) have been awarded to astroparticle physics in this millennium.

The next 10–20 years will see a dramatic progress using new detectors to improve the synergy between cosmic messengers: charged cosmic rays, gamma rays, neutrinos and gravitational waves.

10.5.1 Charged Cosmic Rays

More than one hundred years after their discovery, charged cosmic rays are still, and will be, actively studied through many experiments covering many energy decades. Up to the knee region (10^{15}–10^{16} eV) their origin is basically galactic and the paradigm that associates their origin with SNRs is in a good shape. Other sources of cosmic rays were found in the galaxy; however, only one or two galactic accelerators were found potentially reaching the PeV energies. There is significant evidence that part of the cosmic rays above the EeV come from AGN; however, no individual associations were possible with certainty at these energies. There is evidence that, although GRBs have the energetics for producing CRs above the EeV, their contribution to cosmic rays at extreme energies is negligible.

Measuring with high statistics and precision the different particle (electron, positron, proton, antiprotons, nuclei) spectra, deviations from the Universal power-law behavior expected from the Fermi acceleration mechanism were found with gradual or abrupt changes in energy dependence. Indeed a new era of precision and statistics was recently opened thanks to a new generation of cosmic ray experiments like PAMELA, AMS-02, DAMPE and CALET and, in a different energy-range, ARGO-YBJ and HAWC (see Sect. 10.4); this line will be vigorously pursued in the next years by the present and future (LHAASO, HERD, ...) experiments.

We face thus an enormous challenge to describe cosmic rays, and both the injection (acceleration) and propagation models have to be deeply improved. The increase in computer power allows now multidimensional particle-in-cell (PIC) kinetic simulations able to cope with the non-linear interplay between energetic particles and electromagnetic fields in strong shock wave environments. These simulations are starting nowadays to reproduce the needed Diffuse Shock Acceleration (DSA) mechanisms with the formation of turbulent structures where magnetic fields can be amplified. A better understanding of the SNR interaction with the interstellar medium as well as of the complex damping, unstable and anisotropic transport mechanisms will lead to a clearer picture of the formation and evolution of stars and galaxies. This will need an interplay with X- and gamma-ray detectors (especially in the MeV region, which marks the interactions of CRs with the environment).

The unexpected bump-like structure observed in the positron spectrum by AMS-02, compatible with the products of the self-annihilation of a Dark Matter particle with a mass around 1 TeV (see Sect. 10.4.1.3), remains to be clarified and probably we will have to wait a few years in order that AMS-02 will have enough statistics to reasonably measure the properties of this structure.

The quest for the origin and nature of UHECRs will remain in the list of highlights for the next decade. So far large-scale anisotropies were found at energies around 10^{19} eV (the dipole structure observed by the Pierre Auger Observatory and the indication of a hotspot by the Telescope Array Experiment–see Sect. 10.4.1.6); on the contrary, just possible weak correlations with individual astrophysical sources locations were reported. Statistics is desperately needed and the increase by a factor four of the initial 700 km^2 area of the TA as well as the upgrade of Auger, with with the introduction of scintillators on the top of the Water Cherenkov Detectors, will for sure help.

Composition at extremely high energies and in particular the physical interpretation of a "GZK-like" cutoff in the observed CRs around 10^{20} eV is a central subject. The scenario of an exhaustion of the sources at these energies is making its way in the community. However our QCD-inspired shower models are not able to describe satisfactorily both the electromagnetic and the hadronic EAS components, and thus no firm conclusion may be achieved: scenarios involving "new Physics" at c.m. energies well above those attained by the LHC accelerator can not be discarded. The upgraded Auger will allow disentangling of the electromagnetic and muonic components of the EAS on an event-by-event basis, and thus may shed some light on this long-standing problem.

The idea, pioneered in the 1990s by John Linsley, Livio Scarsi and Yoshiyuki Takahashi, of a wide field-of-view space observatory able to detect from above the UV light produced in the atmosphere by the very energetic EAS is still under intense discussion. What is called nowadays the "EUSO concept" covers a large range of experimental initiatives and projects and a dedicated space mission may be approved in the next decade. The collection area will be huge and may allow the detection of very high energy tau neutrinos (10^{18}–10^{19} eV).

10.5.2 Gamma Rays

10.5.2.1 The Region till a Few MeV

This region has important implications on the science at the TeV and above, since a good knowledge of the spectra in the MeV region can constrain the fit to the emitted spectra at high energies, thus allowing:

- to evidence additional contributions from new physics (dark matter in particular);
- to estimate cosmological absorption, due for example to EBL or to possible interactions with axion-like fields.

On top of this, the 0.3–300 MeV energy range is important per se, since it is the energy region:

- characteristic of nuclear transitions;
- characteristic of the nuclear de-excitation of molecular clouds excited by colliding cosmic rays;
- where one expects the exhaustion of the electromagnetic counterpart of gravitational wave events;
- where one expects gamma rays from the conversion of axions in the core of supernovae.

Unfortunately, it is experimentally difficult to study. It requires an efficient instrument working in the Compton regime with an excellent background subtraction, and possibly with sensitivity to the measurement of polarization. Since COMPTEL, which operated two decades ago, no space instrument obtained extra-solar gamma-ray data in the few MeV range; now we are able to build an instrument one-two orders of magnitudes more sensitive than COMPTEL based on silicon detector technology, state-of-the-art analog readout, and efficient data acquisition.

Several proposals of satellites have been made, and convergence is likely for an experiment to be launched around 2028.

10.5.2.2 The GeV Region

It is difficult to think for this century of an instrument for GeV photons improving substantially the performance of the *Fermi* LAT: the cost of space missions is such that the size of *Fermi* cannot be reasonably overcome with present technologies. New satellites in construction (like the Chinese-Italian mission HERD) will improve some of the aspects of *Fermi*, e.g., calorimetry. For sure a satellite in the GeV region with sensitivity comparable with *Fermi* will be needed in space (*Fermi* could in principle operate till 2028).

10.5.2.3 The Sub-TeV and TeV Regions

CTA appears to have no rivals for the gamma astrophysics in the sub-TeV and TeV (from a few GeV to a few TeV) energy regions. These are crucial regions for fundamental physics, and for astronomy.

PeVatrons and the nature of the emitters in the galaxy will be studied in detail. WIMPs will be tested with the "right" sensitivity up to 1 TeV.

CTA will be probably upgraded including state-of-the art photon detection devices of higher efficiencies with respect to the present ones; it can in principle operate till 2050.

10.5.3 The PeV Region

Due to the opacity of the Universe to gamma rays, less than a handful of sources could be visible in the Northern sky, and less than a dozen in the Southern sky, all galactic. The experiments in the Northern hemisphere (the extended HAWC, LHAASO, TAIGA/HiSCORE) provide an appropriate coverage of the Northern sky and a detailed study of PeVatrons.

The situation in the Southern hemisphere has room for improvement. An EAS detector in the South might give substantial input with respect to the knowledge of the gamma sky, and of possible PeVatrons in the GC, and outperform in this sense the small-size telescopes of CTA. Several proposals are being formulated now, and they will probably merge. A large detector in Southern America could compete in sensitivity with the SSTs of CTA-South already at 100 TeV, offering in addition a serendipitous approach.

10.5.4 High Energy Neutrinos

The discovery of the very High Energy Astrophysical neutrinos (see Sect. 10.4.3.2) opens the era of the High Energy ($>10^{15}$eV) neutrino astronomy.

Neutrino astronomy will progress along three directions:

- The "large volume" direction. The absorption length of Cherenkov light to which the photomultipliers are sensitive exceeds 100 m in ice. Spacings of 250 m, possibly larger, between photomultipliers, are thus acceptable in IceCube. One can therefore instrument a ten-times-larger volume of ice with the same number of strings used to build IceCube. A next-generation instrument using superior light sensors and this enlarged spacing, provisionally called IceCube-Gen2, could have an affordable cost; construction can take 5 years. IceCube-Gen2 can increase, in the next years, the volume and sensitivity of the present detector by more than an order of magnitude and hopefully will be able to identify the neutrino sources and help to decipher the location of the extremely-high-energy cosmic ray accelerators.
- The "precision" direction. If funded, KM3NeT will consist of 115 strings carrying more than 2 000 optical modules, instrumenting a volume of 3 km^3. The vertical distances between optical modules will be 36 meters, with horizontal distances between detection units of about 90 meters; reconstruction accuracy will be thus a factor of 2 better than in IceCube. Construction is now ongoing in Sicily. IceCube has discovered a flux of extragalactic cosmic neutrinos with an energy density that matches that of extragalactic high-energy photons and UHE CRs. This may suggest that neutrinos and high-energy CRs share a common origin, and the better resolution of KM3NeT could be the ket to pinpoint sources.
  A parallel effort is underway in Lake Baikal with the deep underwater neutrino telescope Baikal-GVD (Gigaton Volume Detector). The first GVD cluster, named DUBNA, was upgraded in spring 2016 to its final size (288 optical modules, 120 meters in diameter, 525 meters high, and instrumented volume of 6 Mton). Each of the eight strings consists of three sections with 12 optical modules. Deployment of a second cluster was completed in spring 2017.
- The "extremely high energy" direction, using new technologies. At extremely high energies, above 100 PeV, a cosmogenic neutrino flux is expected from the interaction of highest energy cosmic-ray protons with the CMB. Predicted fluxes are in a range of approximately 1 event/year/km^3 or lower. The idea to increase the effective volume of detectors to be sensitive to such rates seems unfeasible, unless the EUSO concept (see Chap. 4) is adopted; detection of coherent radio emission up to GHz originated by the neutrino interaction in dense, radio-transparent media, the so-called Askar'yan effect, is preferred. Several prototype detectors are being developed.

Neutrino Astronomy has just started and a rich physics program is ahead of us. A global neutrino network (IceCube-Gen2 in the South Pole, Gigaton Volume Detector (GVD) in the lake Baikal and KM3NeT in the Mediterranean sea) will operate.

10.5.5 Gravitational Waves

The direct determination of gravitational waves (see Sect. 10.4.4) opened the new field of gravitational wave astronomy. In the next years an aggressive experimental program will allow to extend it in sensitivity, precision and frequency range. Indeed LIGO, in the USA, that has started operating in 2015, has been joined by the upgraded Virgo detector, in Italy, in 2017, and soon will be joined by the newcomer KAGRA interferometer, in Japan (for a detector description see Chap. 4). These second generation detectors, possibly including the indian LIGO (INDIGO) gravitational wave detector, will form a large international network allowing the improvement of the angular resolution by more than one order of magnitude, and the present sensitivity by a factor of two. This setup will be probably ready before 2024.

A third generation of detector, the Einstein Telescope, with longer baseline (10 km) and cryogenic mirrors, is under study in Europe and, hopefully, will operate around 2024 with an extended observation range (3 Gpc) and a sensitivity 10 times better then the second generation telescopes. It will be built in underground sites, and it will have three arms, in order to measure by itself the direction of a source and to issue autonomously alerts. A similar detector, four times larger, is under study in the US: the Cosmic Explorer. The number of observed events will increase therefore from a couple per month to a few per day allowing the mapping of the gravitational wave astrophysical sources and their detailed study not excluding the (probable) discovery of unexpected new classes of sources.

The lower frequencies, which are relevant to access gravitational waves emitted in the early Universe and thus to test cosmological models, have to be covered from space based detectors. Two space experiments, LISA (ESA) and DECIGO (JAXA) covering respectively the frequency range from 0.03 mHz to 0.1 Hz and from 0.1 Hz to 10 Hz are planned to operate in 20 years. LISA has been scheduled for launch in 2034.

Gravitational waves observatories will be for sure privileged laboratories for general relativity; namely:

- GWs will allow to perform precision tests of General Relativity. The inspiral phase will allow to test if the inspiral proceeds as predicted by General Relativity. Faster inspirals could signal new fields (for example, charged black holes would radiate more and inspiral faster) or even a nontrivial astrophysical environment (if the inspiral is taking place in a large-density dark matter environment, inspiral would also proceed faster).
- GWs will allow to test the Kerr nature of black holes. In GR, the most general black hole solution belongs to the Kerr family, and is specified by only two parameters: mass and angular momentum. This fact is part of the uniqueness or "no-hair" conjecture.[10] The ringdown phase of black holes allow one to measure precisely

[10]The no-hair conjecture, sometimes called "theorem" postulates that all solutions of the equations of gravitation and electromagnetism for a BH can be characterized by only three externally observable parameters: mass, electric charge, and angular momentum. All other information (for which "hair" is a metaphor) disappears behind the BH horizon and is therefore inaccessible to external observers.

the characteristic modes of black holes and to test if they really belong to the Kerr family.
- GWs will allow new probes of quantum gravity.
- GWs will allow us to map the entire compact object content of the universe. Both the inspiral and ringdown phase allow us to measure mass and spin of black holes to an unprecedented precision. If coupled to electromagnetic observations, there is the exciting prospect of determining, in addition, their position. In summary, detailed maps of the black Universe will be possible.

10.5.6 Multi-messenger Astrophysics

Cosmic ray, neutrino and gravitational waves became, in the last years, full right members of the Astronomy club until then just frequented by the electromagnetic waves in all wavelengths (radio, microwaves, IR, optical, UV, X rays, gamma rays, with a clear need for improvement in the MeV region). In the previous sections each of these channels were individually discussed and their ambitious future experimental programs, involving the upgrade and/or the construction of new observatories at ground or in space, were referred.

The challenge for the next years is also to make a fully efficient combined use of all of these infrastructures, not only making available and analysing a posteriori the collected data, but also performing joint observations whenever a transient phenomenon appeared. Wide field of view observatories should be able to launch "alerts" and trigger the narrow FoV ones.

Networks joining some of these observatories do exist already. Examples are: the GCN (Gamma-ray Coordinates Network) , which reports in real-time (or near real-time) locations of GRBs and other transients detected by spacecrafts (Swift, *Fermi*, INTEGRAL, Athena, etc.) producing also follow-up reports of the observations; the AMON (Astrophysical Multimessenger Observatory Network), which provides correlation analyses (real-time or archival) of astrophysical transients and/or sources – among AMON members are ANTARES, Auger, *Fermi*, HAWC, IceCube, LIGO, the Large Millimeter Telescope, MASTER, the Palomar Transient Factory, Swift, MAGIC, VERITAS.

Multi-messenger astronomy is becoming a powerful tool to monitor and understand the Universe we live in.

Further Reading

[F10.1] M. Spurio, "Particles and Astrophysics (a Multi-Messenger Approach)," Springer 2015. Taking a systematic approach, this book comprehensively presents experimental aspects from the most advanced cosmic ray detectors, in particular detectors of photons at different wavelengths.

[F10.2] T. Stanev, "High-Energy Cosmic Rays," Springer 2010. A classic for experts in the discipline.

[F10.3] D.H. Perkins, "Particle Astrophysics," 2nd edition, Oxford University Press 2008.
[F10.4] K.S. Thorne, unpublished, http://elmer.tapir.caltech.edu/ph237.
[F10.5] T.K. Gaisser, R. Engel, E. Resconi, "Cosmic Rays and Particle Physics", 2nd edition, Cambridge University Press 2016. The classic book written by Gaisser in 1990 recently revisited. A reference for particle acceleration and diffusion.
[F10.6] M. Longair, "High Energy Astrophysics", 3rd edition, Cambridge 2011.

Exercises

1. *Fermi acceleration mechanisms.* In the Fermi acceleration mechanism, charged particles increase considerably their energies crossing back and forth many times the border of a magnetic cloud (second-order Fermi mechanism) or of a shock wave (first-order Fermi mechanism). Compute the number of crossings that a particle must do in each of the mechanisms to gain a factor 10 on its initial energy assuming:

   (a) $\beta = 10^{-4}$ for the magnetic cloud and $\beta = 10^{-2}$ for the shock wave;
   (b) $\beta = 10^{-4}$ for both acceleration mechanisms.

2. *Photon spectrum in hadronic cascades.* Demonstrate that in a decay $\pi^0 \to \gamma\gamma$, once boosted for the energy of the emitting π^0, the probability to emit a photon of energy E_γ is constant over the range of kinematically allowed energies.
3. *Top-down production mechanisms for photons: decay of a WIMP.* If a WIMP of mass $M > M_Z$ decays into γZ, estimate the energy of the photon and of the Z.
4. *Acceleration and propagation.* The transparency of the Universe to a given particle depends critically on its nature and energy. In fact, whenever it is possible to open an inelastic channel of the interaction between the *traveling* particle and the CMB, its mean free path diminishes drastically. Assuming that the only relevant phenomena that rules the mean free path of the *traveling* particle is the CMB (CνB), estimate the order of magnitude energies at which the transparency of the Universe changes significantly, for:

   (a) Photons;
   (b) Protons;
   (c) Neutrinos.

   Assume $\langle E_{\gamma_{CMB}} \rangle \simeq 0.24$ meV; $\langle E_{\nu_{C\nu B}} \rangle \simeq 0.17$ meV.
5. *Photon-photon interactions.* Demonstrate that, for an isotropic background of photons, the cross section is maximized for background photons of energy:

$$\epsilon(E) \simeq \left(\frac{900\,\text{GeV}}{E} \right) \text{eV} \,.$$

6. *Neutrinos from SN1987A.* Neutrinos from SN1987A, at an energy of about 50 MeV, arrived in a bunch lasting 13 s from a distance of 50 kpc, 3 h before

the optical detection of the supernova. What can you say on the neutrino mass? What can you say about the neutrino speed (be careful...)?

7. *Neutrinos from SN1987A, again.* Some (including one of the authors of this book) saw in Fig. 10.57 two lines relating arrival times of neutrinos with energy, and derived the masses of two neutrino species. What can you say about the neutrino masses in relation to the current neutrino mass limits?
8. *Time lag in light propagation.* Suppose that the speed c of light depends on its energy E in such a way that

$$c(E) \simeq c_0 \left(1 + \xi \frac{E^2}{E_P^2}\right) ,$$

where E_P is the Planck energy (second-order Lorentz Invariance Violation). Compute the time lag between two VHE photons as a function of the energy difference and of the redshift z.

9. *Difference between the speed of light and the speed of gravitational waves.* Derive a limit on the relative difference between the speed of light and the speed of gravitational waves from the fact that the gamma-ray burst GRB170824A at a distance of about 40 Mpc was detected about 1.7 s after the gravitational wave GW170817.
10. *Flux of photons from Crab.* Consider the expression Eq. 10.56 in the text and let us assume that the flux of cosmic rays between 0.05 TeV and 2 PeV follows this expression.
The flux from the most luminous steady (or almost steady) source of gamma rays, the Crab Nebula, follows, according to the measurements from MAGIC, a law

$$N_\gamma(E) \simeq 3.23 \times 10^{-7} \left(\frac{E}{\text{TeV}}\right)^{-2.47-0.24\left(\frac{E}{\text{TeV}}\right)} \text{TeV}^{-1}\text{s}^{-1}\text{m}^{-2} . \qquad (10.65)$$

Translate this expression into GeV. Compute the number of photons from Crab hitting every second a surface of 10 000 m^2 above a threshold of 50 GeV, 100 GeV, 200 GeV, 1 TeV, up to 500 TeV. Compare this number to the background from the flux of cosmic rays in a cone of 1 degree of radius.

11. *Astronomy with protons?* If the average magnetic field in the Milky Way is 1 μG, what is the minimum energy of a proton coming from Crab Nebula (at a distance of 2 kpc from the Earth) we can detect as "pointing" to the source?
12. *Maximum acceleration energy for electrons.* The synchrotron loss rate is relatively much more important for electrons than for protons. To find the limit placed by synchrotron losses on shock acceleration of electrons, compare the acceleration rate for electrons with the synchrotron loss rate. The latter is negligible at low energy, but increases quadratically with E. Determine the crossover energy, and compare it to supernova ages. Is the acceleration of electrons limited by synchrotron radiation?

13. *Classification of blazars.* Looking to Fig. 10.17, right, how would you classify Markarian 421, BL Lac and 3C279 within the blazar sequence? Why?
14. $\gamma\gamma \rightarrow e^+e^-$. Compute the energy threshold for the process as a function of the energy of the target photon, and compare it to the energy for which the absorption of extragalactic gamma-rays is maximal.
15. *Hadronic photoproduction vs. photon-pair production mechanisms.* High-energy protons traveling in the intergalactic space may interact with CMB photons either via a photoproduction mechanism ($p\gamma \rightarrow N\pi$) or via a pair production mechanism ($p\gamma \rightarrow pe^+e^-$). Assume for the first process a cross section of about 0.5 mb, while for the second process it is some 40 times larger.

    (a) Compute the threshold energies for either production mechanism.
    (b) Calculate the propagation length for protons to lose 90% of their energies in either mechanism.

16. *Mixing photons with paraphotons.* The existence of a neutral particle of tiny mass μ, the paraphoton, coupled to the photon, has been suggested to explain possible anomalies in the CMB spectrum and in photon propagation (the mechanism is similar to the one discussed to the photon-axion mixing, but there are no complications related to spin here). Calling ϕ the mixing angle between the photon and the paraphoton, express the probability of oscillation of a photon to a paraphoton as a function of time (note: the formalism is the same as for neutrino oscillations). Supposing that the paraphoton is sterile, compute a reasonable range of values for ϕ and μ that could explain an enhancement by a factor of 2 for the signal detected at 500 GeV from the AGN 3C279 at $z \simeq 0.54$.
17. *Photon absorption affects the shape of the SED.* TXS 0506 +056 has a redshift of 0.34. What is the fraction of gamma rays absorbed due to interaction with EBL at an energy $E = 400$ GeV? If the measured spectral index if of 2.3, what can you say about the spectral index at emission?
18. *Estimating the energy of a cosmic accelerator from the energy of emitted neutrinos.* How would you estimate the energy of the proton generating a 300 GeV neutrino in the flare of a blazar?
19. *The standard model of particle physics cannot provide dark matter.* Name all particles which are described by the SM and write down through which force(s) they can interact. Why can we rule out that a dark matter particle does interact through the electromagnetic force? Why can we rule out that a dark matter particle does interact through the strong force? Now mark all particles which pass the above requirements and could account for dark matter, and comment.
20. *How well do we know that Dwarf Spheroidals are good targets for hunting Dark Matter?* Draco is a dwarf spheroidal galaxy within the Local Group. Its luminosity is $L = (1.8 \pm 0.8) \times 10^5 L_\odot$ and half of it is contained within a sphere of radius of (120 ± 12) pc. The measured velocity dispersion of the red giant stars in Draco is (10.5 ± 2.2) km/s. What is our best estimate for the mass M of the Draco dSph? What about its M/L ratio? Which are our main uncertainties in such determinations?

21. *Tremaine-Gunn bound.* Assume that neutrinos have a mass, large enough that they are non-relativistic today. This neutrino gas would not be homogeneous, but clustered around galaxies. Assume that they dominate the mass of these galaxies (ignore other matter). We know the mass $M(r)$ within a given radius r in a galaxy from the velocity $v(r)$ of stars rotating around it. The mass could be due to a few species of heavy neutrinos or more species of lighter neutrinos. But the available phase space limits the number of neutrinos with velocities below the escape velocity from the galaxy. This gives a lower limit for the mass of neutrinos. Assume for simplicity that all neutrinos have the same mass. Find a rough estimate for the minimum mass required for neutrinos to dominate the mass of a galaxy. Assume spherical symmetry and that the escape velocity within radius r is the same as at radius r.